The role of coupled gating of L-type calcium channels in arrhythmogenesis in Timothy syndrome (LQT8)

Edward Peiyang Cheng

A dissertation
submitted in partial fulfillment of the
requirements for the degree of

Doctor of Philosophy

University of Washington

2012

Reading Committee

Luis Fernando Santana, Chair
Andres Barría
Michael Laflamme

Program Authorized to Offer Degree:

Physiology and Biophysics

University of Washington

Abstract

The role of coupled gating of L-type calcium channels in arrhythmogenesis in Timothy syndrome (LQT8)

Edward Peiyang Cheng

Chair of the Supervisory Committee:

Professor Luis Fernando Santana
Department of Physiology and Biophysics

L-type Ca^{2+} ($Ca_V1.2$) channels shape the cardiac action potential waveform and are essential for excitation-contraction (EC) coupling in the heart. We find that a transient subpopulation of 2 to 6 $Ca_V1.2$ channels gate concertedly via a novel coupled gating modality. In the presence of the scaffolding protein AKAP150: PKCα, calmodulin inhibition, and the G406R mutation that causes Timothy syndrome (TS), also known as long QT syndrome type 8 (LQT8), increase the probability of coupled gating. As for the mechanism of coupled gating, we propose that $Ca_V1.2$ channels interact with each other via their carboxy tails when calmodulin is dislodged from the IQ domain, and coupled gating requires AKAP150 to bind to the $Ca_V1.2$ carboxy tails via its leucine zipper domain and to act as a scaffold. To study further the role of coupled gating and AKAP150 in arrhythmogenesis in LQT8, we created a LQT8 transgenic mouse expressing cardiac-specific $Ca_V1.2$-LQT8-tRFP channels. Importantly, we then crossed these LQT8 transgenics with AKAP150$^{-/-}$ mice, and the LQT8/ AKAP150$^{-/-}$ mice show a rescue of the wild-type (WT) phenotype. Compared to WT and LQT8/ AKAP150$^{-/-}$ ventricular myocytes, LQT8 ventricular myocytes have delayed inactivation in whole-

cell I_{Ca}, and there is increased frequency in coupled gating and open time in cell-attached i_{Ca}. These myocytes also have prolonged action potential duration and arrhythmogenic voltage fluctuations, such as early and delayed afterdepolarizations. With respect to EC coupling, LQT8 ventricular myocytes have increased [Ca^{2+}] transient amplitudes and more frequent arrhythmogenic spontaneous Ca^{2+} releases. On the whole animal level, LQT8 mice have prolonged QT_C interval and more frequent incidence of Torsades de Pointes ventricular tachycardia than WT or LQT8/ AKAP150$^{-/-}$. In conclusion, AKAP150 mediated coupled gating of $Ca_V1.2$ channels plays a central role in the pathophysiology of LQT8, causing local perturbation on EC coupling that lead to arrhythmogenesis.

Table of Contents

List of Figures

List of Tables

Preface

All the world's a stage,

And all the men and women merely players,

They have their exits and entrances,

And one man in his time plays many parts,-Shakespeare

As an aspiring physician scientist, I have to prepare myself for multiple roles on world's stage-at times comic, at times tragic, but hopefully never soporific. It was with this idea in mind that I set about finding my calling in both scientific research and clinical medicine. My younger self once viewed medicine with the jejune idea that being a physician is simply being a healer, and being a scientist is an intrepid foray into the virgin yet fecund land of the unknown, ever to expand my apothecary's shelf. My mind, once filled with numbers, equations, formulas, and structures, hubristically thought like Faust that I would one-day battle mortality itself. Fortunately, like Faust worthy of redemption, my jejune self was also a dreamer of sort, and I still love Shakespeare and a good philosophical debate. Being in the hospital as a medical student, I quickly abandoned any naïve fantasies as I had the privilege to feel and to witness the abject decline of old age as well as the indomitable fighting spirit of life, those souls who would battle and live life to their utmost, to the very last breathe. I was much humbled; panacea was not to be found; neither I nor any soul wiser by far could or should solve mortality itself.

However, in the heart, I find the metaphor that speaks of life's struggle for one more beat, to love and be loved, and that, at the end, is the essence of life. That, and what remains of the numbers, formulas, and equations from my former days as an engineering student could help me understand the mystery of this great, inexorable pump of life. Perhaps the knowledge that I gleam from nature would help souls to better live, love, and be loved while their hearts still beat, or perhaps my failures would simply remind me of my own mortality, telling me how better to live, love, and be loved, as a man, a physician, a scientist, a lover of life and knowledge.

I have the fortune to find a home in the Physiology and Biophysics Department, under the guidance of Fernando, who inspires me to continue to think, feel, and philosophize beyond numbers, formulas, and equations. We are in the science of life, after all. I have learned much from him, and one day I too hope to mentor, inspire, and even dare to seed a little sedition at times, in someone much like myself just as he has for the past four years. I am in awe of the fact that I am under the supervision of an august committee of intellects whose acumen, perseverance, as well as humble humanity that I can only hope to emulate: Drs. Andres Barría, Stan Froehner, Bertil Hille, Michael Laflamme, and Fernando Santana. I am equally fortunate and much humbled to work with my lab mates, who continue to be my friends as well as teachers.

My wife, who loves me through good and bad, and those in my family who saw me through some of my darkest hours, you who stand with me on life's stage, in the hot

glare of the limelight, from Pasadena to Fort Knox, 19-Kilo to Doctor of Philosophy, all the accolades go to you, and may we have many more encores together.

So, now, exeunt poor Yorick from his small role in a memorable yet fleeting scene, out of the infinite variety on the world's stage. Hopefully well played. Onward, life.

-Edward Cheng, né 鄭沛洋

Acknowledgements

Once again I want to thank Fernando for being my mentor as well as my good friend for the past four years. From him I learned how to pose a hypothesis, and to balance science with life. And once again, I want to thank Drs. Andres Barría, Stan Froehner, Bertil Hille, and Michael Laflamme for guiding me toward this day. I want to thank everyone in the Physiology and Biophysics Department for being my teachers and friends, and being supportive as I go through this long gestation as a graduate student. I want to thank Dr. Rick Rossow for introducing me to Fernando, and for being my "bro" for the past six years, and even when he is now in residency we still meet up for a drink. I want to thank Dr. Manuel Navedo for showing me the ropes in the world of patch clamping and for putting up with my mess in the office. I want to thank Jennifer Cabarrus for just about everything. If it were not for her I would have to kill thousands more mice with little result to show for it. I promise you that I will not go into surgery. I want to thank Suzie Kozawa for always stocking the special drawer with chocolates and helping to keep my mice alive and well. I want to thank Dr. Can Yuan for being the master molecular biologist and the hardest working person around. I also want to thank you for always telling the truth, no matter how ugly it may be! Santana lab: I will miss you.

Many people have provided invaluable assistance towards my thesis project, leading to the publication of the two original research articles in *Circulation Research* that I present as Chapters 2 and 3 of this dissertation. For Chapter 2, I want to thank Drs.

Bertil Hille, Carmen A. Ufret-Vincenty, and Madeline Nieves-Cintrón for reading the original manuscript. For Chapter 3, I want to thank Ms. Jennifer Cabarrus and Katherine Forbush for technical assistance and Dr. Michael T. Chin for reviewing ECG records.

I want to thank the Cardiovascular Pathology Training Grant and Drs. Steve Schwartz and Mark Majesky for financially supporting my training as well as mentally challenging me to be constantly aware of the bigger picture of vascular biology. And last but not least, I also want to thank the Medical Scientist Training Program (MSTP) of the University of Washington School of Medicine and its amazing directors, Drs. Larry Loeb, Mary-Claire King, Alexander Clowes, and Marshall Horwitz, as well as its amazing administrators Maureen Holstad and Marcie Buckner, for this amazing opportunity to prepare me for a career where I could combine both basic science and clinical medicine, as well as financially supporting my training.

Dedication

To Karen

Copyright Permissions

Portions of this dissertation have been previously published in separate manuscripts, and I have obtained all the proper permissions allowed me as a copyright holder to re-publish these works as parts of this dissertation.

A section of Chapter 1 was previously published as:
Santana LF, **Cheng EP**, Lederer WJ. How does the shape of the cardiac action potential control calcium signaling and contraction in the heart?. *Journal of Molecular and Cellular Cardiololgy*. 2010 Dec;49(6):901-3.

Chapter 2 was previously published as:
Navedo MF, **Cheng EP**, Yuan C, Votaw S, Molkentin JD, Scott JD, Santana LF. Increased coupled gating of L-type Ca^{2+} channels during hypertension and Timothy syndrome. *Circulation Research*. 2010 Mar 5;106(4):748-56.

Chapter 3 was previously published as:
Cheng EP, Yuan C, Navedo MF, Dixon RE, Nieves-Cintrón M, Scott JD, Santana LF. Restoration of normal L-type Ca2+ channel function during Timothy syndrome by ablation of an anchoring protein. *Circulation Research*. 2011 Jul 22;109(3):255-61.

Chapter 4 will be published as a chapter in *The Biophysics of the Failing Heart*:
Cheng EP, Santana LF. Biophysics of signaling in heart failure.

Chapter 1: Introduction

1.1 Historical perspective of cardiac physiology

> The heart . . . is the beginning of life; the sun of the microcosm . . . for it is the heart by whose virtue and pulse the blood is moved, perfected, made apt to nourish, and is preserved from corruption and coagulation; it is the household divinity which, discharging its function, nourishes, cherishes, quickens the whole body, and is indeed the foundation of life, the source of all action.—William Harvey, 1628 (Robert A Harrington, Mark E Silverman, & Charles F Wooley, 2011)

The ancients believed that the heart was the abode of the soul, and the great Roman physician Galen was only partially correct when he proposed that the heart was the great pump that propelled *pneuma*, the vital fluid of life through the body (Robert A Harrington et al., 2011). Galen's humorist theory of medicine became the central dogma of western medicine for over a thousand years, enshrined by the Church as being compatible with the Scripture. Yet, with the arrival of the Renaissance, intrepid souls, like Servetus and Vesalius, dared to explore the human anatomy for answers that would either confirm or deny the church's dogmas. Upon close examination, it was obvious that many of Galen's theories were incorrect. For

example, Vesalius showed that no foramen connected the two ventricles, and that the circulatory system's origin was the heart, not the liver (Robert A Harrington et al., 2011). William Harvey finally ushered in the modern era of cardiovascular physiology in his seminal 1628 work *Exercitatio Anatomica de Motu Cordis et Sanguinis in Animalibus*, which contains the first correct description of the circulatory circuit:

> It must of necessity be concluded that the blood is driven into a round by a circular motion and that it moves perpetually; and hence does arise the action or function of the heart, which by pulsation it performs. (Robert A Harrington et al., 2011)

With the advent of industrialization, modern societies have been confronted with a growing burden of cardiovascular disease (CVD) that has been linked to a shift to a sedentary lifestyle, over-nourishment, and tobacco use (Zachariah, Vasan, & D'Agostino, 2011). According to the WHO, CVD is the leading cause of mortality in the world (Zachariah et al., 2011). By 2020, an estimated 20 million people would die annually from CVD (Zachariah et al., 2011). The human and economic costs of CVD have added to the urgency to understand better the physiology and pathophysiology of the heart.

1.2 Gross anatomy and physiology of the heart

1.2.1 Anatomy and physiology of the heart

So, what is the heart? It is a muscular organ that acts as the great pump of life by circulating blood throughout the body, meeting its metabolic demands by providing oxygen and nutrients and removing waste. Anatomically, the normal adult male heart weighs ~300 g, and it is mostly composed of striated cardiac myocytes, whose fibers are arranged in a complex geometry with multiple orientations, resulting in a twisting, wringing motion of the heart during contraction (Scholz, Kitzman, Hagen, Ilstrup, & Edwards, 1988). The heart is located in the mediastinum within the thorax, surrounded by a fibrous sac, the pericardium. The heart consists of four chambers- the right and left atrium and the right and left ventricle. The heart is the mechanical pump that is the center of the closed loop circulatory system composed of the low-pressure (~20 mmHg) pulmonary circulation and the high-pressure (~100 mmHg) systemic circulation. The two-stroke mechanical cycle of this great pump is defined with respect to the ventricles: during systole, the ventricles contract, while during diastole, the ventricles relax (Martin & Lilly, 2007).

During systole, the right atrium receives venous blood from the systemic circulation, and the right ventricle contracts and ejects blood into the pulmonary circulation. Also during systole, the left heart receives oxygenated blood from the pulmonary

circulation into the left atrium, and the left ventricle pumps oxygenated blood into the high-pressure systemic circulation. During diastole, the left and right ventricles relax, and they are filled with blood from the left and right atria, which contract to aid ventricular filling during late diastole (Martin & Lilly, 2007). There are also four valves that regulate proper blood flow in and out of the ventricles. During systole, the tricuspid valve prevents the regurgitation of blood from the right ventricle into the right atrium, and the mitral valve prevents the left ventricle from regurgitating blood into the left atrium. During diastole, the pulmonic valve prevents flow back into the right ventricle from the pulmonary trunk, and the aortic valve prevents flow back into the left ventricle from the ascending aorta. Valvular diseases, which can be stenotic or insufficient (regurgitative), are a common morbidity, and if left untreated, the additional mechanical stress from volume overload can lead to hypertrophy of the myocardium and heart failure, the condition where the heart has reduced capacity to perfuse the body and to meet its metabolic demands (Padala, Keeling, Guyton, & Thourani, 2011). The myocardium is itself perfused by a network of coronary arteries that have two origins located at the base of the ascending aorta, just above the aortic valve, and from these two origins the left main and right coronary arteries branch off into ever smaller branches, and the network of smaller arteries penetrates into the myocardium, supplying it with oxygen and nutrients (Iyer, Edelman, & Lilly, 2007). Atherosclerosis, or hardening, of the coronary arteries due to the formation of cholesterol-laden atheromas, or plaques, is the leading cause of mortality and morbidity in the first world (Young & Libby, 2007). During a myocardial infarction, the endothelial lining covering an atheroma ruptures, and a thrombus quickly forms

and occludes the lumen of the coronary artery over the plaque, infarcting the myocardium supplied by the artery (Young & Libby, 2007). Venous blood from the myocardium is collected into a network of cardiac veins that drains into the coronary sinus, located in the right atrium just above the tricuspid valve (Iyer et al., 2007).

Within the mediastinum, the heart's shape could be approximated as a trigonal prism with five faces. The heart's base, or the posterior surface, consists of the left atrium, a portion of the right atrium, the superior and inferior venae cavae, and the pulmonary vein (Drake, Vogl, & Mitchell, 2005). The base is fixed, and it extends from the thoracic vertebrae levels 5 to 8. From the base, the long axis of the heart projects anteriorly and inferiorly leftward. The apex of the heart consists of the left ventricle, and it is located at the fifth intercostal space just medial of the left mid-clavicular line (Drake et al., 2005). The heart's anterior surface consists of the right ventricle, a portion of the right atrium, and a portion of the left ventricle, and it faces the sternum. Its inferior surface consists of the left ventricle and a portion of the right ventricle, and it faces the diaphragm. The right and left lungs appose the right and left faces of the heart, respectively.

1.2.2 Cardiac mechanics

The inexorable beatings of the heart define life. The gross mechanics of the heartbeat can be divided into two phases: the diastole and the systole. The stereotypical “lub-dub” heart sounds, which are called S1 and S2 respectively, mark the start and end of systole. If we were to plot the mechanical work of the left ventricle on a graph with volume as the abscissa and pressure as the ordinate, it would form a closed loop with the area enclosed equal to the net mechanical work performed during one cycle, and it is called the pressure-volume (PV) loop (Fig 1.1).

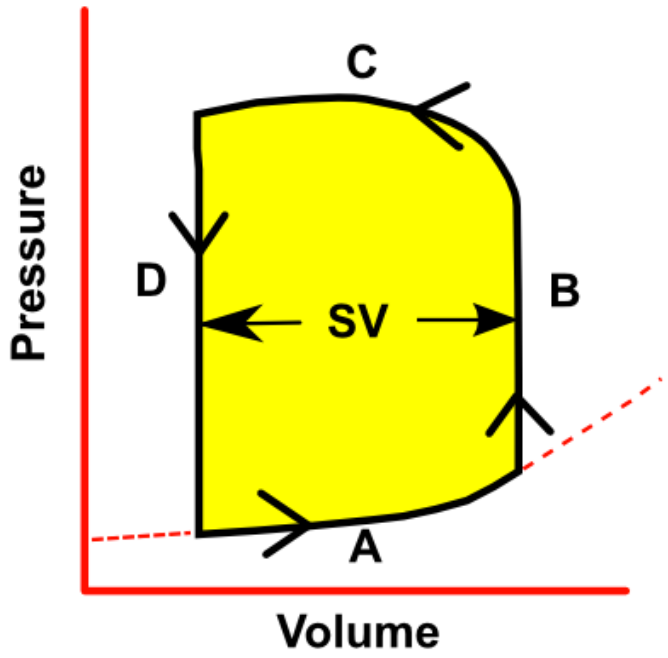

Figure 1.1. The cardiac pressure-volume (PV) loop.
Abscissa is the left-ventricular volume. The ordinate is left-ventricular pressure (LVP). The area colored yellow represents the net work expanded by the ventricular wall during one cardiac contraction cycle. The dashed red curve represents the passive compliance of the ventricle. SV is the stroke volume.

During diastole, which makes up approximately 2/3 of one cardiac cycle, the ventricles relax, and the aortic and pulmonic valves are closed (Martin & Lilly, 2007). In Figure 1.1, the left ventricle undergoes isovolumic relaxation during diastole (labeled D in Figure 1.1) until its pressure drops below that within the left atrium, which opens the mitral valve (junction of segments D and A in Figure 1.1), refilling the ventricles with blood from the atria (labeled A in Figure 1.1). The curvature of A represents the passive mechanical compliance of the left ventricular wall. Ventricular filling is aided by atrial contraction towards the end of diastole; however, atrial contraction is not necessary for ventricular filling; for example, patients with atrial fibrillation can still fill their ventricles without the atrial kick. The ventricles begin to contract at the start of systole, and the left ventricular pressures quickly exceed the left atrial pressures, closing the mitral valve (junction of segments A and B in Figure 1.1). The end-diastolic ventricular volume, corresponding to the junction of segments A and B in Figure 1.1, is called the preload. According to the Frank-Starling law, the ventricle increases the ejection fraction with an increase in preload as a way to maintain volume homeostasis (Kemp & Conte, 2012).

After the closure of the mitral valve, the ventricles then undergo isovolumic contraction and pressurization (labeled B on Figure 1.1) until the pressure within the left ventricle exceed that in the ascending, which push the aortic valve to open (junction of segments B and C on Figure 1.1). Blood is continuously ejected, and the pressure the left ventricle needs to generate during systole is called the afterload (labeled C on Figure 1.1). The ventricles begin to relax toward the end of systole,

and when the left ventricular pressures drop below those within the aorta, the aortic \ valve shuts, signaling the end of systole. The mean arterial pressure within the systemic circulation (~100 mmHg) is typically much higher than that within the pulmonary circulation (~20 mmHg), and the demand to generate a much higher work causes the left ventricular wall being much more muscular than that of the right ventricle. The stroke volume (SV), or the amount of blood ejected per cycle, is the width of the PV loop. In heart failure caused by chronic, untreated hypertension, the area enclosed by the PV loop would be larger for a given SV, given the longer lengths of segments B and D in the PV loop, and the chronic elevation in work to meet the cardiac output demands of the body causes the left ventricular wall to hypertrophy (Shah & Fifer, 2007).

1.3 The heart is an electrical organ

1.3.1 The cardiac resting potential

The physiology behind the rhythm of the heart is a unique coupling of electricity and mechanical force generation. The heart is primarily composed of striated cardiac myocytes. Like all cells, an electrical potential exists across the plasma membrane, also called sarcolemma in myocytes. In a human cardiac myocyte, at rest, this potential is approximately -90 mV. The negative resting potential is set by the large concentration gradient that exists across the sarcolemma for different ions and the

selective permeability of the sarcolemma, which can be described by the Goldman-Hodgkin-Katz (GHK) Equation:

$$E_m = \frac{RT}{F} \ln \left(\frac{\sum_i^N P_{M_i^+} \left[M_i^+ \right]_{out} + \sum_j^M P_{A_j^-} \left[A_j^- \right]_{in}}{\sum_i^N P_{M_i^+} \left[M_i^+ \right]_{in} + \sum_j^M P_{A_j^-} \left[A_j^- \right]_{out}} \right),$$

where *R* is the universal gas constant; *T* is the temperature in Kelvin; *F* is the Faraday constant; and *P* is the permeability for each ion (Goldman, 1943). The typical intra- and extracellular concentrations for the ions that chiefly contribute to the resting potential are given in Table 1.1 (Berne, Spreelakis, & Geiger, 1979).

Ion	Extracellular Concentration (mM)	Intracellular Concentration (mM)	Ratio of extracellular to intracellular Concentration	Nernst Potential (mV)
Na^+	145	15	9.7	+60
K^+	4	150	0.0027	-94
Cl^-	120	5-30	4-24	-83 to -36
Ca^{2+}	2	10^{-7}	2×10^4	+129

Table 1.1. The typical intra- and extracellular concentrations of ions

1.3.2 The electrophysiology of the cardiac pacemaker

However, a cardiac myocyte that remains at resting potential does not beat, and a cardiac myocyte contains a whole complement of voltage-gated ion channels that allows it to fire action potential (AP) and to contract. Unlike skeletal muscle fibers,

the contraction of the heart does not require innervation from the nervous system. The heart contains pacemaker cells capable of automaticity, which is the ability spontaneously fire APs, in the sinoatrial (SA) and the atrioventricular (AV) node. Under normal physiology, the SA node is the dominant pacemaker due to its higher intrinsic rate, and it suppresses the AV node via a mechanism known as overdrive suppression (Rolls, Stevenson, Strichartz, & Lilly, 2007). The SA node is a spindle shaped structure that lies just beneath the epicardium within the right atrial sulcus terminalis, which is located at the junction of the superior vena cava and the right atrium (Rubart & Zipes, 2008).

The physiology of automaticity in SA nodal pacemaker cells is controversial, with groups who are proponents of the model where Ca^{2+} oscillation conducted via the sodium-calcium exchanger (NCX) is responsible for depolarization to the threshold potential, and others who believe that the gradual depolarization to the threshold potential is regulated by an hyperpolarization-activated inward current, known as the "funny current" (I_f) conducted through the hyperpolarization-activated, cyclic-nucleotide gated HCN channels (Lakatta 2010, Liao et al., 2012). While proponents of the Ca^{2+} oscillation model points to NCX's well-known role as a target for phosphorylation by protein kinase A (PKA) as physiological evidence in favor of their model, since PKA activation by adrenergic signaling is an integral part of the signaling cascade of the fight or flight response, which raises the heart rate; however, there is evidence for both direct activation of HCN channels by cyclic adenosine monophosphate (cAMP) and modulation of HCN channels via PKA

phosphorylation (Lakatta, Maltsev, & Vinogradova, 2010; Z. Liao, Lockhead, Larson, & Proenza, 2010). In any case, the automaticity of SA nodal cells is remarkably consistent, commanding the adult heart to beat at a native rate of ~100 beats/min when vagal innervation, which slows down the rate, were blocked. When a SA nodal cell reaches the threshold potential, the opening of L-type and T-type calcium channels causes an AP to fire. The combined effects of voltage-gated potassium channels' activation and L-type calcium channels' inactivation bring about the termination of the AP in the SA pacemaker cell.

1.3.3 The electrophysiology of conduction

The wavefront of depolarization propagates out of the SA node into the atrial myocardium, following two pathways established by connexin gap junction channels at the upper and lower margins of the SA node that provide a low resistance pathway between the cytoplasm of nodal and atrial myocytes. Connexin gap junctions also connect atrial myocytes, which allow the rapid propagation of the depolarization wavefront throughout the atria. Depolarization of the atrial myocytes cause them to contract via the process of excitation-contraction (EC) coupling. The atrioventricular (AV) node, which is located near the coronary sinus in the interatrial septum, normally provides the sole electrical connection via the His-Punkinje bundle system between the atria and the ventricle. The AV node has a much slower conduction velocity of the depolarization wavefront compared to either atrium, which

allows sufficient time for ventricular filling before the ventricles contract. The AV node is also capable of automaticity, at a slower intrinsic rate, in pathological states when it becomes uncoupled from the SA node (Rolls et al., 2007). In Wolff-Parkinson-White (WPW) syndrome, an accessory pathway, which is a congenital structural defect, provides an alternative faster conduction pathway between the atria and ventricles (Rolls et al., 2007). Patients with WPW have a high risk of developing paroxysmal superventricular tachycardia (PSVT) that can lead to sudden cardiac death (SCD). After ~50 ms delay through the AV node, the depolarization impulse then travels rapidly through specialized conduction fibers of the His-Purkinje system, composed of specialized cardiac myocytes, down the interventricular septum and penetrating into ventricular myocardium. Ventricular myocytes are electrically coupled to the His-Purkinje system, and their depolarization triggers EC coupling, progressing from the endocardium to the epicardium, and from the apex up. At the end of ventricular systole, repolarization of the ventricles progress in the opposite direction. A normal cardiac cycle ends with the completion of ventricular repolarization, and it continuously resets with the firing of the SA node.

1.3.4 The electrocardiogram (ECG)

The electrical activity of the myocardium, the propagation of the wave of depolarization and repolarization, can be monitored via skin surface leads using the electrocardiogram (ECG). The movement of ionic charge in the myocardium generates an electrical field with a measurable electrical dipole moment, even on the

torso surface (Hecht, 1961; Mirvis & Goldberger, 2008). The standard limb leads are a combination of bipolar leads that represent three non-orthogonal electrical axes 60^{o} apart in the coronal plane. The angles in between the axes are defined by a left-handed coordinate system, with the clockwise direction being positive. Lead I lie along the horizontal axis, at 0°, with the positive pole on the left arm, and the negative pole on the right arm. Lead II lies $+60^{0}$ with respect to lead I, with its positive pole on the left leg, and its negative lead is on the right arm. Lead III is again $+60^{0}$ with respect lead II, with its positive pole on the left leg, and its negative pole on the left arm. The standard limb leads forms a triangle, known as the Einthoven triangle, with the potential sensed by lead II being the sum of those sensed by leads I and II (Mirvis & Goldberger, 2008). By tying together any pair of the standard limb electrodes, one obtains the augmented leads avR, avL, and avF, which bisect the angles formed by the standard limb leads in the coronal plane. Additionally, in the transverse plane, there are six unipolar precordial leads, and they are especially important clinically for localizing myocardial injury, such as ischemia and infarction.

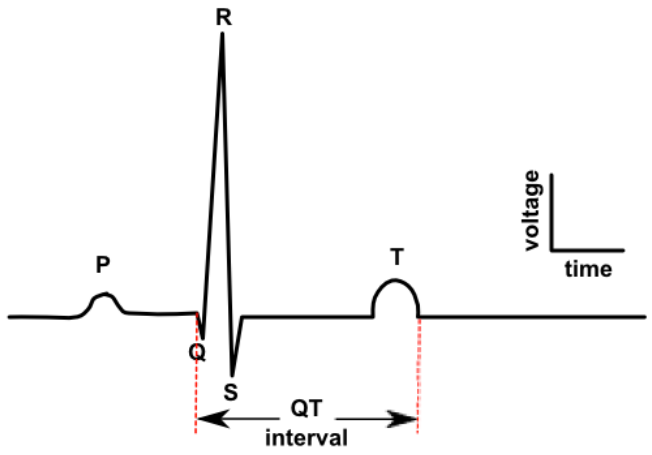

Figure 1.2. Cartoon of a typical lead II electrocardiogram (ECG) waveform.

Each ECG lead can be viewed as a vector. A positive deflection in its record represents a depolarization wavefront traveling towards its positive direction or a repolarization wavefront moving away from its positive direction, and vice versa for a negative deflection. Figure 1.2 represents a normal electrocardiogram. The P wave represents atrial activation; however, atrial repolarization is not seen as the QRS complex obscures it. The PR segment, the isoelectric region between the end of the P wave and the start of the QRS complex, corresponds to the slow conduction through the AV node. The QRS complex corresponds to the sequence of ventricular activation, spreading from the endocardium outwards. The QRS complex is normally positive between -30^{o} and 90^{o}, reflecting the physiologic hypertrophy of the left ventricular myocardium (Garibyan & Lilly, 2007). The ST segment corresponds to the plateau of the cardiac AP, and the normally upright T wave corresponds to ventricular repolarization, which progresses from the epicardium inward (Hecht, 1961; Mirvis & Goldberger, 2008). The QT interval, the period between the start of

the QRS complex to the end of the T wave, grossly represent the duration of the ventricular AP. QT interval prolongation and shortening are both pathologic, and they can be caused by congenital abnormalities, metabolic disturbances, and medication (Zimetbaum & Josephson, 2008). Disturbance to the QT interval outside of the physiologic range can quickly lead to the development of arrhythmias. Polymorphic ventricular tachycardia (PVT), also known as torsades de pointes (TdP), is a dangerous form of arrhythmia that can be a sequela of QT prolongation, and if left untreated, SCD can quickly ensue (Zimetbaum & Josephson, 2008).

1.4 Cellular cardiac physiology

1.4.1 The cardiac action potential (AP)

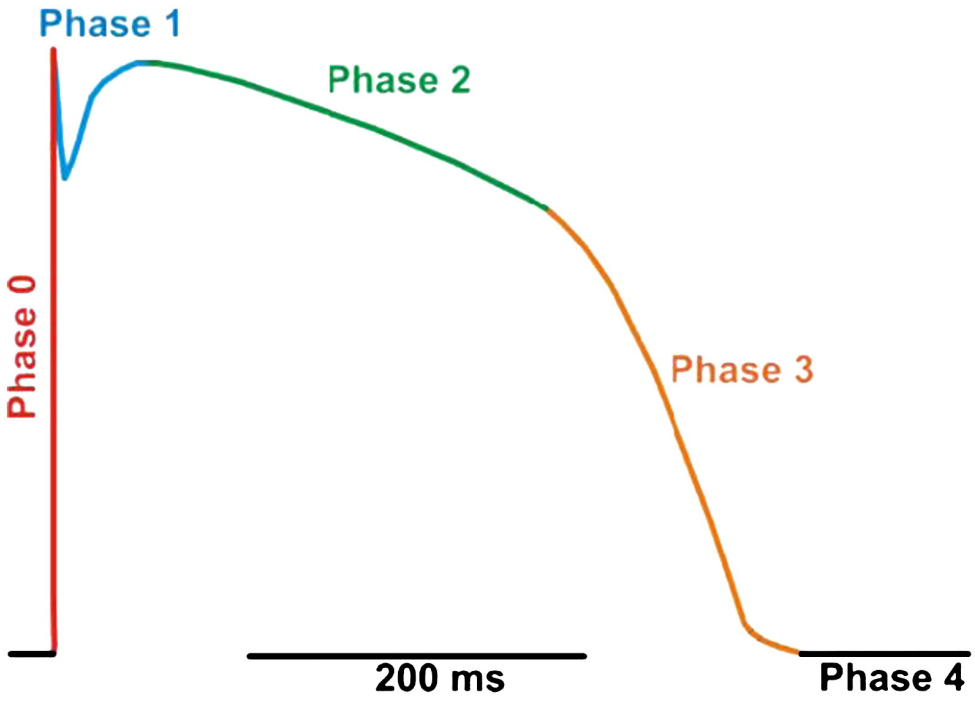

Figure 1.3. A typical action potential (AP) waveform of an adult human ventricular myocyte modified from Cooper et al. (Cooper, Soeller, & Cannell, 2010).

While on the gross level the electrophysiology of the myocardium can be viewed as sequential wavefronts of positive and negative currents propagating through the myocardium, the electrophysiology of the cardiac AP on the cellular level is more complex and intricate. In Fig. 1.3, a color-coded human ventricular myocyte AP is used to illustrate its five phases. Phase 0 (red) is the leading edge of the AP and

corresponds to the period of rapid depolarization (depolarization rate ≈ 250 V/s) from the diastolic membrane potential of ≈ −90 mV to + 50 mV (Hecht, 1961). It is produced primarily by the activation of cardiac voltage-gated Na^+ channels ($Na_V1.5$) with a contribution from cardiac voltage-gated L-type Ca^{2+} channels ($Ca_V1.2$) (Nerbonne & Kass, 2005).

Phase 1 (blue), also referred as the “notch”, is produced by termination of the depolarizing inward Na^+ current due to inactivation and the concomitant activation of the transient outward K^+ (I_{to}) and Na^+/Ca^{2+} exchanger (I_{NCX}) currents. This results in a transient repolarization period as the membrane potential goes from ≈ +50 to +30 mV (or more negative). The I_{to} currents have two components, the fast and the slow, carried by the $K_V4.3$ and $K_V1.4$ channels respectively, and their magnitudes have great effect on action potential duration (APD) and the driving force for the L-type Ca^{2+} current (Cooper et al., 2010; Harris et al., 2005; Sah, Ramirez, & Backx, 2002). Reduction of this current occurs after myocardial injury, and it contributes to arrhythmogenesis (Cooper et al., 2010; Rossow et al., 2009) Indeed, according to the Goldman-Hodgkin-Katz (GHK) equation, repolarization from +50 to +30 mV during phase 1 would triple the Ca^{2+} electrochemical driving force 3.09-fold, which would play an important difference during phase II of the cardiac AP.

Phase 2 (green) is the long (hundreds of milliseconds) plateau phase of the AP during which the membrane potential changes little. The balance of long opening $Ca_V1.2$ Ca^{2+} current (I_{Ca}) and a small, non-inactivated Na^+ current against

hyperpolarizing K^+ currents forms the plateau. The hyperpolarizing K^+ currents consist of two components: the rapid and slow delayed rectifier voltage-gated K^+ currents (I_{Kr} and I_{Ks}), which pass through the hERG and K_VLQT1 K^+ channels respectively (Nerbonne & Kass, 2005). The tug-of-war between I_{Ca} versus I_{Kr} and I_{Ks} plays a critical role in determining APD. A mutation in $Ca_V1.2$ that causes delay in I_{Ca} inactivation and consequently APD prolongation causes LQT8, also known as Timothy syndrome, a congenital long QT syndrome characterized by early SCD (Splawski et al., 2004). Blockade of the hERG channel by drugs such as quinidine is a widespread cause of acquired long QT and frequently lead to the development of TdP and SCD (Sanguinetti & Tristani-Firouzi, 2006).

During Phase 3 (orange), reductions of Ca^{2+} and Na^+ currents and increasing K^+ currents contribute to the repolarization of the myocyte. Towards the end of phase 3 the repolarizing actions of these K^+ currents are opposed by an inward I_{NCX} produced by the Na^+/Ca^{2+} exchanger operating in its Ca^{2+} extrusion mode. A period comprising of phases 0, 1, 2, and a portion of phase 3 is called the effective refractory period, when depolarization from a neighboring cell is unable to trigger the firing of a new AP (Dressler & Jonas, 1964).

Phase 4 (black) is the diastolic membrane potential of the quiescent ventricular myocytes at ≈ -90 mV, and the non-voltage gated inward rectifying K^+ channel (K_{ir}) helps to establish the phase 4 potential close to the K^+ reversal potential (Doupnik, Davidson, & Lester, 1995; Nerbonne & Kass, 2005). While the AP morphology

shown in Figure 1.3 illustrates that found in the human ventricular myocyte and Purkinje cells, the exact AP morphology varies between anatomic location of the tissue as well as the species and developmental age of the animal (Nerbonne & Kass, 2005).

1.4.2 Excitation-contraction (EC) coupling

"Ja, Kalzium das ist alles…"-Otto Loewi, Nobel Laureate (Heping Cheng & Lederer, 2008)

The process by which cardiac myocyte couples the electrical stimuli of AP with mechanical contractions is known as excitation-contraction (EC) coupling. In cardiac myocytes, the sliding filament model explains how Ca^{2+} plays a central role in allowing the motor protein myosin to generate mechanical force during contraction (A. F. Huxley & Niedergerke, 1954; H. Huxley & Hanson, 1954). In this model, the myosin head groups bind to actin filaments, forming cross-bridges, and ATP powered conformational change in the head groups, in an oar-like motion, translates into a sliding motion against the actin filaments and the conversion of chemical energy into mechanical force. The cross-bridge formation requires Ca^{2+} to bind to troponin, which then undergoes conformational change and moves tropomyosin out of the myosin binding-site. $[Ca^{2+}]$ elevation is critical for contraction, and EC

coupling is the process that translates membrane depolarization into a global [Ca^{2+}] transient.

Ca^{2+} is perhaps the simplest and most primordial of signaling molecules. All living cells spend tremendous amount of metabolic energy in compartmentalizing and regulating [Ca^{2+}]. During diastole, the cytosolic [Ca^{2+}] in cardiac myocytes is only ~150 nmol/L, which represents a ~10^4 time gradient across the sarcolemma (Heping Cheng & Lederer, 2008; Yuan & Bers, 1994). A similar gradient exists between the cytoplasm and the sarcoplasmic reticulum (SR), the highly specialized endoplasmic reticulum of cardiac myocytes (Heping Cheng & Lederer, 2008). The SR contains Ca^{2+} buffering proteins that greatly increase the Ca^{2+} storage capacity, and the most important buffer is calsequestrin, which has a K_d=2 mmol/L for Ca^{2+} (di Barletta et al., 2006; Qin et al., 2008). During a systolic [Ca^{2+}] transient in cardiac myocytes, ~1/3 of the [Ca^{2+}] elevation is due to Ca^{2+} influx through the L-type $Ca_V1.2$ channels, and ~2/3 of the [Ca^{2+}] elevation is due to Ca^{2+} release from the SR via type 2 ryanodine receptors (RyR2) (Heping Cheng & Lederer, 2008). Unlike skeletal muscles, where the skeletal muscle isoform of the L-type Ca^{2+} channel ($Ca_V1.1$) is directly coupled to type 1 ryanodine receptors (RyR1), and membrane depolarization directly triggers SR Ca^{2+} release and EC coupling (Dayal, Schredelseker, Franzini-Armstrong, & Grabner, 2010). Membrane depolarization in cardiac myocytes does not directly lead to SR Ca^{2+} release. Trans-sarcolemmal $Ca_V1.2$ Ca^{2+} current triggers the opening of RyR2 on the surface of the SR via the mechanism of calcium-induced calcium release (CICR) (Fabiato, 1985). Like the Greek god Janus,

$Ca_V1.2$ channels have two faces: the Ca^{2+} gateway controlling EC coupling as well as the long-opening ion channel responsible for the phase II cardiac AP plateau. Therefore, the biophysics of $Ca_V1.2$ channels is of key importance to the study of both the electrophysiology and the mechanics of cardiac myocytes.

1.4.3 L-type ($Ca_V1.2$) calcium channels

$Ca_V1.2$ channels are sensitive to the dihydropyridine family of pharmacologic blockers like nifedipine, which is why they are classically referred to as dihydropyridine receptors (DHPR) in the parlance of muscle physiology (Reuter, 1979). In cardiac myocytes, $Ca_V1.2$ channels are made up of heteromeric complexes composed of the pore forming α1c, and the accessory β, and α2δ subunits (Arikkath & Campbell, 2003). The α1c is a large protein of approximately 2,000 amino acids long, with a molecular weight of ~170 kD before and ~250 kD after glycosylation, and it is structurally divided into four transmembrane (TM) domains (DI-IV), with each domain having six TM α helices, linked together by cytoplasmic loops (Catterall, 2000, 2011). A three-dimensional structure from X-ray crystallography does not currently exist for $Ca_V1.2$; however, recent crystallographic structure of the carboxy terminal and high-resolution electron microscopy both show that these channels may exist as dimers (Fallon et al., 2009; M.-C. Wang, Collins, et al., 2004).

Like the S4-family of voltage-gated Na^+ and K^+ channels, the S4 helix in each domain of $Ca_V1.2$ acts as the voltage sensor (Catterall, 2011; Nerbonne & Kass, 2005). The S4 voltage sensor putatively functions via Coulomb force on a series of basic residues it contains, and the cell-wide movement of these positive charges contained within S4 helices can be experimentally recorded as gating currents (Bezanilla, 2000). The S5 and S6 helices make up the pore, and a cluster of glutamate residues in the loop connecting S5 and S6 confers Ca^{2+} selectivity (Catterall, 2011; Heinemann, Terlau, Stuhmer, Imoto, & Numa, 1992). The S5 and S6 helices also may contribute to the inactivation mechanism of $Ca_V1.2$ channels.

Unlike other voltage-gated ion channels, $Ca_V1.2$ channels undergo two forms of inactivation: the slower voltage dependent inactivation (VDI) and the faster Ca^{2+} dependent inactivation (CDI) (Brehm & Eckert, 1978; Catterall, 2000). From the perspective of scientific parsimony, it is more likely that these two mechanisms both act convergent (Cens, Rousset, Leyris, Fesquet, & Charnet, 2006; Findlay, 2004). The most well understood molecular mechanism during $Ca_V1.2$ inactivation is how Ca^{2+} triggers feedback inhibition in the form of CDI. Calmodulin (CaM), the ubiquitous Ca^{2+} sensor, exists as the Ca^{2+} free apoCaM form and binds to the pre-IQ domain on the carboxy terminal of $Ca_V1.2$ when the channel is closed (Soldatov, Oz, O'Brien, Abernethy, & Morad, 1998). Upon binding to four Ca^{2+} ions, CaM switches its binding site to the IQ domain on the $Ca_V1.2$ carboxy termininal, and this association drives the channel to undergo CDI (Soldatov et al., 1998; Soldatov, Zühlke, Bouron, & Reuter, 1997; Zühlke & Reuter, 1998). The mechanism of how

CaM-IQ interaction allosterically translates into CDI is still unclear (Cens et al., 2006; Findlay, 2004).

Although the molecular mechanism of the inactivation step in $Ca_V1.2$ channels remain in dispute, with no definitive inactivation particle like the tethered plug found in voltage-gated Na^+ and K^+ channels, evidence from site-directed mutagenesis and chimera studies suggest that the cytoplasmic loop linking DI and DII (I-II loop) form a "hinged-lid" that occludes the channel during inactivation (Cens et al., 2006; P. Liao & Soong, 2010; Stotz & Zamponi, 2001; J.-F. Zhang, Ellinor, Aldrich, & Tsien, 1994). Site-directed mutagenesis studies that substitute hydrophilic residues for certain hydrophobic residues on the S6 helices in DII-IV show delayed VDI and CDI, which suggest that the hydrophobic ring lining lower vestibule of the pore may play a role in VDI and CDI (Cens et al., 2006; Shi & Soldatov, 2002). While one would like to assume that introduced mutations only act locally, the results of these studies need to be weighed against the possibility that these mutations create allosteric changes, alterations to the macromolecular structure of the channel, and the effects seen may be due to some novel gain-of-function mutation unknowingly introduced. An additional level of complication is added via $Ca_V1.2$ phosphorylation, by kinases such as PKA and calmodulin kinase II (CaMKII), which also acts allosterically and promotes the channels to go into mode 2 gating, which is characterized by frequent occurrence of long duration openings, and delays VDI of the macroscopic current (Findlay, 2004; Hess & Tsien, 1984). Findlay proposed an attractive model that unifies CDI, VDI, and the effects of kinases, where channels that undergo mode 1

gating, which is characterized by frequent but short duration openings, undergo VDI exclusively, and they shift to mode 2 gating and CDI with phosphorylation (Findlay, 2004; Hess & Tsien, 1984).

The accessory subunits play important roles in determining the physiological characteristics of $Ca_V1.2$ channels. The α2δ subunit is composed of two halves, α2 and δ, that are cleaved from a single gene product via post-translational modification, and they are covalently linked together via disulfide bonds (De Waard, Gurnett, & Campbell, 1996). A glycophosphatidylinositol (GPI) on the tail of the δ portion anchors the α2δ subunit on the extracellular face of the membrane (Catterall, 2011). The β subunit binds to α1c subunit via the α-interaction domain (AID) present on the intracellular DI-II loop, and it modulates inactivation kinetics (Lacerda et al., 1991; Pragnell et al., 1994). It has four variants, β1-4, and they all act as chaperones in the proper trafficking α1c pore into the sarcolemma (Chien et al., 1995; Colecraft et al., 2002). In cardiac myocytes, β2b is the most common variant, and it confers the slowest inactivation kinetics when compared to other variants of the β subunit because of it is anchored to the sarcolemma via GPI anchors (Cens et al., 2006; Colecraft et al., 2002).

1.4.4 Ca^{2+} sparklets and sparks: the physiology of local control of EC coupling

Although $Ca_V1.2$ channels exist everywhere on the sarcolemma in cardiac myocytes, in ventricular cardiac myocytes they are mostly concentrated in transverse tubules (T-tubules), which are invaginations in the sarcolemma, perpendicular to the long-axis of the myocyte (Guatimosim, Hull, Von Gersdorff, & Prado, 2002). The T-tubules are located at the Z-lines, the orthogonal striations that are the hallmark of microscopic images of striated muscle cells, located approximately ~2 μm apart (Guatimosim et al., 2002) The T-tubules allow clusters of ~10 $Ca_V1.2$ channels to appose clusters of RyR2s on the surface of junctional SR (jSR) cisternae forming a "dyad," with a subspace of ~15 nm in between (Langer & Peskoff, 1996). RyR2s are homotetrameric Ca^{2+} channels with large cytosolic domains that are clearly visible as "feet" in electron microscopy (EM) (Franzini-Armstrong, Protasi, & Ramesh, 1999; Meng et al., 2007). The RyR2 are packed within a ~30 nm wide quasi-crystalline array in the jSR membrane, forming calcium release units (CRUs) (Hayashi et al., 2009). A widely accepted EM study by Franzini-Armstrong et al. finds that ~100 RyR2 are packed into CRUs in ventricular myocytes (Franzini-Armstrong et al., 1999). However, a recent study using super-resolution optical microscopy finds that the RyR2 are packed into smaller, elongated subunits of ~13 RyR2, and these smaller subunits communicate with neighboring subunits ~50 nm away to form CRUs (Baddeley et al., 2009). Apposing $Ca_V1.2$ channels and CRUs in a dyad functionally couple to form "couplons," the fundamental functional units of EC coupling (Stern, 1992).

Inward I_{Ca}, during phase II of the cardiac AP, elevates the local [Ca^{2+}] to ~10 μM in the 15 nm wide subspace within a couplon, between the membranes of adjoining T-tubules and jSR, which activates the opening of RyR2s in CRUs (Heping Cheng & Lederer, 2008; Langer & Peskoff, 1996). Because they could be visualized *in situ* as an increase in fluorescence of Ca^{2+} indicators, the [Ca^{2+}] elevation caused by the opening of individual or clusters of $Ca_V1.2$ channels is known as sparklets, and the [Ca^{2+}] elevation caused by the opening of RyR2s in an individual CRU is known as a Ca^{2+} spark (H Cheng, Lederer, & Cannell, 1993; H Cheng & Lederer, 2008; Navedo, Amberg, Votaw, & Santana, 2005; S.-Q. Wang, Song, Lakatta, & Cheng, 2001). Although previous single-channel patch clamp recordings showed that there is temporal heterogeneity in $Ca_V1.2$ channels' activity, with channels shifting between modes, 0, 1, and 2, recent studies from our group using TIRF microscopy to visualize Ca^{2+} sparklets in large surface membrane areas in myocytes and tsA-201 cells demonstrated that the activity of Ca^{2+} sparklets is highly spatially heterogeneous due to PKCα phosphorylation of $Ca_V1.2$ channels, with a sub-population of $Ca_V1.2$ channels showing "persistent," long-opening, Ca^{2+} sparklet activity (Hess & Tsien, 1984; Navedo, Amberg, Nieves, Molkentin, & Santana, 2006; Navedo et al., 2005). Such spatial heterogeneity can affect the synchrony of EC coupling. During systole, the near concurrent activation of ~10^4 sparks by just as many sparklets via CICR amalgamates into a whole cell [Ca^{2+}] transient, which provides the [Ca^{2+}] (~1 μM) required for myofilament cross-bridge formation (Blayney & Lai, 2009; H Cheng & Lederer, 2008).

Ca^{2+} sparks are discrete units of EC coupling, and they mostly occur in a stochastic fashion during diastole due to a non-zero probability of spark occurrence at diastolic [Ca^{2+}], even when $Ca_V1.2$ channels are blocked (H Cheng et al., 1993; H Cheng & Lederer, 2008). However, evoked sparks are always triggered by Ca^{2+} sparklets, and this coupling means that evoked sparks occur deterministically instead of stochastically (H Cheng et al., 1993; H Cheng & Lederer, 2008; S.-Q. Wang et al., 2001). In the presence of a $Ca_V1.2$ agonist FPL64176, approximately two-thirds of all Ca^{2+} sparklets trigger Ca^{2+} sparks, with a triggering delay of ~0.6 ms (S.-Q. Wang et al., 2001). Using Ca^{2+} sparklets as an optical "yardstick," Wang et al. found by confocal imaging of both Ca^{2+} sparklets and their evoked sparks at the mouth of a loose-seal patch electrode that Ca^{2+} sparks are much larger in amplitude than sparklets, corresponding to ~1.2 pA of Ca^{2+} current (S.-Q. Wang et al., 2001). Activation of RyR2 follows a steep logistic function, somewhat analogous to voltage-gated ion channels, but instead of having voltage as the abscissa, $[Ca^{2+}]_{subspace}$ is the abscissa (H Cheng & Lederer, 2008). Ca^{2+} spark frequency is also a function of the SR Ca^{2+} load, with Ca^{2+} spark frequency increasing with SR Ca^{2+} load (Lukyanenko, Viatchenko-Karpinski, Smirnov, Wiesner, & Györke, 2001). In a reconstituted system, the SR Ca^{2+} buffer calsequestrin forms a complex with RyR2 and the jSR membrane proteins triadin and junction, and this complex confers on RyR2s' open probability responsiveness with respect to SR luminal [Ca^{2+}] (Györke, Hester, Jones, & Györke, 2004). Currently, there is no clear consensus on whether all the RyR2s in a CRU open simultaneously or whether only a few open during a spark (Sobie, Dilly, dos Santos Cruz, Lederer, & Saleet Jafri, 2002; S. Q. Wang,

Stern, Ríos, & Cheng, 2004). However, there is evidence that neighboring RyR2s gate cooperatively in a coupled fashion via interactions with the FKBP12.6 protein, which contributes to the steepness and positive cooperativity of the *in situ* RyR2 activation curve when compared to RyR2 in artificial planar lipid bilayers (Heping Cheng & Lederer, 2008; Marx et al., 2001). Under normal physiology, local CICR from RyR2 is under the exclusive control of local Ca^{2+} influx via $Ca_V1.2$ channels (i_{Ca}), and this observation is known as the local control theory of EC coupling (M. B. Cannell & Kong, 2012; M. Cannell, Cheng, & Lederer, 1995; Stern, 1992; Wier, Egan, López-López, & Balke, 1994; Xie & Weiss, 2009). By investigating the voltage dependence of both Ca^{2+} spark probability of occurrence P_S and the whole-cell $Ca_V1.2$ current I_{Ca}, Santana et al. was able to mathematically derive the local EC coupling gain, which is the coupling fidelity between local Ca^{2+} sparklet $Ca_V1.2$ current i_{Ca} and Ca^{2+} spark activation, assuming local control of EC coupling (H Cheng & Lederer, 2008; L.F. Santana, Cheng, Gómez, Cannell, & Lederer, 1996). Santana et al. assumed that P_S is the products of the open probability P_O of local $Ca_V1.2$ channels and the probability that a channel opening would trigger CICR, P_i (L.F. Santana et al., 1996):

$$P_S = P_O P_i.$$

And if we assume that P_i is proportional to the single-channel $Ca_V1.2$ current i_{Ca} to an unknown power x, then the local EC coupling gain follows the following power law with respect to i_{Ca},

$$P_S = P_O \cdot k \cdot i_{Ca}^{x},$$

where *k* is a constant. The whole-cell $Ca_V1.2$ current I_{Ca} is equal to:

$$I_{Ca} = n \cdot i_{Ca} \cdot P_O,$$

where *n* is the number of $Ca_V1.2$ channels. By dividing P_S with I_{Ca}, we obtain the following equation,

$$\frac{P_S}{I_{Ca}} = \frac{(k \cdot i_{Ca}^{x-1})}{n}.$$

It is obvious that the ratio of Ca^{2+} spark probability of occurrence P_S and the whole-cell $Ca_V1.2$ current I_{Ca} follows an unknown power-law relationship with respect to local $Ca_V1.2$ current i_{Ca}. By fitting the empirically determined ratio of Ca^{2+} spark probability and I_{Ca} as a function of membrane voltage, Santana et al. found that it is linear with respect to the Nernst-Planck equation for i_{Ca} as a function of membrane voltage (L.F. Santana et al., 1996). Therefore, the ratio is linear with respect to i_{Ca}, ergo x=2, and the local EC coupling gain is proportional to i_{Ca}^2. Because the $[Ca^{2+}]_{subspace}$ is related linearly with i_{Ca}, then we can also make the following conclusion (Heping Cheng & Lederer, 2008; Soeller & Cannell, 1997):

$$P_S \propto [Ca^{2+}]_{subspace}{}^2$$

The quadratic relationship between Ca^{2+} spark activation to local i_{Ca} and $[Ca^{2+}]_{subspace}$ agrees well with what we expect from the large positive-feedback that we observe in EC coupling. Interestingly, recent study found that at the plateau phase of the cardiac AP, a Ca^{2+} sparklet due to the opening of a single $Ca_V1.2$ channel would be insufficient to trigger a Ca^{2+} spark due to the reduced Ca^{2+} electrochemical driving force at +30 mV (Inoue & Bridge, 2003). Even at 0 mV, Cheng and Lederer found that only 1 out of 60 Ca^{2+} sparklet is capable of triggering a spark (Heping Cheng & Lederer, 2008). Therefore, it would be of great and tantalizing utility if $Ca_V1.2$ channels also undergo coupled gating like RyR2, given this quadratic dependence on $[Ca^{2+}]_{subspace}$ during EC coupling.

Even though CICR appears to be an extreme example of positive feedback, Ca^{2+} sparks cannot trigger sparks from neighboring CRUs in healthy cardiac myocytes. However, CICR is under local $[Ca^{2+}]_{subspace}$ control, and this lack of all-or-none behavior would appear to be a paradox given the large positive-feedback built into EC coupling (M. Cannell et al., 1995; Heping Cheng & Lederer, 2008; L.F. Santana et al., 1996). In his seminal work on CICR, Fabiato varied the strength of CICR by varying both the amplitude and the rate of applied $[Ca^{2+}]$, which would suggest that CICR is graded despite the large positive feedback built into the local control of EC coupling (Fabiato, 1985). There were early proponents of a parsimonious "common pool Ca^{2+}" model of EC coupling, which hypothesizes that trans-sarcolemmal Ca^{2+}

influx via $Ca_V1.2$ channels produce a homogeneous global $[Ca^{2+}]$, which then uniformly trigger all CRUs in a myocyte (Heping Cheng & Wang, 2002). However, even though a parsimonious model would appear to be fulfilling Occam's razor, both experimental and computer modeling evidences show that the "common pool" model is both unphysiological, and if it were true, would lead to highly unstable, all-or-none behavior in EC coupling (Heping Cheng & Wang, 2002; Stern, 1992). A global increase in $[Ca^{2+}]$, which Niggli and Lederer produced using flash photolysis of caged Ca^{2+}, is less effective than increase in local i_{Ca} at triggering the activation of CICR (Niggli & Lederer, 1990).

During diastole, we can observe isolated, spontaneous Ca^{2+} sparks, which occur due to the finite open probability of RyR2 at diastolic subspace $[Ca^{2+}]$ of 150 nmol/L, when I_{Ca} is practically nil (M. Cannell et al., 1995). This observation illustrates $Ca_V1.2$'s exclusive role in triggering global EC coupling, as most spontaneous Ca^{2+} sparks are inadequate to trigger CICR from the adjacent CRUs (H Cheng et al., 1993; Heping Cheng & Lederer, 2008). However, even though Parker and Wier found that the anatomy of EC coupling precludes Ca^{2+} sparks from "jumping" from one Z-line to the next, ~2 μm away, Izu et al. found that Ca^{2+} sparks are able to increase the local frequency of Ca^{2+} sparks through local $[Ca^{2+}]_{subspace}$ elevation, causing an apparent "coupling" between sparks, but this local positive-feedback is far from all-or-none (Izu, Bányász, Balke, & Chen-Izu, 2007; Parker & Wier, 1997). EC coupling gain is also a positive function of SR Ca^{2+} load (L F Santana, Kranias, & Lederer, 1997). Ca^{2+} spark triggered CICR occurs more frequently when SR Ca^{2+} is

overloaded, which causes RyR2 to become more sensitive to cytoplasmic [Ca^{2+}] via an unknown mechanism (Lukyanenko & Györke, 1999; Lukyanenko et al., 2001). Sometimes, when the extreme-positive feedback in these spark triggered CICR becomes self-renewing, the SR Ca^{2+} release propagate through the myocyte as Ca^{2+} waves (H Cheng et al., 1993; Heping Cheng & Lederer, 2008; Díaz, O'Neill, & Eisner, 2004).

Inactivation of $Ca_V1.2$ channels, by a combination of VDI and Ca^{2+}-dependent inactivation (CDI) mechanisms, terminates the global [Ca^{2+}] transient near the end of phase 2 of the cardiac AP. The mechanism of Ca^{2+} spark termination remains unclear, with evidence for either RyR2 inactivation via cisternal SR Ca^{2+} depletion or coupled gating (Heping Cheng & Lederer, 2008). There is conflicting evidence as to whether RyR2 themselves undergo CDI (Heping Cheng & Lederer, 2008). At the termination of EC coupling, after both influx of Ca^{2+} from extracellular space and Ca^{2+} released from the SR, the cardiac myocyte needs to restore Ca^{2+} homeostasis, returning to the resting [Ca^{2+}] in both the cytoplasm and the SR. Homeostasis is maintained within the cytoplasm and the SR compartments by active transport, using the energy of ATPs. The SR Ca^{2+} ATPase (SERCA) pumps Ca^{2+} into the SR, and it is responsible for recovering the Ca^{2+} released by the SR during EC coupling. Phospholamban (PLB) is an important regulator of SERCA, having a constitutive inhibitory effect on SERCA's function, unless phosphorylated (Hicks, Shigekawa, & Katz, 1979). Cardiac myocytes from PLB KO mice have larger SR Ca^{2+} load, which also increases the frequency and amplitude of Ca^{2+} sparks as these cells maintain

Ca^{2+} homeostasis at a different steady state level (L F Santana et al., 1997). The sarcolemmal sodium-calcium exchanger (NCX), extrudes extracellular Ca^{2+} that entered via $Ca_V1.2$ channels during EC coupling, and they operate at a stoichiometry of 3 Na^+:1 Ca^{2+} (Sipido, Volders, Vos, & Verdonck, 2002). Because it conducts a net inward depolarizing current, NCX can play an important role in arrhythmogenesis. When Ca^{2+} waves form during SR Ca^{2+} overload, the large depolarizing NCX current triggered by the Ca^{2+} waves can cause delayed afterdepolarizations (DADs), arrhythmogenic voltage fluctuations that prematurely depolarize a myocyte before the next systole, and they are associated with ventricular tachycardias (Sipido et al., 2002).

1.4.5 Local modulation of EC coupling by macromolecular complexes

The amplitude of the global $[Ca^{2+}]_i$ transient during EC coupling is not an all-or-none phenomenon such as the firing of an AP. Instead, the force of cardiac contraction is graded by the amplitude of the global $[Ca^{2+}]_i$ transient. This represents the mechanistic basis of a vital function of the heart: to match its pumping force to physiological needs.

The principal modulator of cardiac contractility in order to meet the body's metabolic demands and the environment is the sympathetic nervous system (SNS). The SNS is responsible for the fight-or-flight response, which increases cardiac output via both increases in contractility and heart rate. The catecholamines epinephrine, released

by the adrenal glands into the circulation, and norepinephrine, released locally by post-ganglionic sympathetic fibers, are the neurotransmitters of the SNS, and they bind to β-adrenergic receptors (βAR) (Y. Xiang & Kobilka, 2003; Xiao et al., 2004). ~75% of the βARs in cardiac myocytes are the β_1 isoform, with the rest belonging to the β_2 isoform (Xiao et al., 2006). Under normal physiology, βARs are heterotrimeric G-protein coupled receptors (GPCR), and both isoforms of βAR are normally coupled to G_s. Upon catecholamines binding to βAR, G_S becomes activated via the exchange of GTP for GDP in the $G\alpha_S$ subunit, which separates from the Gβγ subunit (Dai, Hall, & Hell, 2009). $G\alpha_S$ activates adenylate cyclases (AC) and the production of cyclic adenosine monophosphate (cAMP), a ubiquitous, freely diffusible second messenger molecule that in term activates PKA (Dai et al., 2009; Walsh, Perkins, & Krebs, 1968).

Both $Ca_V1.2$ and RyR2 channels are substrates for PKA during βAR stimulation. In $Ca_V1.2$ channels, serine-1928 in the carboxy-terminal is the only phosphorylation site for PKA (De Jongh et al., 1996). Phosphorylation of $Ca_V1.2$ by PKA causes a left shift in the current-voltage curve, which means that more channels are open at lower membrane potentials where the driving force for Ca^{2+} is higher, resulting in greater influx (Bean, Nowycky, & Tsien, 1984). On the single channel level, PKA phosphorylation promotes $Ca_V1.2$ to shift out of mode 0, where the channel is inactive, into mode 1, characterized by frequent short openings, and mode 2, characterized by long openings (Hess & Tsien, 1984). The ramification of greater open probability results in potentiation of the whole cell trans-sarcolemmal Ca^{2+}

current (I_{Ca}). In RyR2, serine-2808 is the phosphorylation site for PKA (Marx et al., 2000). Mice expressing a knock-in RyR2 with the S2808A substitution, which removes the PKA phosphorylation site, exhibit blunted fight-or-flight response (Shan et al., 2010). βAR stimulation in S2808A mice fails to elicit an increase in inotropy, or contractility, which shows that PKA phosphorylation of $Ca_V1.2$ and I_{Ca} potentiation are not sufficient for increasing the strength of EC coupling without RyR2 phosphorylation at S2808 (Shan et al., 2010). Whether S2808 phosphorylation contributes to the pathophysiology of heart failure and SCD is controversial, but a recent study by Zhang et al. found not evidence of S2808 hyperphosphorylation in mice after myocardial infarction (Marks, 2001; H. Zhang et al., 2012).

In cardiac myocytes, the A-kinase adaptor protein 79/150 (AKAP79/150), with AKAP79 being the human and AKAP150 being the murine ortholog, acts as a scaffold for PKA, localizing PKA to the locale of $Ca_V1.2$ channels (Coghlan et al., 1995; Nichols et al., 2010). AKAP79/150 associates with the carboxy-terminal of $Ca_V1.2$ via a leucine-zipper (LZ) domain (Nichols et al., 2010; Oliveria, Dell'Acqua, & Sather, 2007). *In vitro*, a recent study by Gold et al. using mass spectrometry finds that AKAP79/150 exists as dimers in complex with two PKA enzymes (Gold et al., 2011). AKAP79/150 targeting of PKA to couplons is directly responsible for EC coupling potentiation during βAR stimulation, with $AKAP150^{-/-}$ mice showing complete absence of EC coupling potentiation when βARs are stimulated with 100 nmol/L isoproterenol (ISO) (Nichols et al., 2010). Critically, in addition to its association with $Ca_V1.2$ channels, AKAP79/150 recruits a supramolecular signaling

complex involving βAR, AC5/6, and caveolin-3 (Nichols et al., 2010). Interestingly, AKAP150$^{-/-}$ mice still show I_{Ca} potentiation under βAR stimulation by 100 nmol/L ISO; however, the failure of this increase to translate into an increase in [Ca^{2+}] transient illustrates the necessity for the assemblage and colocalization of the components in this supramolecular complex built around AKAP79/150 in the βAR regulation of EC coupling (Nichols et al., 2010). The implication of this AKAP79/150 supramolecular signaling complex is that adrenergic signaling is locally targeted to couplons via $Ca_V1.2$, increasing the open probability of both $Ca_V1.2$ and RyR2 and the strength of local EC coupling. Although RyR2 has its own AKAP partner-mAKAP, which recruits an unique signaling complex containing PKA and PDE4D3, its role is primarily involved in regulating local [cAMP] and excitation-transcription coupling via the nuclear transcription factor NFAT (Bauman, Michel, Henson, Dodge-Kafka, & Kapiloff, 2007; Dodge et al., 2001)

While there are other AKAP proteins that associate with $Ca_V1.2$, and amongst them AKAP15/18 has also been proposed as an alternative candidate as the AKAP responsible for targeting βAR signaling to $Ca_V1.2$ channels and EC coupling during the fight-or-flight response (Fuller, Emrick, Sadilek, Scheuer, & Catterall, 2010; Mauban, O'Donnell, Warrier, Manni, & Bond, 2009; Tasken & Aandahl, 2004). In cultured HEK293 cells one can reconstitute a rudimentary flight-or-flight response with the heterologous expression βAR, AKAP15/18, and $Ca_V1.2$ (Fuller et al., 2010). Disruption of $Ca_V1.2$-AKAP15/18 interaction with a synthetic peptide mimicking the $Ca_V1.2$ C-terminal LZ domain inhibits βAR regulation of I_{Ca} in rat ventricular

myocytes exposed to 1 μmol/L ISO (Hulme, Lin, Westenbroek, Scheuer, & Catterall, 2003). However, the authors failed to demonstrate the effect, if any, of this peptide on EC coupling. Also, ISO at 1 μmol/L would saturate βARs and produce a supra-physiological amount of activation, which would remove the very necessity for spatial localization of cAMP-PKA signaling (De Arcangelis, Liu, Zhang, Soto, & Xiang, 2010). Therefore, the evidence supporting AKAP79/150 as being the primary AKAP responsible for fast, local βAR modulation of EC coupling, which is under local control, is stronger. However, AKAP15/18 plays other roles in global βAR mediated signaling in cardiac myocytes. Lygren et al. found that AKAP15/18 binds to PLN and colocalizes with SERCA and PLN in the SR membrane, and AKAP15/18 is responsible for targeting PKA for PLN phosphorylation (Lygren et al., 2007).

In addition to integrating adrenergic signaling, AKAP79/150 also acts as a scaffold for protein kinase C (PKCα) and the phosphatase calcineurin (PP2B) (Gao et al., 1997; Klauck et al., 1996; Luis F. Santana & Navedo, 2010). Both PKCα and PP2B are activated by [Ca^{2+}] elevation produced by $Ca_V1.2$ Ca^{2+} sparklets (Scott & Santana, 2010). Recently, a study from our group showed that PKCα phosphorylation causes persistent $Ca_V1.2$ openings at -70 mV in arterial myocytes (Navedo et al., 2005; Luis F. Santana & Navedo, 2010). In fact, previous studies of $Ca_V1.2$ Ca^{2+} sparklets from our group using Total Internal Reflection Fluorescence (TIRF) microscopy in neonatal cardiac myocytes, arterial myocytes, and tsA-201 cells show that $Ca_V1.2$ activity is highly spatially heterogeneous, and AKAP79/150 is necessary and sufficient in establishing this spatial heterogeneity (Navedo et al.,

2005; Luis F. Santana & Navedo, 2010). This finding reveals the advantage of Ca^{2+} sparklets, an optical technique, versus traditional cell-attached surface recordings of single-channel $Ca_V1.2$ current (i_{Ca}), when technically feasible. TIRF microscopy can visualize a large footprint of the cell membrane and simultaneously monitor the activity of $Ca_V1.2$ channels across space. In contrast to kinases like PKA and PKCα, whose activity is directed at the $Ca_V1.2$ channel itself, PP2B plays a significant role in excitation-transcription (ET) coupling (Rossow et al., 2009; Scott & Santana, 2010). Under chronic βAR stimulation, PP2B dephosphorylate NFAT, a transcription factor, which causes the reduction of I_{to} current gradient across the left ventricular wall (Rossow et al., 2009). In addition to its role in modulating EC coupling, the signaling complex constructed around AKAP79/150 plays a critical role in establishing spatial heterogeneity of $Ca_V1.2$ activity and ET coupling.

1.5 Timothy syndrome (LQT8)-a congenital disease of arrhythmias

Cardiac arrhythmia is a pathologically disturbed heart rhythm that is not normal sinus rhythm, properly conducted through the AV node and the His-Purkinje system. Cardiac arrhythmia is the leading cause of death in patients with heart failure and acutely after a myocardial infarction (Zachariah et al., 2011). Every year, 300,000-400,000 die from SCD in the United States (Rubart & Zipes, 2005). While the pathophysiology of arrhythmias is multifactorial, all arrhythmia fundamentally arise from disorders in the ionic currents that shape the cardiac action potential.

Arrhythmias can be divided into three classes based on their mechanism: automaticity, triggered activity, or reentry (Rubart & Zipes, 2005). Automaticity arises when an ectopic focus in either the AV node or the His-Purkinje system takes over pacemaking from the SA node. Triggered activity is caused by abnormal foci of automaticity, when clusters of rogue myocytes undergo synchronized early afterdepolarizations (EADs) or delayed afterdepolarizations (DADs) (Michael Rubart & Zipes, 2005; Sato et al., 2009; Weiss, Nivala, Garfinkel, & Qu, 2011). As illustrated in Figure 1.4, afterdepolarizations are abnormal depolarizations during the cardiac AP, with EADs occurring during phase 2 or 3, and DADs occurring during phase 4 of the cardiac AP.

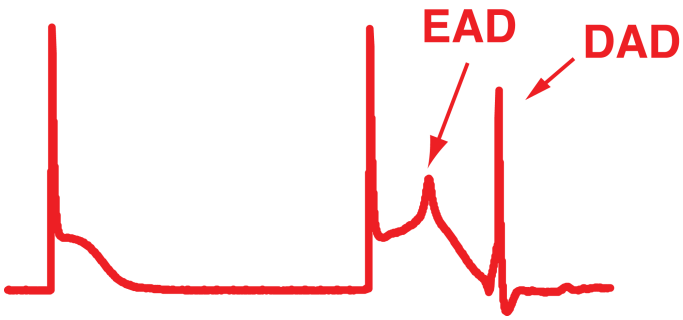

Figure 1.4. Exemplar AP trace showing an EAD and a DAD.

DAD is caused by spontaneous Ca^{2+} release, often in the form of Ca^{2+} waves during SR Ca^{2+} overload (Michael Rubart & Zipes, 2005; Sipido et al., 2002; Weiss et al., 2011). In addition to the previously stated mechanism of EAD being caused by $Ca_V1.2$ channels reactivating during prolonged APD, EAD can also be caused by spontaneous SR Ca^{2+} release, just like DAD (Choi, Burton, & Salama, 2002; Michael

Rubart & Zipes, 2005). A classic example of triggered activity is polymorphic ventricular tachycardia, or Torsades de Pointes (TdP), French for “ribbon of points,” describing the apparent twisting of the QRS axis on an ECG rhythm strip, and it can be a serious sequela of prolonged QT interval (Michael Rubart & Zipes, 2008; Sato et al., 2009). Reentry results from aberrant or blocked conduction of the depolarization wavefront through the myocardium, creating an island of unexcited myocardium, which becomes excited and conduct a retrograde depolarization wavelet once the main front has bypassed it (Michael Rubart & Zipes, 2008). The backward propagation wavelet can start a rotating, hurricane like, spiral wave of depolarization. Reentry is caused by variations in refractoriness across the myocardium, marked by ECG T-wave alternans (Michael Rubart & Zipes, 2005) While often caused by myocardial injury, dispersion in refractoriness is also associated with spontaneous SR Ca^{2+} release and EAD (Huffaker, Lamp, Weiss, & Kogan, 2004; Michael Rubart & Zipes, 2005). A very deadly example of a reentry arrhythmia is ventricular fibrillation, which requires immediate defibrillation, which is the delivery of electrical shock in an attempt to restore sinus rhythm in patients (Michael Rubart & Zipes, 2008).

Congenital long QT syndromes are of great interest to cardiac physiology because many are caused by channelopathies, which are congenital ion channel disturbances (Kaufman, 2009). In long QT syndromes, the mutations either reduce repolarizing K^+ currents or increase depolarizing Na^+ and Ca^{2+} currents. Channelopathies allow us insights into how disturbances to the ionic currents in a

cardiac myocyte can lead to abnormal EC coupling and arrhythmogenesis, with the potential that these pathophysiologic mechanisms also play roles in acquired diseases that have increased incidence of arrhythmias, such as heart failure. Long QT syndromes are characterized by the ECG QT interval prolongation and greatly elevated risks of syncope and SCD from TdP (Kaufman, 2009). Table 1.2 lists the known congenital long QT syndromes and their associated mutations (Kaufman, 2009).

Type	Locus	Gene	Protein	Function	Frequency
LQT1	11p15.5	KCNQ1	$K_V7.1$ α	I_{Ks} ↑	30-35%
LQT2	7q35	KCNH2	$K_V11.1$ α	I_{Kr} ↓	25-30%
LQT3	3p21	SCN5A	$Na_V1.5$ α	I_{Na} ↓	5-10%
LQT4	4q25	ANK2	Ankyrin- β	$I_{Na\,K}$ ↓ I_{NCX} ↓	1-2%
LQT5	21q22.1	KCNE1	minK β	I_{Ks} ↓	RARE
LQT6	21q22.1	KCNE2	MiRP1 β	I_{Kr} ↓	RARE
LQT7*	17q23	KCNJ2	$K_{ir}2.1$ α	I_{K1} ↓	RARE
LQT8**	12p13.3	CANA1C	$Ca_V1.2$ α1c	$I_{Ca,L}$ ↑	RARE
LQT9	3p25	CAV3	Caveolin-3	I_{Na} ↑	RARE
LQT10	11q23	SCN4B	$Na_V1.5$ β4	I_{Na} ↑	RARE
LQT11	7q21	AKAP9	Yotiao	I_{Ks} ↓	RARE
LQT12	20q11.2	SNTA1	A-dystrophin	I_{Na} ↑	RARE
***Andersen-Tawil syndrome **Timothy syndrome**					

Table 1.2. Congenital long QT syndromes and their genetic basis

Characterized by a greatly increased risk for fatal arrhythmias, Timothy syndrome (TS) is the long QT syndrome type 8 (LQT8) identified in humans (Splawski et al., 2004). In addition to being a long QT syndrome, TS also causes disorders in multiple organ systems, including congenital heart disease, cardiomegaly,

syndactylyl, facial dysmorphia, immune deficiency, intermittent hypoglycemia, and neurological disorders such as autism spectrum disorder (ASD) and cognitive deficits (Splawski et al., 2004). A case report from Reichenbach et al., first identified the spectrum of symptoms associated with TS clinically in 1992, and in 2004 Splawski et al. identified its genetic etiology-a point mutation in exon 8A of the CACNA1C gene encoding the human $Ca_V1.2$ channel (Reichenbach, Meister, & Theile, 1992; Splawski et al., 2004). Half of known TS patients have died by the age of ~2.5 years (Splawski et al., 2004). Because of the autosomal dominant nature of the TS mutation and lethality before reaching reproductive maturity, most documented cases of TS have been *de novo* mutations, with the exception of cases where a parent is mosaic for TS (Splawski et al., 2004). The multisystem nature of TS gives us insight into the importance of $Ca_V1.2$ channels in development and ET coupling, in addition to its primary role in EC coupling in the cardiac system. In fact, the ASD associated with TS is of great interest to neurophysiologists seeking a disease model to help us understand autism (Bader et al., 2011). The severity of the TS phenotype, though highly unfortunate for those afflicted, gives us a model system to study how increased $Ca_V1.2$ activity contributes to the pathophysiology of arrhythmogenesis.

TS is caused by the G1216A point mutation in exon 8A of the CACNA1C gene that encodes the human L-type $Ca_V1.2$ calcium channel, which causes a glycine to arginine substitution in position 406 (G406R) located on the cytoplasmic side of IS6 (Splawski et al., 2004). Exon 8A is an alternatively spliced form of exon 8, and they

are mutually exclusive (Splawski et al., 2005). 20% of cardiac $Ca_V1.2$ mRNA contains exon 8A. A variant of TS, found in two individuals, has the identical G406R mutation in exon 8, and they exhibited more severe symptoms, presumably due to a dose dependent effect of the mutation (Splawski et al., 2005). The cytoplasmic loop linking DI and DII (I-II loop) plays an important role in inactivation, possibly acting as the inactivating "lid" in $Ca_V1.2$ channels during VDI, and the G406R substitution indeed causes a dominant, gain-of-function mutation that significantly delays open state VDI in $Ca_V1.2$ channels (Splawski et al., 2004; Tadross & Yue, 2010). In computer simulations using the Luo-Rudy model of the cardiac myocyte, impaired VDI in TS produces prolonged APD (Splawski et al., 2004; Faber et al., 2007). When the ratio of repolarizing to depolarizing current is decreased in cardiac myocytes, as in TS, the arrhythmogenic voltage fluctuations EAD can occur during the plateau phase (phase II) of the cardiac AP (Sato et al., 2009). In whole heart preparations, EAD leads to TdP and ventricular fibrillation (VF) (Sato et al., 2009).

While it is clear that VDI is impaired in TS, TS may have effects on calcium dependent inactivation (CDI) and deactivation as well (Raybaud et al., 2006; Barrett and Tsien, 2008; and Yarotskyy et al., 2009). Different reports disagree over the effect of TS on CDI, with Raybaud et al. reporting slower CDI by comparing the effect of non-functional $CaM_{1,2,3,4}$ on inactivation (Raybaud et al., 2006). However, others report slightly enhanced CDI by comparing the fraction of whole-cell current that is inactivated with either Ba^{2+} or Ca^{2+} as the charge carrier (Barrett and Tsien, 2008; Yarotskyy et al., 2009). This disagreement is not surprising, given that CDI is

modulated by the binding of CaM to the IQ domain on the C-terminus, producing an allosteric effect on inactivation, instead of direct modulation on the I-II loop hinged lid (Tadross et al., 2010). On the other hand, deactivation, the return of the S6 gate to the closed conformation, is significantly slowed down in TS, which is illustrated by the exaggerated tail currents following repolarization to resting potential in HEK293 cells transfected with $Ca_V1.2$-TS (Yarotskyy et al., 2009). In computer simulations, the delayed deactivation caused by TS causes prolongs APD, which is arrhythmogenic (Yarotskyy et al., 2009).

While the effect of the G406R mutation on the whole cell Ca^{2+} current is well-established, the specific mechanism of how the G406R mutation affects inactivation in $Ca_V1.2$ warrants further investigation. By using mass-spectroscopy analysis of synthetic peptide fragments with sequence corresponding to the region around the TS mutation in the I-II loop, exposed *in vitro* to CaMKII, the G406R mutation creates a phosphorylation site for CaMKII at serine-409 (S409) (Erxleben et al., 2006). CaMKII, which is activated by CaM under elevated $[Ca^{2+}]$ and becomes autocatalytic, plays a physiologically important role in the positive feedback phenomenon of I_{Ca} use-dependent potentiation known as facilitation (Couchonnal & Anderson, 2008). Unlike either PKA or PKC, CaMKII does not require AKAP79/150 to act as its scaffold for localization to $Ca_V1.2$, but instead it directly associates with the β subunit (Abiria & Colbran, 2010; Couchonnal & Anderson, 2008). Therefore, the positive feedback effect of CaMKII phosphorylation would be logically consistent with the pathophysiology of TS, where VDI delay results in an increase in I_{Ca}.

Furthermore, single-channel patch-clamp recordings of $Ca_V1.2$-TS expressed in HEK293 cells show an increase in mode 2 gating activity, characterized by frequent and prolonged openings seen in single channel records (Erxleben et al., 2006). The CaMKII antagonist KN-62 abolishes this increase in mode 2 gating at 5 μmol/L; however, the authors of the study failed to demonstrate that KN-62 correct the kinetics of delayed VDI on whole-cell currents, which should be expected if an increase in mode 2 gating due to CaMKII phosphorylation were solely responsible for delayed VDI in TS (Erxleben et al., 2006).

To further investigate the role of CaMKII phosphorylation in TS, another study by Thiel et al. in cultured rat ventricular myocytes, lentiviral transfection with $Ca_V1.2$-TS channels significantly prolongs APD and shows increased I_{Ca} facilitation with repeat stimulation, and these effects are abolished by 5 μmol/L KN-62 (Thiel et al., 2008). However, the increases in mode 2 gating activity and I_{Ca} facilitation by CaMKII are mechanistically distinct from VDI impairment, as the study by Yarotskyy et al. shows that the G406R/S409A double mutation fails to abolish G406R's effect on VDI in transfected HEK293 cells (Tadross & Yue, 2010; Viktor Yarotskyy, Gao, Peterson, & Elmslie, 2009). Until the study on the role of AKAP79/150 in the mechanism of TS that I present as Chapter 3 of this dissertation, the only intervention that has any effect on partially restoring WT-like inactivation in $Ca_V1.2$-TS is roscovitine, a tri-substituted purine cyclin-kinase inhibitor (V Yarotskyy & Elmslie, 2007). Roscovitine at 100 μmol/L enhances open state VDI and delays activation in heterologously expressed $Ca_V1.2$ channels (V Yarotskyy & Elmslie, 2007).

TS is of great interest to the field of induced pluripotent stem cells (iPSCs) because of the multisystemic pathology that it exhibits. Cardiac myocytes differentiated from iPSCs generated by the Dolmetsch Group from dermal fibroblasts of TS patients exhibit APD prolongation, arrhythmogenic voltage perturbations, and irregular EC coupling (Yazawa et al., 2011). Roscovitine at 33 μmol/L is able to decrease EC coupling irregularity, VDI prolongation, and APD prolongation; however, in contrast to the authors claim of rescue using roscovitine, it fails to restore fully rescue WT-like VDI kinetics (Yazawa et al., 2011). The same group has also differentiated cortical neurons from TS iPSCs, and these neurons exhibit defective Ca^{2+} signaling and gene transcription (Pasca et al., 2011). These findings could be the mechanistic basis for the behavioral impairments reported in a recent report on a TS mouse model for ASD (Bader et al., 2011). The effect of defective $Ca_V1.2$ dependent ET coupling plays an important role in the pathogenesis of ASD and other neurological deficits in TS.

The existing literature on TS is rather narrowly focused on the mutation's phenotype with respect to delayed inactivation of the $Ca_V1.2$ channel. I believe that they do not provide a clear and conclusive mechanism of how the G406R mutation causes this phenotype of delayed inactivation. Current literature also does not offer an animal model of how the gain-of-function mutation leads to arrhythmogenesis. Based on our group's past studies on the spatial heterogeneity in Ca^{2+} sparklet activity, we tested the hypothesis that $Ca_V1.2$ channels undergo a novel AKAP79/150-facilitated

coupled gating modality that becomes more frequent due to the TS mutation, which is presented as Chapter 2 in this study. In Chapter 3 we further tested the hypothesis that increase in AKAP79/150 dependent coupled gating activity plays a critical role in arrhythmogenesis in TS/LQT8. In summary, in the studies that I am presenting as Chapters 2 and 3 of this dissertation, I demonstrate evidence from the resolution of single $Ca_V1.2$ channel up to a mouse model of LQT8, that $Ca_V1.2$ channels undergo an AKAP79/150 dependent coupled gating modality that is significantly elevated in TS, leading to arrhythmogenesis.

1.6 Specific aims

1.6.1 Aim 1

To test the hypothesis that the Timothy syndrome (LQT8) mutation causes higher coupled gating frequency in both tsA-201 cells and ventricular myocytes.

I use a $Ca_V1.2$-LQT8 transgenic mouse model to study the effects of the TS mutation *in situ.* Because TS is an autosomally dominant condition, there is no need to knock-in the mutant TS CACNA1C construct, and a transgenic mouse model is used in this study (Splawski et al., 2004). The *trans* $Ca_V1.2$-LQT8 channels are labeled with a red fluorescent tagRFP® protein. As in previous studies using arterial myocytes and tsA-201 cells, Ca^{2+} sparklets will be detected in tsA-201 cells transiently expressing $Ca_V1.2$-LQT8 channels expressed in the LQT8 mouse, dialyzed with Fluo-5F and voltage clamped at -70 mV using total internal reflection fluorescence (TIRF) microscopy (Navedo et al., 2007, 2006, 2005). The lack of transverse tubules is critical for our ability to visualize Ca^{2+} sparklets using TIRF microscopy. I also record cell-attached patch clamp current records from adult ventricular myocytes from both WT and LQT8 mice, as electrophysiology remains the “gold standard” for the study of ion channels. I analyze the degree of coupled gating from sparklet recordings and cell-attached patch clamp current records using a lumped parameter Markov chain model that was previously used to test for

coupled gating in ligand-gated GABA channels (Chung & Kennedy, 1996). I expect that in LQT8 ventricular myocytes, there is increased Ca^{2+} sparklet activity and coupled gating frequency would correlate.

1.6.2 Aim 2

To test the hypothesis that coupled $Ca_V1.2$-LQT8 channels correlate with foci of increased Ca^{2+} spark frequency.

I test the effects of the presence of $Ca_V1.2$-LQT8 channels on EC coupling, specifically if the increased Ca^{2+} influx that I expect from coupled gating would lead to larger EC coupling gain. I record Ca^{2+} sparks from LQT8 and WT cardiac myocytes loaded with fluo-4-AM Ca^{2+} indicator using swept field confocal microscopy. Spark sites are detected using custom software written in the IDL language as previously described (Navedo et al., 2006). Colocalization of Ca^{2+} spark and wave sites with tRFP tagged $Ca_V1.2$-LQT8 channels are analyzed using the ImageJ software (Bolte & Cordelières, 2006).

I expect to see sites of increased spark frequency to spatially correlate with clusters of $Ca_V1.2$-LQT8 channels due to the dependence of spark frequency on the square of local $[Ca^{2+}]$ (Heping Cheng & Lederer, 2008; L.F. Santana et al., 1996).

1.6.3 Aim 3

To test the hypothesis that the Timothy syndrome (LQT8) mutation leads to an increased frequency of arrhythmogenic voltage fluctuations and increased incidence of cardiac arrhythmias in the LQT8 transgenic mice.

I test the hypothesis that the TS mutation leads to an increased frequency of arrhythmogenic fluctuations by recording action potentials (APs) from ventricular cardiac myocytes isolated from the LQT8 mice and their littermates. APs are stimulated under current clamp by brief depolarizing pulses given at 1 Hz. I expect LQT8 cardiac myocytes to have increased action potential duration (APD), which has been linked to arrhythmias (23). I also expect LQT8 ventricular myocytes to have more frequent arrhythmogenic early afterdepolarizations (EADs) and delayed afterdepolarizations (DADs).

I want to test the hypothesis that the TS mutation will lead to increased incidence of cardiac arrhythmias in the LQT8 transgenic mice by surgically implanting ECG telemetry transmitters into both our transgenic LQT8 and WT littermate mice. I induce arrhythmias by exercising the mice on a treadmill equipped with an electric shocker. I expect to see higher frequency of arrhythmic events in the LQT8 transgenic mice when compared to their littermates.

Chapter 2: Increased coupled gating of L-type Ca^{2+} channels during hypertension and Timothy syndrome

2.1 Summary

L-type ($Ca_V1.2$) Ca^{2+} channels are critical regulators of muscle and neural function. Although in previous studies from our group, we found that $Ca_V1.2$ channel activity varies regionally through a PKCα and AKAP79/150 dependent mechanism. Based on our previous observation in a subpopulation of our Ca^{2+} sparklet recordings that a variable number (2 to 6) of $Ca_V1.2$ channels appeared to open and close concertedly in a transient fashion, we wanted test the hypothesis that $Ca_V1.2$ channels can gate coordinately. We used optical and electrophysiological approaches to record $Ca_V1.2$ channel activity in cardiac, smooth muscle, and tsA-201 cells expressing $Ca_V1.2$ channels. Consistent with our hypothesis, we found that small clusters of $Ca_V1.2$ channels can open and close in tandem. FRET and electrophysiological studies suggest that this coupling of $Ca_V1.2$ channels involves transient interactions between neighboring channels via their C-termini. The frequency of coupled gating events increases in hypertensive smooth muscle and in cells expressing a mutant $Ca_V1.2$ channel that causes arrhythmias and autism in humans with Timothy syndrome (LQT8). In conclusion, we propose that coupled gating of $Ca_V1.2$

channels may represent a novel mechanism for the regulation of Ca^{2+} influx and excitability in neurons, cardiac, and arterial smooth muscle under physiological and pathological conditions.

2.1.1 Abbreviations

AKAP150 = A-kinase anchoring protein 150
CaM = calmodulin
CaMKII = Ca^{2+}/calmodulin-dependent kinase II
EGFP = enhanced green fluorescent protein
FRET = fluorescence resonance energy transfer
jSR = junctional sarcoplasmic reticulum
PDBu = phorbol 12,13-dibutyrate
PKCα = protein kinase C α
RyR = ryanodine receptor
SR = sarcoplasmic reticulum
TS = Timothy syndrome
tRFP = tag red fluorescent protein
TIRF = total internal reflection fluorescence
WT = wild type

2.2 Introduction

Voltage-gated L-type ($Ca_V1.2$) Ca^{2+} channels are expressed in the surface membrane of many different types of excitable cells, including neurons and muscle cells, where they regulate multiple processes including excitability, contraction, gene expression, and memory storage (M. Cannell, Berlin, & Lederer, 1987; Fourcaudot et al., 2009; Gomez-Ospina, Tsuruta, Barreto-Chang, Hu, & Dolmetsch, 2006; Marrion & Tavalin, 1998). As introduced in Chapter 1, recent studies revealed an unexpected feature of $Ca_V1.2$ channels: their activity (i.e. open probability, P_o) varies within the cell membrane (Navedo et al., 2006, 2005; Tour et al., 2007). Low activity $Ca_V1.2$ channels open randomly and infrequently at rest, producing brief elevations in intracellular Ca^{2+} concentration ($[Ca^{2+}]_i$) called "Ca^{2+} sparklets" (S.-Q. Wang et al., 2001). In contrast, small clusters of $Ca_V1.2$ channels can function in a high open probability mode that generates localized zones of relatively high Ca^{2+} influx ("persistent Ca^{2+} sparklets"). In a subpopulation of our Ca^{2+} sparklet records, we also observed concerted openings and closings of groups of $Ca_V1.2$ channels producing $[Ca^{2+}]$ change corresponding to that produced by 2 to 6 adjacent $Ca_V1.2$ channels on the cell membrane. Recall that a previous study by Marx et al. introduced in Chapter 1 demonstrated that RyR2s within a CRU undergo coupled gating, which is a mechanistic basis for the fidelity and the large positive feedback inherent in EC coupling (Marx et al., 2001). Another recent study by Inoue and Bridge, also previously introduced, showed that the opening of a single $Ca_V1.2$

channel during the plateau phase of the cardiac AP under physiological extracellular [Ca^{2+}] (2 mmol/L) is not sufficient to pass the threshold for activating a Ca^{2+} spark (Inoue & Bridge, 2003). These findings combined with our observation of concerted gating events in a subpopulation of Ca^{2+} sparklet records, lead us to hypothesize that $Ca_V1.2$ channels also undergo coupled gating during EC coupling.

Although targeting of PKCα to the surface membrane by the kinase anchoring protein AKAP150 (the rodent ortholog of human AKAP79) increases the probability of persistent $Ca_V1.2$ channel activity, the mechanisms by which small clusters of these channels open concertedly are unknown (Navedo et al., 2008). Interestingly, as was introduced in-depth in Chapter 1, a recent study also discovered a gain-of-function mutation (G406R) in $Ca_V1.2$ that causes a multisystem disorder called Timothy syndrome, or long QT syndrome type 8 (LQT8) because of the cardiac phenotype of prolonged QT intervals and greatly increased incidence of lethal arrhythmias (Splawski et al., 2004). The mutation putatively creates a phosphorylation site for CaMKII, and phosphorylation of these $Ca_V1.2$-TS channels promote these channels to go into mode 2 gating, which we found to be highly analogous to the role PKCα plays in persistent $Ca_V1.2$ channel activity (Erxleben et al., 2006). Here, we employed FRET approaches with optical and electrophysiological recordings of Ca^{2+} influx via $Ca_V1.2$ channels to investigate this important issue. Our data indicate that activators of PKCα, calmodulin antagonists, or a specific $Ca_V1.2$ channel mutation that causes arrhythmias and autism in humans with the Timothy syndrome (LQT8) move the ubiquitous Ca^{2+}-binding

protein calmodulin from the IQ domain in the C-terminal tail of the channel. This induces functional interactions between nearby $Ca_V1.2$ channel via their C-termini that could lead to coupled gating of these channels.

2.3 Materials and Methods

2.3.1 Isolation of arterial and adult and neonatal cardiac myocytes

Mice and rats were euthanized as approved by the University of Washington Institutional Animal Care and Use Committee. Adult arterial myocytes and neonatal cardiac myocytes were prepared as described previously (Devic, Xiang, Gould, & Kobilka, 2001; Navedo et al., 2006).

Mice (PKCα$^{-/-}$, AKAP150$^{-/-}$, and corresponding wild type littermates) and Sprague Dawley (SD) rats were euthanized with a lethal dose of sodium pentobarbital as approved by the University of Washington Institutional Animal Care and Use Committee. Spontaneously beating neonatal cardiac myocytes were prepared from hearts of 1–2 day old mouse pups as described previously (Devic et al., 2001). Arterial myocytes were prepared from freshly dissected basilar, middle and posterior cerebral arteries as described in detail elsewhere (Navedo et al., 2006).

2.3.2 $Ca_V1.2$ and CaM constructs and their expression in tsA cells

Plasmids encoding the pore forming subunit of the wild type (WT) dihydropyridine-sensitive, voltage-gated Ca^{2+} channel pore-forming and accessory subunits (rabbit

and mouse $Ca_V1.2$ (α_{1c}), Ca_V-β_3 and Ca_V-$\alpha_2\delta_1$) were provided by Dr. Diane Lipscombe. We generated the rabbit homolog of the human Timothy syndrome $Ca_V1.2$ (G436R, Rabbit; G406R Human) (Erxleben et al., 2006). The $Ca_V1.2$ mutant with a stop codon at amino acid 1670 (CaV1.2Δ1670X) and calmodulin (CaM) were kindly provided by Dr. David T. Yue. Plasmids for the enhanced green fluorescent protein (EGFP) and the tag-RFP® (tRFP) were purchased from Invitrogen and Evrogen, respectively. We chose tRFP specifically for its relative brightness when compared to other red fluorescent proteins and its inability to dimerize (Merzlyak et al., 2007). tRFP and EGFP were fused to the C-tail of $Ca_V1.2$ and $Ca_V1.2$-TS, yielding $Ca_V1.2$-TS-tRFP, $Ca_V1.2$-TS-EGFP, $Ca_V1.2$-tRFP, and $Ca_V1.2$-EGFP. For experiments examining CaM association with the IQ domain in the C-terminal of WT $Ca_V1.2$ via FRET, we used a $Ca_V1.2$ channels with a C-tail truncated just after the IQ site without stop codon and tagged with EGFP as described previously (Erickson, Alseikhan, Peterson, & Yue, 2001). The CaM-tRFP construct was generated by PCR amplification of rat CaM cDNA followed by fusion to the carboxyl terminus of the tRFP. tsA-201 cells were cultured in Dulbecco's Modified Eagle Medium supplemented with 10% fetal bovine serum, L-glutamine (2 mmol/L), and a 1% streptomycin and penicillin solution. Cells were transiently transfected with using JetPEI. Successfully transfected cells were identified on the basis of EGFP or tRFP fluorescence.

2.3.3 Inducible PKCα translocation

A rapamycin-induced PKCα translocation system similar to the one developed by Liberles *et al* and Suh *et al* was developed for some of the experiments included in this study (Liberles, Diver, Austin, & Schreiber, 1997; Suh, Inoue, Meyer, & Hille, 2006). The system requires the expression of a FKBP12-rapamycin-binding element (FRB) that is anchored to the plasma membrane via the myristoylation and palmitoylation modification sequence Lyn_{11}. It also expresses PKCα fused to the enhanced green fluorescent protein and a FK506 binding protein. Application of rapamycin promoted heterodimerization of protein domains from FKBP-PKCα-EGFP and the membrane anchored FRB. This recruited FKBP-PKCα-EGFP to the membrane from the cytosol upon addition of rapamycin.

The membrane anchored Lyn11-FRB and CFP-FKBP vectors were obtained from Agilent Technologies. Mouse PKCα cDNA (kindly provided by Dr. John Exton) was amplified and fused to the carboxyl terminus of EGFP in pEGFP-C2 vector. Then, FKBP was PCR amplified from CFP-FKBP vector and inserted in the middle of EGFP and PKCα within the correct reading frame. EGFP-FKBP-PKCα fragment was then PCR amplified and sub-cloned downstream of IRES in pIRES vector. Finally, membrane-anchored Lyn11-FRB was PCR amplified from Lyn11-FRB vector and inserted upstream of IRES to obtain the final Lyn11-FRB-pIRES-EGFP-FKBP-PKCα construct. We transfected tsA-201 cells with this construct and the calcium

channel subunits using JetPEI. For those experiments involving neonatal myocytes, an adenovirus vector delivering Lyn11-FRB-pIRES -EGFP-FKBP-PKCα was generated. To do this, the 4.2 kb Lyn11-FRB-IRES-EGFP-FKBP-PKCα fragment was amplified and subcloned into pENTR 1A (Invitrogen) vector using Quick PCR Cloning Kit (BPS Bioscience). Then the target sequence was recombined into adenoviral expression vector pAd/CMV/V5-DEST. The adenoviral expression clone was digested with Pac I and purified using phenol-chloroform extraction followed by ethanol precipitation. We used 1 μg of Pac I-digested plasmid DNA to transfect 293A producer cell line using jetPEI DNA transfection reagent. Crude viral lysate was harvested 2 days after transfection. The adenoviral construct was amplified by infecting 293A producer cells using 100 μl crude lysate. Virus lysate was harvested 2 days later and stored in -80°C. A 500 μL of virus lysate was used to transduce mouse neonatal myocytes. Transgene expression was detected 2 days after infection.

2.3.4 Electrophysiology

Membrane potential was controlled using the whole-cell configuration of the patch-clamp technique using a HEKA EPC10 amplifier. Cells were patched in the presence of a solution with the following constituents (mmol/L): 140 NaCl, 5 $CsCl_2$, 2 $CaCl_2$, 1 $MgCl_2$, 10 glucose, 10 HEPES adjusted to pH 7.4. Once a GΩ seal was formed and successful conversion to whole-cell patch-clamp configuration was achieved, this

solution was exchanged for a solution containing a similar composition except that it had no Na^+, $CaCl_2$ was 20 mmol/L and NMDG concentration was 120 nmol/L. Pipettes for whole-cell patch-clamp experiments were filled with a solution containing (in mmol/L): 87 Cs-aspartate, 20 CsCl, 1 $MgCl_2$, 5 MgATP, 10 EGTA, 10 HEPES, and 0.2 Fluo-5F or Rhod-2 adjusted to pH 7.2 with CsOH. All experiments were performed at room temperature (22-25^{o}C).

We recorded L-type Ca^{2+} channel currents from cell-attached patches from neonatal ventricular myocytes and tsA-201 cells expressing WT $Ca_V1.2$ and $Ca_V1.2$-TS channels. The patch pipette solution contained 20 mmol/LM Ca^{2+} (charge carrier), 10 µmol/L tetrodotoxin (TTX), 130 mmol/L TEA^+ and no Na^+ or K^+ to eliminate Na^+ and K^+ channel currents (pH = 7.2). The L-type Ca^{2+} channel opener BayK-8644 (500 nmol/L) was included in the pipette solution to increase the mean open time and open probability (P_o) of these channels. With this solution, patch pipette resistances ranged from 4-5 MΩ. Currents were recorded while cells were exposed to a solution containing 145 mmol/L KCl, 10 mmol/L HEPES, and 10 mmol/L NaCl (pH = 7.4). L-type Ca^{2+} channel currents were evoked by a 2 s step depolarization to -30 mV from the holding potential of -80 mV. In some experiments, a modified patch-pipette including the L-type Ca^{2+} channel blocker nifedipine (10 µmol/L) was used. Inward Ca^{2+} currents were never recorded in the presence of nifedipine, indicating that L-type Ca^{2+} channels produced the currents recorded at -30 mV. Membrane currents were recorded and analyzed using pCLAMP 9 software.

2.3.5 TIRF and confocal microscopy

Ca^{2+} sparklet images were acquired using a through-the-lens TIRF microscope built around an inverted Olympus IX-71 microscope equipped with an Olympus PlanApo (60X, NA = 1.45) oil-immersion lens and an Andor iXON 597 EMCCD camera. Images were acquired at 100-200 Hz using TILL Image software. To monitor $[Ca^{2+}]_i$, cells were loaded with the calcium indicators fluo-5F or rhod-2. Rhod-2 was used in all experiments in which the enhanced green fluorescent protein was expressed. Excitation of fluo-5F and rhod-2 was achieved with 491 or 563 nm solid state lasers. Excitation and emission light was separated with the appropriate set of filters. Ca^{2+} sparklets were recorded in cells exposed to 1 μmol/L thapsigargin to eliminate Ca^{2+} release from intracellular stores.

Background-subtracted fluorescence signals were converted to concentration units using the "F_{max}" equation (Maravall, Mainen, Sabatini, & Svoboda, 2000):

$$\left[Ca^{2+}\right] = K_d \frac{F/F_{\max} - 1/R_f}{1 - F/F_{\max}},$$

where F is fluorescence, F_{max} is the fluorescence intensity of fluo-5F or rhod-2 in the presence of a saturating free Ca^{2+} concentration; K_d is the dissociation constant of

the fluorescence indicator used (fluo-5F = 1100 nmol/L; rhod-2 = 600 nmol/L); and R_f (fluo-5F = 210; rhod-2 = 150) is this indicator's F_{max}/F_{min}. F_{min} is the fluorescence intensity of fluo-5F or rhod-2 in a solution where the Ca^{2+} concentration is 0. K_d and R_f values for Fluo-5F and rhod-2 were determined *in vitro* using standard methods (Woodruff et al., 2002). F_{max} was determined at the end of experiments by exposing cells to a solution to which the Ca^{2+} ionophore ionomycin (10 mmol/L) and 20 mmol/L external Ca^{2+} had been added.

Ca^{2+} sparklets were detected and defined for analysis using an automated algorithm written in IDL language. Ca^{2+} sparklets had an amplitude equal to or larger than the mean basal $[Ca^{2+}]_i$ plus three times its standard deviation. For a $[Ca^{2+}]_i$ elevation to be considered a sparklet, a grid of 3 X 3 contiguous pixels had a $[Ca^{2+}]_i$ value at or above the amplitude threshold. These detection criteria for Ca^{2+} sparklets are similar to those used by other investigators (Heping Cheng et al., 1999; Demuro & Parker, 2004, 2005).

We determined that Ca^{2+} sparklets were produced by Ca^{2+} influx via L-type Ca^{2+} channels using multiple strategies. First, sparklet activity in smooth muscle cells, neonatal ventricular myocytes, and tsA-201 cells transfected with CaV1.2 was rapidly eliminated by the application of the L-type Ca^{2+} channel inhibitor nifedipine (10 µmol/L) or by superfusion of a Ca^{2+}-free external solution (*data not shown*). Second, as reported previously, Ca^{2+} sparklets were never observed in untransfected tsA-201 cells (Navedo et al., 2005). Third, Ca^{2+} sparklets in arterial

and neonatal ventricular myocytes have the same amplitude of quantal event, activity, and pharmacology (e.g. insensitive to 1 μmol/L thapsigargin, eliminated by 10 μmol/L nifedipine) as Ca^{2+} sparklets in tsA-201 cells expressing $Ca_V1.2$ channels (Navedo et al., 2005; Selvin, 1995).

By simultaneously recording single Ca^{2+} channel currents and Ca^{2+} sparklets in arterial myocytes, we recently reported that at -70 mV and with 20 mmol/L external Ca^{2+}, a single Ca^{2+} channel current of ≈0.7 pA produced a Ca^{2+} sparklet of ≈40 nmol/L (Navedo et al., 2005). As shown in previous studies, histograms from all $[Ca^{2+}]_i$ records obtained from arterial myocytes had multiple, clearly separated peaks and could be fit with the following multi Gaussian function:

$$N = \sum_{j=1}^{n} a_j * \exp\left[-\frac{([Ca^{2+}]_i - jq)^2}{2jb}\right],$$

where *a* and *b* are constants and $[Ca^{2+}]_i$ and *q* are intracellular Ca^{2+} and the quantal unit of Ca^{2+} influx, respectively (Navedo et al., 2006, 2005). Using this analysis, and consistent with our previous studies, we obtained a *q* value of 38 nmol/L in the histogram, a value that is similar to that obtained previously (see above). This analysis provides further support to the hypothesis that Ca^{2+} sparklets are quantal in nature and that the size of Ca^{2+} sparklet depends on the number of quanta activated.

Quicktime movie tutorials of this analysis are available in our lab webpage: (http://web.mac.com/fernando_santana/Lab_website/Sparklet_tutorials.html).

We determined the number of Ca^{2+} sparklet sites with coupled gating events per cell as follows. First, we identified Ca^{2+} sparklet sites in each cell as described above. Next, we analyzed the Ca^{2+} sparklets records from these sites using the coupled Markov model described below to determine the coupling co-efficient of the Ca^{2+} channels underlying these sparklets. We created bar plots of the number of sites per cell with coupling coefficients > 0. Because Ca^{2+} sparklets were recorded using TIRF, this analysis was limited to the portion of the cell within the evanescent field (typically 100-400 μm^2).

Confocal images were obtained using the 60X lens (NA = 1.4 or 1.2) of an inverted microscope coupled to a BioRad Radiance 2100 confocal system. The all-points histograms shown in Figure 2.1 and 2 were fitted using a least-squares routine with a multi-component Gaussian function using Graphpad Prism v5 (San Diego, CA)

2.3.6 Coupled Markov chain model

Membrane currents and time courses of $[Ca^{2+}]_i$ from Ca^{2+} sparklet sites were analyzed using a binary coupled Markov chain model originally described by Chung and Kennedy to simulate and fit independent records of partially coupled channels

(Chung & Kennedy, 1996). The program was written in Matlab® language, and the full source code is provided in Appendix A. Channel openings were identified using a half-amplitude protocol, with the quantal level for a unitary event set at 0.50 pA for currents and 38 nmol/L for Ca^{2+} sparklets (Navedo et al., 2005). The activity of $Ca_V1.2$ channels was modeled as a first order, discrete Markov chain, and the Markovian transition matrix was estimated from the current and sparklet records and their corresponding channel opening time courses using the built-in Hidden Markov parameter estimation function in Matlab®. The estimated transition matrix was modeled as a partially coupled Markov chain where a dimensionless parameter (κ) is the coupling coefficient between fully uncoupled and fully coupled cases. In addition to the coupling coefficient (κ), the model has two additional parameters: the channel open-to-open probability (ρ) and the channel closed-to-closed probability (ς), and together they fully describe the contribution from the fully uncoupled case to the transition matrix. For each record, the optimum set of parameters (κ, ρ, ς) for the partially coupled Markov chain model was fitted using a gradient descent algorithm.

The utility of this model is that it is a “lumped” model, where the channels switch between the binary observable states of either “open” or “closed,” and therefore, instead of trying to deduce the gating kinetics of multiple channels, which involves many free parameters, our model has only three free parameters, including the coupling coefficient. It does not completely describe the actual kinetics of the channel and consequently the transition probabilities obtained from this lumped model are not interpreted as rate constants.

2.3.7 FRET imaging

For these experiments, we used tsA-201 cells transfected with $Ca_V1.2$-EGFP and CaM-tRFP, $Ca_V1.2$-TS-EGFP and CaM-tRFP, $Ca_V1.2$-EGFP and $Ca_V1.2$-tRFP, or $Ca_V1.2$-TS-EGFP and $Ca_V1.2$-TS-tRFP as described above. FRET was determined using a confocal microscope using approaches similar to those described by Tadross et al. (Tadross, Park, Veeramani, & Yue, 2009). Cells were imaged using a Nikon swept field confocal system coupled to a Nikon TE300 inverted microscope equipped with a Nikon 60x lens (NA = 1.2) and using a slit aperture of 60 μm (maximum apperture). This optical configuration has been shown to produce robust sub-cellular FRET imaging (Tadross et al., 2009). EGFP and tRFP were excited using 488 and 563 nm light, respectively and appropriate dichroic (500/543 nm long-pass) and emission (dual 535/30 nm and 610/40) filters. Images were acquired with a Cascade EMCCD camera.

The efficiency of FRET between EGFP and tRFP was determined using the donor de-quenching method as described elsewhere (Day et al., 2003; Erickson et al., 2001). Briefly, images of EGFP-tagged proteins (donor) were collected before and after the PKC activator PDBu (500 nmol/L) or the CaM inhibitor W7 (100 μmol/L) and after approximately complete photobleaching of tRFP-tagged (acceptor) proteins. During analysis, we generated fluorescence intensity profiles (1 μm wide) of portions of the images that included the surface membrane and cytosol of each cell analyzed

before and after photo-bleaching tRFP (i.e. acceptor). FRET was reflected by an increase in EGFP fluorescence intensity following tRFP bleaching. The effective FRET was calculated using the following equation: $E_{EFF} = 1 – (F_{DA}/F_D)$, where E_{EFF} is the effective FRET, F_{DA} is the fluorescence intensity of EGFP before acceptor photo-bleaching, and F_D is the fluorescence intensity of EGFP after tRFP photo-bleaching with 563 nm light (Selvin, 1995).

2.3.8 Statistics

Data are presented as mean ± SEM. Two-sample comparisons were made using a students' T-test or a Wilcoxon signed-rank test. A *p* value of less than 0.05 was considered significant. The asterisk (*) symbol is used in the figures to illustrate a significant difference between groups.

2.4 Results

2.4.1 Optical recordings of coupled L-type Ca^{2+} channels

A TIRF microscope was used to image Ca^{2+} sparklets in arterial smooth muscle cells, neonatal ventricular myocytes, and tsA-201 cells expressing wild type $Ca_V1.2$ channels. All Ca^{2+} sparklet experiments were performed in voltage clamped cells using the whole-cell configuration of the patch-clamp technique. Ca^{2+} sparklets were recorded in cells treated with the SERCA pump inhibitor thapsigagin (1 μmol/L) to eliminate Ca^{2+} release from intracellular Ca^{2+} stores. To image Ca^{2+} sparklets, cells were dialyzed with patch pipette solution containing the fluorescent Ca^{2+} indicator fluo-5F and EGTA. The inclusion of the relatively slow Ca^{2+} buffer EGTA (on rate ≈100-fold slower than fluo-5F) in the intracellular solution serves an important purpose: it restricts fluo-5F fluorescence to the site of Ca^{2+} entry (≈ 1 μm). This occurs because with EGTA in the cytosol, Ca^{2+} entering the cell initially interacts with the faster fluo-5F, producing a fluorescence signal, but then quickly (≈ 2 ms) binds to the more abundant and non-fluorescent EGTA. Thus, in our TIRF experiments, $[Ca^{2+}]_i$ signals are limited to the sub-membrane space near the mouth of surface membrane Ca^{2+} channels.

Figure 2.1A shows representative Ca^{2+} sparklets from arterial smooth muscle cells, neonatal ventricular myocytes, and tsA-201 cells expressing $Ca_V1.2$ channels.

These Ca^{2+} sparklets were recorded while cells were held at -70 mV to increase the driving force for Ca^{2+} influx and maintain a low L-type Ca^{2+} channel activity, which increased contrast and hence our ability to detect discrete Ca^{2+} entry sites. A $\Delta[Ca^{2+}]_i$ amplitude histogram of these records revealed two discrete peaks corresponding to closed channels ($\Delta[Ca^{2+}]_i$ = 0 nmol/L) and openings of ≈38 nmol/L, which as demonstrated previously, represents the amplitude of quantal Ca^{2+} sparklet events in tsA-201 cells expressing $Ca_V1.2$ and arterial myocytes (Navedo et al., 2007, 2006, 2005). A previous study[6] suggests quantal Ca^{2+} sparklets are likely produced by the opening of a single Ca^{2+} channel.

It is important to note that, consistent with previous work[5, 6], Ca^{2+} sparklet activity in smooth muscle cells, neonatal ventricular myocytes, and tsA-201 cells transfected with $Ca_V1.2$ was rapidly eliminated by the application of the L-type Ca^{2+} channel inhibitor nifedipine (10 μmol/L) or by superfusion of a Ca^{2+}-free external solution (*data not shown*). Importantly, and as reported recently, Ca^{2+} sparklets were never observed in untransfected tsA-201 cells (Navedo et al., 2006). Furthermore, Ca^{2+} sparklets in arterial and neonatal ventricular myocytes have the same amplitude of quantal event, activity, and pharmacology (e.g. insensitive to 1 μmol/L thapsigargin, eliminated by 10 μmol/L nifedipine) as Ca^{2+} sparklets in tsA-201 cells expressing $Ca_V1.2$ channels (Navedo et al., 2007, 2006). Collectively these observations strongly suggest that Ca^{2+} sparklets in arterial smooth muscle cells, neonatal ventricular myocytes, and tsA-201 cells expressing $Ca_V1.2$ channels are produced by Ca^{2+} influx via L-type Ca^{2+} channels.

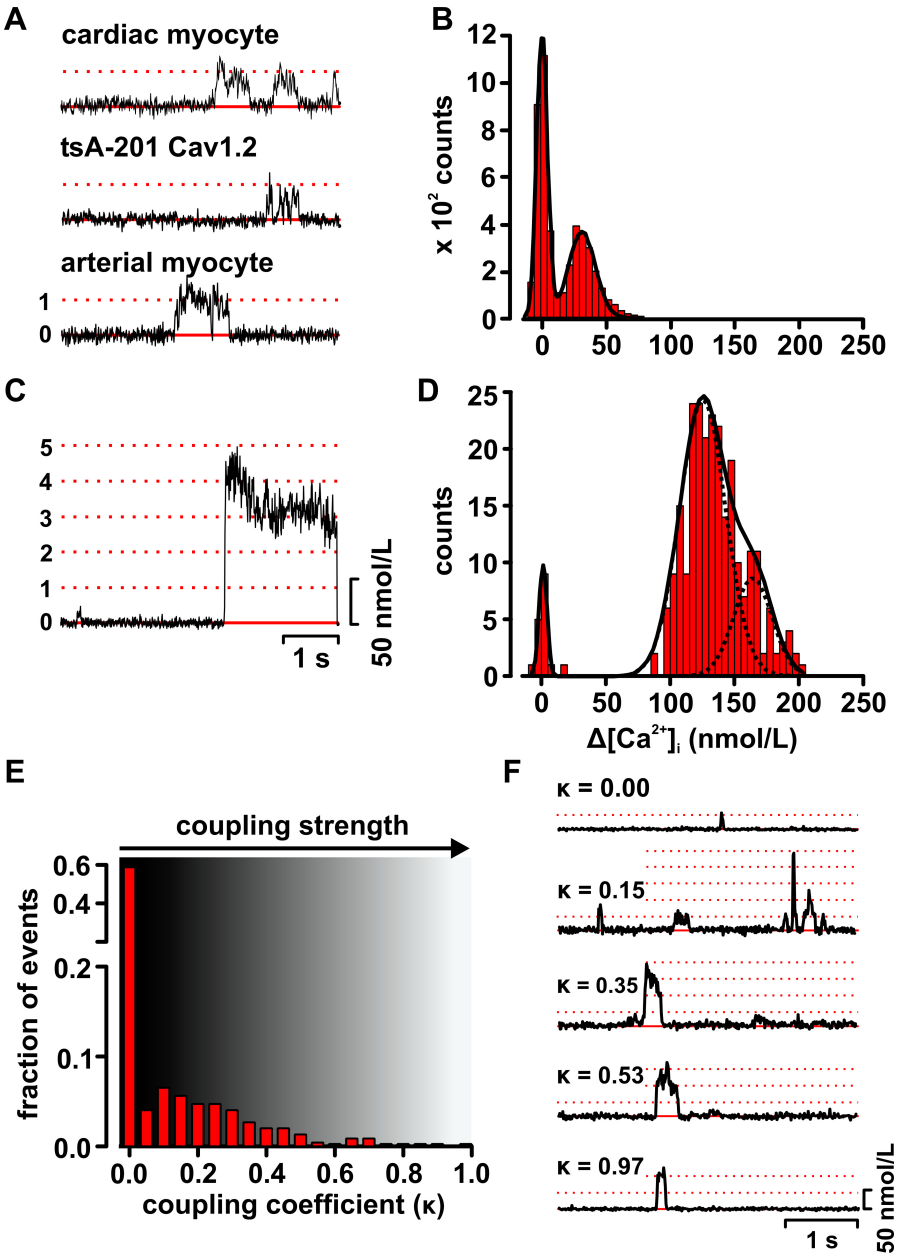

Figure 2.1. Optical recordings of coupled gating of $Ca_V1.2$ channels.
(A) Representative records of Ca^{2+} influx via Cav1.2 channels in neonatal cardiac myocytes (*top*), tsA-201 cells (*middle*), and arterial myocytes (*bottom*). (B) All-points histogram of Ca^{2+} sparklet traces in panel A. The solid black line is the fit (χ^2 = 2.1) to the data with a multi-component Gaussian function with centers at 0 and 38 nmol/L. (C) $\Delta[Ca^{2+}]_i$ from a Ca^{2+} sparklet site in an arterial myocyte with coupled Cav1.2 channels. (D) All-points histogram of the Ca^{2+} sparklet trace in panel C. The solid black line is the best-fit (χ^2 = 2.5) to the data with a three-component Gaussian function with centers at 0, 120, and 160 nmol/L. (E) Histogram of the coupling coefficients (κ) of multiple Ca^{2+} sparklet records from cardiac, arterial, and tsA-201 cells. (F) Ca^{2+} sparklet records with varied κ values.

Although most Ca^{2+} sparklets recorded in these cells were similar to those in Figure 2.1A, we noticed that in a number of Ca^{2+} sparklet sites (191 of 491 sites) small clusters of $Ca_V1.2$ channels opened and closed simultaneously to promote greater elevation in subcellular $[Ca^{2+}]_i$ (Figure 2.1C). The $\Delta[Ca^{2+}]_i$ histogram of the trace in Figure 2.1D had three distinct peaks at a $\Delta[Ca^{2+}]_i$ of 0, 120, and 160 nmol/L. The peaks at 120 and 160 nmol/L likely resulted from the simultaneous activation of 3 and 4 $Ca_V1.2$ channels, respectively. Note the absence of a peak near the quantal amplitude of Ca^{2+} influx (i.e. 38 nmol/L).

The observation of Ca^{2+} sparklets resulting from the simultaneous openings of small clusters of $Ca_V1.2$ channels is surprising because the P_o of a single $Ca_V1.2$ channel is only $\approx 10^{-6}$ at -70 mV (M Rubart, Patlak, & Nelson, 1996). The probability of independently gating channels opening simultaneously at this potential should be very low: $\approx 10^{-12}$, 10^{-18}, and 10^{-24} for the random, coincidental opening of 2, 3, or 4 channels. Thus, the probability of observing simultaneous openings of Ca^{2+} channels should be progressively lower as the number of participating channels increase, which should result in a histogram with peaks of decreasing amplitudes as multichannel events become rarer. On the basis of that analysis, Ca^{2+} sparklet events like the one in Figure 2.1C should be very rare. Yet, Ca^{2+} sparklets resulting from the coincident activation of 2 or more $Ca_V1.2$ channels were frequently observed. This suggests that this is not simply the consequence of overlapping stochastic openings of independently activated $Ca_V1.2$ channels. Rather, our data provide evidence for the coordinated activation of a small cluster of these channels.

To test this hypothesis, we implemented a coupled Markov chain model to determine the coupling coefficient (κ) among $Ca_V1.2$ channels within Ca^{2+} sparklet sites (Figures 2.1E and 2.1F). The model was originally developed by Chung and Kennedy and used to analyze individual records of partially coupled GABA-activated chloride channels (Chung & Kennedy, 1996). Briefly, this model is a simplified Markov chain model with only 3 free parameters that takes the form of a set of binary chains that are interdependent according to a lumped coupling coefficient parameter called κ. The other two parameters (called ρ and ς) describe the intrinsic characteristics of the binary chains. The κ value could range from 0 for independently gating channels to 1 for "tightly" coupled channels that open and close simultaneously all the time. A detailed description of this model is provided in the Methods section.

Using this analysis, we found that although the majority of Ca^{2+} sparklets (59%) were likely the result of Ca^{2+} influx via independently gating $Ca_V1.2$ channels (i.e. $\kappa = 0$), numerous Ca^{2+} sparklets were produced by $Ca_V1.2$ channels with a $\kappa > 0$. Indeed, the coupling coefficient of non-independent events (i.e. $\kappa > 0$) ranged from 0.1 to 1 with a median value of 0.2. Together with the Ca^{2+} sparklet data above, this Markov analysis suggested that a subpopulation of $Ca_V1.2$ channels was capable of gating coordinately.

2.4.2 Electrophysiological recordings of coupled L-type Ca^{2+} channels

We used electrophysiological techniques to record L-type Ca^{2+} channel currents (Figure 2.2). In these experiments, we recorded elementary L-type Ca^{2+} channel currents from cell-attached patches from neonatal ventricular myocytes. L-type Ca^{2+} channel currents were evoked by a 2 s step depolarization to -30 mV from the holding potential of -80 mV. The patch pipette solution contained 20 mmol/L Ca^{2+} (charge carrier), 10 µmol/L tetrodotoxin (TTX), 130 mmol/L TEA^+ and no Na^+ or K^+ to eliminate Na^+ and K^+ channel currents. The L-type Ca^{2+} channel opener BayK-8644 (500 nmol/L) was included in the pipette solution to increase the mean open time and P_o of these channels and the probability of PKCα-dependent, persistent L-type Ca^{2+} channel activity (Navedo et al., 2006).

As expected from our Ca^{2+} sparklet studies, depolarization to -30 mV evoked relatively low levels of Ca^{2+} channel activity in most (112 out of 134 sweeps, or 84%; from 5 cells) of the sweeps examined (Figure 2.2A). A current amplitude histogram from these records show two distinct peaks with centers at 0 mV (i.e. closed channel) and 0.53 pA, which corresponds to the expected single channel current level for an L-type Ca^{2+} channel at -30 mV with 20 mmol/L Ca^{2+} (Navedo et al., 2007). The κ value of the $Ca_V1.2$ channels in these patches was 0, suggesting that these currents were produced by independently gating channels. At this point it is

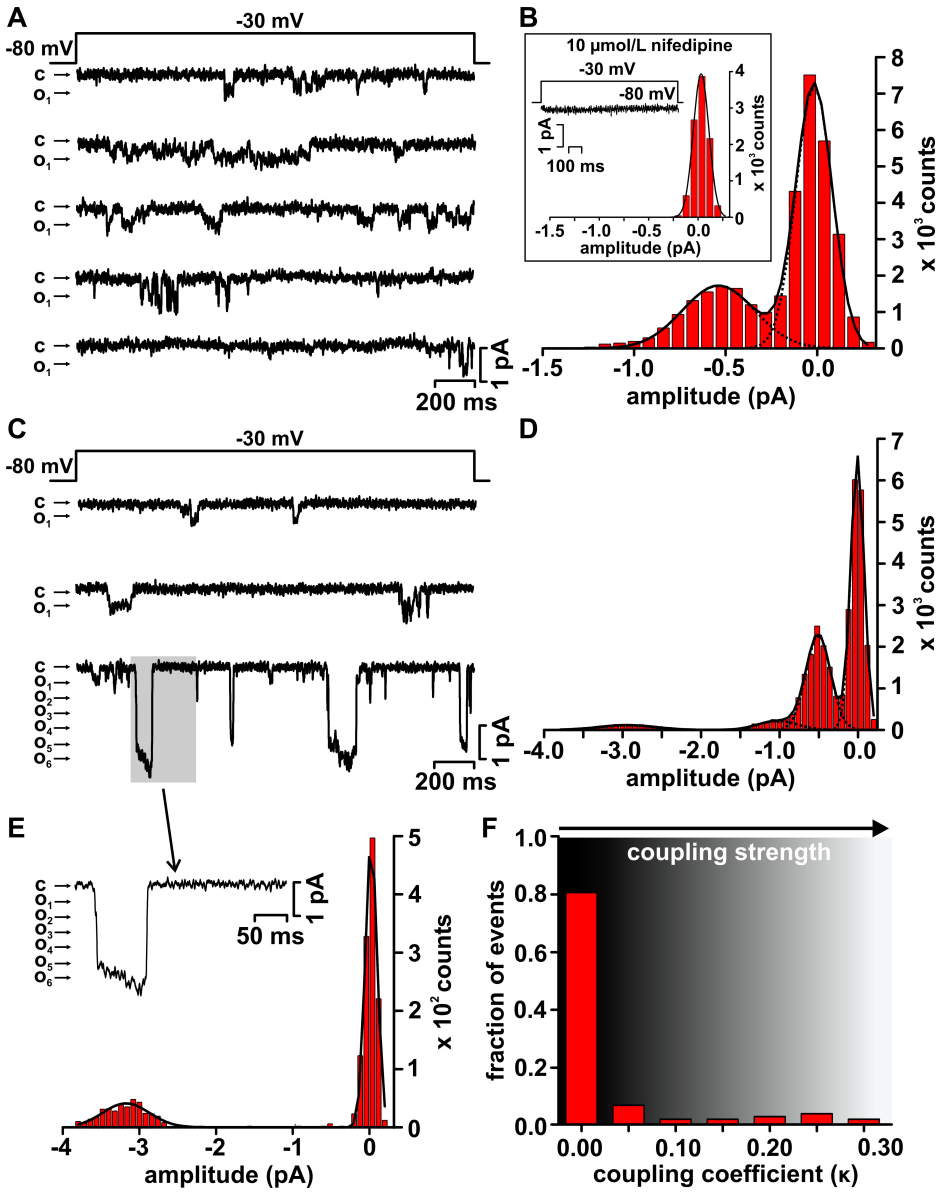

Figure 2.2. Electrical recordings of coupled L-type Ca^{2+} channels.
(A) Representative elementary L-type Ca^{2+} channel records obtained during a step depolarization (2 s) from -80 mV to -30 mV. Openings are shown as downward deflections, with the close state denoted by "c", and the open state by "o". (B) Histogram of L-type Ca^{2+} currents traces in panel A. The solid black line is the fit to the data with a multi-component Gaussian function with centers at 0.0 and 0.5 pA. The inset shows a histogram from a representative record obtained in the presence of 10 µmol/L nifedipine. (C) Representative single and coupled L-type Ca^{2+} channel current records obtained during step depolarizations from -80 mV to -30 mV. (D) Histogram of the L-type Ca^{2+} currents records in panel C. The solid black line is the fit to the data with a multi-component Gaussian function with centers at 0.0, -0.5, -1.0, and -2.9 pA. (E) Trace shows a portion (gray box) of the record in panel C showing a L-type Ca^{2+} current resulting from the simultaneous opening and closing of multiple channels. A histogram from this portion of the trace is shown below. The histogram was fitted with a Gaussian function with centers at 0.0 and -3.1 pA. (F) Histogram of the coupling coefficients (κ) of multiple L-type Ca^{2+} current records from cell-attached patches from neonatal ventricular myocytes.

important to note that in control experiments inclusion of 10 μmol/L nifedipine prevented all Ca^{2+} channel activity, indicating that L-type Ca^{2+} channels produced these currents (*inset* in Figure 2.2B).

Consistent with our Ca^{2+} sparklet data, we found that in a minority of the records (22 out 134 sweeps or 16%; from 5 cells) membrane depolarization to -30 mV evoked elementary as well as relatively large currents that were likely produced by the simultaneous opening and closing of multiple L-type Ca^{2+} channels (Figure 2.2C). The amplitude histogram of the current records in Figure 2.2C had four prominent peaks at 0.0, 0.5, 1.0, and 2.9 pA, likely resulting from the activation of a single or simultaneous activation of two or six L-type Ca^{2+} channels, respectively. Closer examination (Figure 2.2E) of one of the large current events highlighted by the gray box in the bottom sweep in Figure 2.2D, indicates that in this patch 5-6 channel likely opened and then closed simultaneously multiple times. Three additional multichannel current events of similar amplitude were observed in this sweep. As noted above, the prominence of the peak with a center at 2.9 pA in the histogram in Figure 2.2C and absence of peaks of larger amplitude between this peak and the peak at 1 pA suggests coupled gating between L-type Ca^{2+} channels. Consistent with this, the coupling coefficient of the L-type Ca^{2+} channels in this section was 0.22, suggesting this current was produced by partially coupled channels. Indeed, analysis of all L-type Ca^{2+} channel records indicates that the vast majority of the currents were likely the result of independent openings of L-type Ca^{2+} channels (i.e. $\kappa = 0$; Figure 2.2F). In combination with the Ca^{2+} sparklet data above, these findings

strongly support to the hypothesis that small clusters of $Ca_V1.2$ channels can open and close coordinately.

2.4.3 Activation of PKCα increases coupled gating of $Ca_V1.2$ channels

Activation of PKCα has been linked to elevated persistent Ca^{2+} sparklet activity in arterial myocytes (Navedo et al., 2008, 2006, 2005). Thus, we investigated whether membrane translocation and activation of this kinase increases coupled gating of $Ca_V1.2$ channels. To do this, we used two complementary approaches. First, we generated a chemically-induced PKCα translocation system (Liberles et al., 1997; Suh et al., 2006). Briefly, we created an adenoviral vector expressing a FKBP12-rapamycin-binding element (FRB) that is anchored to the plasma membrane via myristoylation and palmitoylation modification sequence Lyn_{11}. This adenoviral vector also expressed PKCα fused to the enhanced green fluorescent protein and a FK506 binding protein. Application of rapamycin promoted heterodimerization of protein domains from FKBP-PKCα-EGFP and the membrane anchored FRB. This recruited FKBP-PKCα-EGFP to the membrane from the cytosol upon addition of rapamycin (Figure 2.3A). We used this inducible PKCα in neonatal ventricular myocytes and tsA-201 cells expressing $Ca_V1.2$. We found that induction of membrane translocation of PKCα (Figure 2.3A) increased Ca^{2+} sparklet activity and

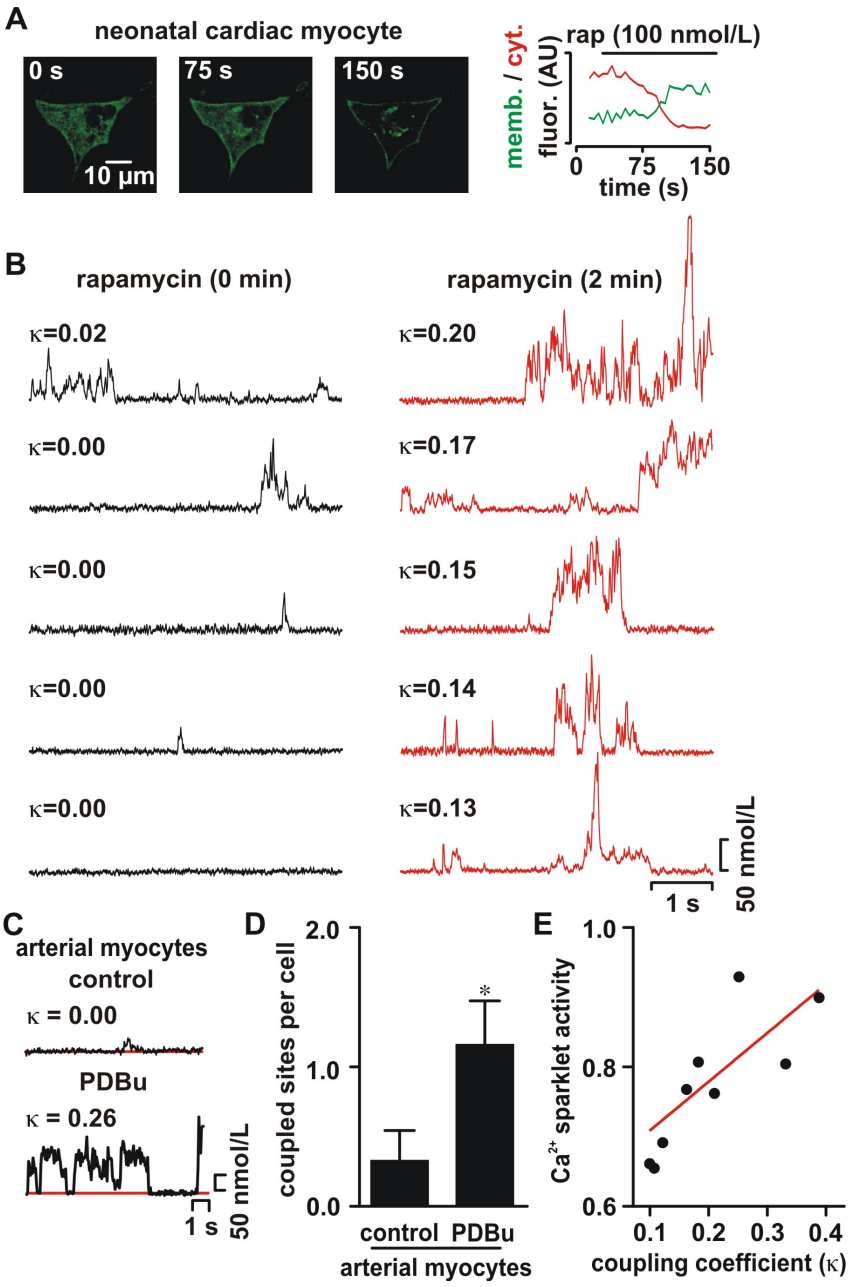

Figure 2.3. Activation of PKCα increases coupled gating between CaV1.2 channels.
(A) Confocal images of neonatal ventricular cells expressing the inducible PKCα translocation system before (0 s) and after (75 and 150 s) application of 0.1 µmol/L rapamycin to induce membrane translocation of this kinase. The graph on the right side shows the time course of PKCα fluorescence intensity in the membrane and cytosol in this cardiac myocyte. $\Delta[Ca^{2+}]_i$ records from multiple Ca^{2+} sparklet sites before (left) and after (right) induction of PKCα-EGFP translocation are shown below the confocal images. (B) $\Delta[Ca^{2+}]_i$ records from a Ca^{2+} sparklet site before and after application of PDBu. The κ of the Cav1.2 channels in this site is shown above each record. (C) Ca^{2+} sparklet records from an arterial myocyte before and after PDBu (500 nmol/L). (D) Bar plot of the mean number of coupled sites per cell in arterial myocytes under control condition and after application of 500 nmol/L PDBu. (E) Relationship between Ca^{2+} sparklet activity and coupling coefficient. Red line is a linear fit to the data (r^2 = 0.64).

coupled gating of $Ca_V1.2$ channels in cardiac myocytes (n = 5 cells, Figure 2.3B) and tsA-201 cells (n = 6 cells, Figure 2.4).

Our second approach involved the activation of endogenous PKC using the phorbol 12,13-dibutyrate (PDBu; 500 nmol/L). Activation of PKC with PDBu had a similar effect in arterial myocytes (n = 17 cells, Figure 2.3C and 3D). Taken together these data suggest that membrane translocation and activation of PKCα increases the probability of coupled gating between $Ca_V1.2$ channels.

2.4.4 Inducible PKCα translocation in tsA-201 cells increases coupled $Ca_V1.2$ channel activity

We recorded Ca^{2+} sparklet activity in voltage-clamped tsA-201 cells (-70 mV) expressing $Ca_V1.2$ channels as well as membrane-anchored Lyn11-FRB and FKBP-PKCα-EGFP (Figure 2.4). Under control conditions, FKBP-PKCα-EGFP fluorescence was distributed broadly throughout the cytosol of tsA-201 cells. Application of rapamycin (0.1 μmol/L) induced a rapid decrease in cytosolic fluorescence and an increase in membrane-associated fluorescence, which was produced by the translocation of FKBP-PKCα-EGFP to the surface membrane of these cells. The translocation of FKBP-PKCα-EGFP to the sarcolemma of these cells was complete 85 ± 5 seconds (n = 6 cells) after the introduction of rapamycin.

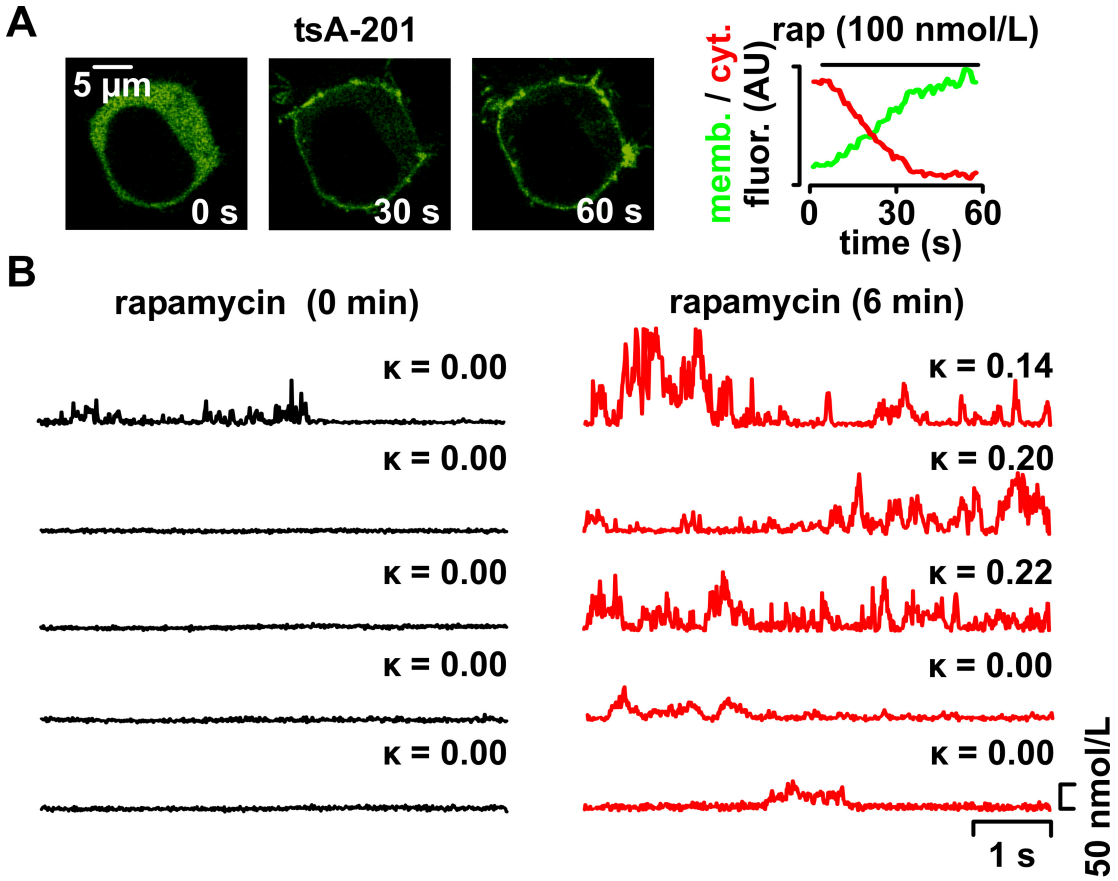

Figure 2.4. Activation of PKCα induces coupled gating of L-type Ca^{2+} channels in tsA-201 cells expressing $Ca_V1.2$ channels.
(A) Confocal images of tsA-201 cells expressing FKBP-PKCα-EGFP and membrane-anchored Lyn11-FRB before (0 s) and after (30 and 60 s) application of 0.1 µmol/L rapamycin. The graph on the right side of the images shows the time course of PKCα fluorescence intensity in the membrane (green) and cytosol (red) in this cell. (B) $\Delta[Ca^{2+}]_i$ records from multiple Ca^{2+} sparklet sites (-70 mV) before (left) and after (right) induction of FKBP-PKCα-EGFP translocation. The coupling coefficient (κ) of Cav1.2 at each site is shown above the trace.

As in neonatal ventricular myocytes, membrane-anchored Lyn11-FRB, and FKBP-PKCα-EGFP (Figure 2.3), Ca^{2+} sparklet activity in general and coupled activity in specific was low in tsA-201 cells under control conditions (i.e. -70 mV, before application of rapamycin) (Figure 2.4B).

However, PKCα translocation to the surface membrane of these cells evoked an increase in coupled $Ca_V1.2$ activity in previously active and silent Ca^{2+} sparklet sites ($p < 0.05$).

2.4.5 Movement of calmodulin away from the IQ domain in the C-tail of $Ca_V1.2$ channels increases coupled gating of these channels

We observed that the activity of Ca^{2+} sparklets produced by coupled $Ca_V1.2$ channels was higher than those produced by independently gating channels (Figure 2.3E). This raised the intriguing possibility that the probability of coupled gating of $Ca_V1.2$ channels might be enhanced by deficient Ca^{2+}-dependent inactivation (CDI) of these channels. Calmodulin (CaM) mediates CDI of CaV1.2 channels (Imredy & Yue, 1994; Zuhlke, Pitt, Deisseroth, Tsien, & Reuter, 1999). Thus, we tested the hypothesis that inhibition of CaM increases the probability of coupled gating of $Ca_V1.2$ channels.

Consistent with this hypothesis, we found that application of the CaM antagonist W7 (100 μmol/L) increased the number of sites with coupled $Ca_V1.2$ channels ≈7-fold

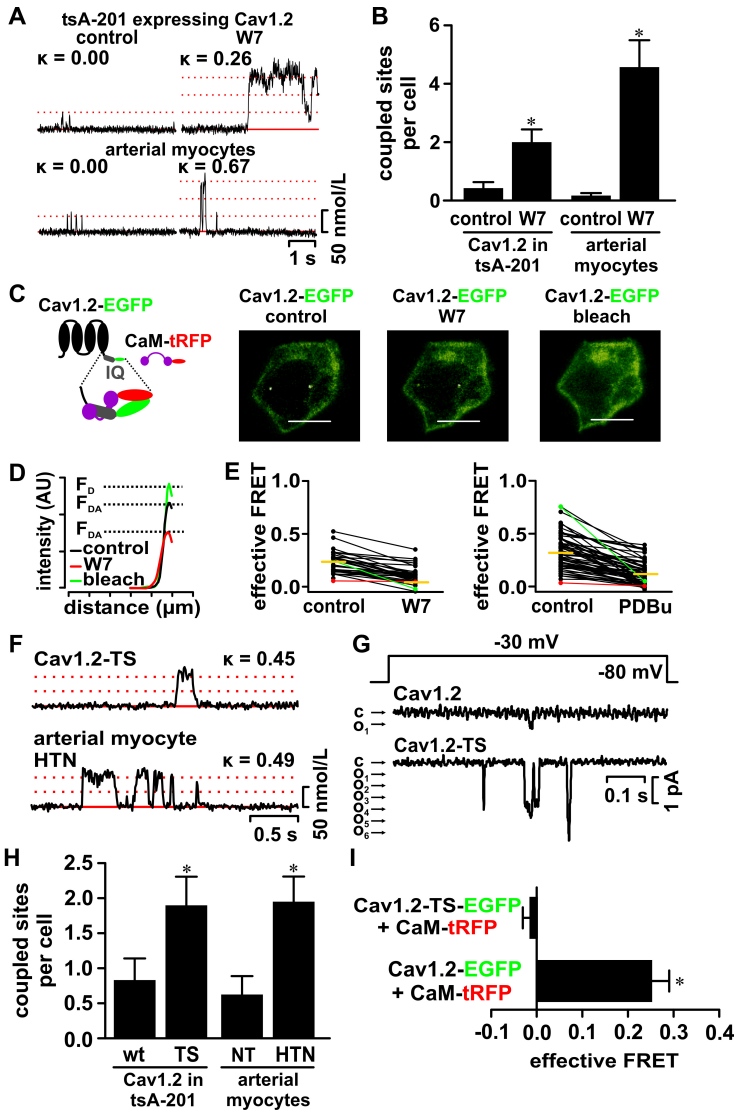

Figure 2.5. Removing CaM from the IQ domain of $Ca_V1.2$ increases coupled gating of WT and TS $Ca_V1.2$ channels.
(A) Ca^{2+} sparklet records from tsA-201 and arterial myocytes showing induction of coupled gating by W7 (100 μmol/L). κ values are shown above each trace. (B) Number of coupled sites per cell before and after W7. (C) Cartoon of Cav1.2-EGFP and CaM-tRFP. *Right*, images of Cav1.2-EGFP in tsA-201 cells under control conditions, during W7 treatment, and following CaM-tRFP photobleaching. (D) Cav1.2-EGFP fluorescence intensity at an example cross section of the membrane marked by the white line in each of the images in panel C. Dotted lines show the F_{DA} and F_A values used to calculate effective FRET (=1-F_{DA}/F_A). (E) FRET in specific sites before and after W7 (center, lower row) or PDBu (right, lower row) application. Yellow bars are mean values. (F) Ca^{2+} sparklet records with coupled Cav1.2 channels from tsA-201 cells expressing Cav1.2-TS and hypertensive smooth muscle. (G) Representative Cav1.2 channel currents evoked by depolarization from -80 to -30 mV in patches (cell-attached) from tsA-201 cells expressing WT (upper trace) and Cav1.2-TS channels (lower trace). The close state is denoted by a "c" and the open state by an "o". (H) Number of sites with coupled Cav1.2 channels per cell in cells expressing WT and TS Cav1.2 and in normotensive (NT) and hypertensive (HTN) smooth muscle. (I) FRET data between EGFP-tagged WT or TS Cav1.2 and CaM-tRFP.

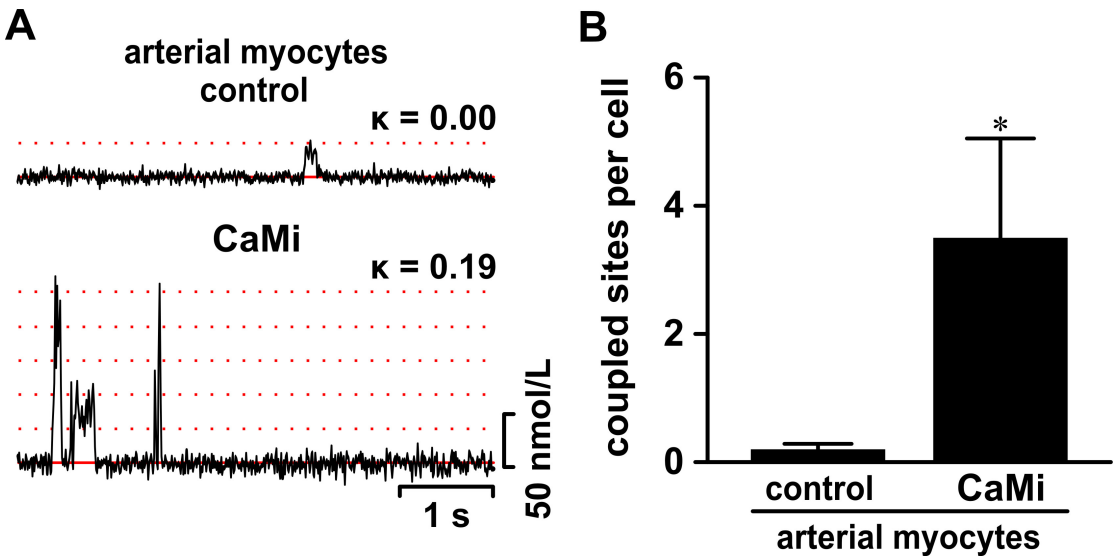

Figure 2.6. CaM-inhibitory peptide increases coupled gating of $Ca_V1.2$ channels.
(A) Representative $\Delta[Ca^{2+}]_i$ records from Ca^{2+} sparklet sites in smooth muscle cells under control conditions (top) and during dialysis with the CaM inhibitory (CaMi) peptide (1 μmol/L; bottom). The coupling coefficient (κ) of these Cav1.2 channels is shown above each trace. Dotted lines show the amplitude of quantal levels. (B) Bar plot of the mean number of coupled sites per cell.

and 27-fold in tsA-201 cells (n =4 cells) and myocytes (n = 7 cells), respectively (p < 0.05; Figures 2.5A and 2.5B). Similar findings were obtained in myocytes injected with the CaM-inhibitory peptide (1 μmol/L; n = 4 cells; Figure 2.6). Application of either CaM antagonist increased the number of Ca^{2+} sparklet sites with coupled $Ca_V1.2$ channels, but not the median κ value (0.2) of coupled channels (p > 0.05).

To examine the dynamics of this phenomenon, we used **f**luorescence **r**esonance **e**nergy **t**ransfer (FRET) to visualize the interaction between $Ca_V1.2$ channels and CaM. The C-terminal of $Ca_V1.2$ was tagged with the enhanced green fluorescent protein ($Ca_V1.2$-EGFP) and CaM was fused with tag-RFP® (CaM-tRFP) (Figures

2.5C and 2.5D). CaM associates with the IQ domain in the C-terminal of $Ca_V1.2$, which is critical for CDI of these channels (Erickson et al., 2001; Zuhlke et al., 1999). Accordingly, FRET was relatively high (0.32 ± 0.02, n = 10 cells) between $Ca_V1.2$-EGFP and CaM-tRFP under control conditions. Application of the CaM antagonist W7 (100 µmol/L) or the PKC activator PDBu (500 nmol/L) decreased FRET between $Ca_V1.2$-EGFP and CaM-tRFP from 0.21 ± 0.04 to 0.08 ± 0.03 (n = 10 cells) and from 0.33 ± 0.02 to 0.12 ± 0.10 (n = 11 cells), respectively (Figure 2.5E) ($p < 0.05$). Note, however, that the magnitude of the decrease in FRET induced by W7 and PKCα activation varied within cells. The relative change in FRET ranged from 0 in some sites (red line in Figure 2.5E) to 100% in others (green line in Figure 2.5E). A decrease in FRET suggests an increase in the distance between $Ca_V1.2$-EGFP and CaM-tRFP. This could result from two potential scenarios. *First*, CaM-tRFP dissociates from the IQ domain of $Ca_V1.2$-EGFP channels. *Second*, CaM-tRFP changes in position within the C-tail of $Ca_V1.2$ channels, moving away from the EGFP fused to the C-terminal of these channel enough to decrease or even eliminate FRET. Although our FRET experiments cannot distinguish between these two possibilities, they evidently suggest that displacement of CaM away from the IQ domain of $Ca_V1.2$ channels may be a critical step in the induction of coupled gating of these channels.

2.4.6 Calmodulin-inhibitory peptide increases coupled gating of $Ca_V1.2$ channels

In these experiments, we used a 17-residue peptide based on the calmodulin (CaM)-binding domain of myosin light chain kinase. This peptide inhibits CaM by binding to it with high affinity (K_d = 6 pmol/L). We tested the hypothesis that the CaM inhibitory peptide increases coupled gating of $Ca_V1.2$ channels in arterial myocytes. To test this hypothesis, we recorded Ca^{2+} sparklet activity at -70 mV in control myocytes and in cells dialyzed via the patch pipette with an intracellular solution similar to the one used for control cells, but containing 1 μmol/L of the CaM inhibitory peptide (Figure 2.6). As with the CaM antagonist W7 (Figure 2.5), we found a higher frequency ($p < 0.05$) of coupled gating $Ca_V1.2$ events in cells exposed to the CaM inhibitory peptide than in control cells. Together with the W7 data, these findings strongly suggest that CaM inhibition increases the probability of coupled gating between $Ca_V1.2$ channels.

2.4.7 Increased coupled gating of $Ca_V1.2$ channels during hypertension and Timothy syndrome

Increased $Ca_V1.2$ channel activity underlies lethal cardiac arrhythmias and autism in humans with Timothy syndrome (TS) (Splawski et al., 2004). In TS, a single amino acid substitution (Gly-436-Arg) in $Ca_V1.2$ (CaV1.2-TS) increases the open time and P_o of these channels (Erxleben et al., 2006; Splawski et al., 2004). We recorded

Ca^{2+} sparklets (-70 mV) and depolarization-evoked currents in tsA-201 cells expressing WT and $Ca_V1.2$-TS channels (Figures 2.5F and 2.5G, respectively). We found a higher frequency of Ca^{2+} sparklets with coupled $Ca_V1.2$ channels in tsA-201 cells expressing $Ca_V1.2$-TS (n = 10 cells) than WT channels (n = 10 cells; Figure 2.5H; $p < 0.05$). Next, we used experimental conditions similar to those used to record Ca^{2+} currents in neonatal cardiac myocytes above.

Membrane depolarization to -30 mV activated WT and $Ca_V1.2$-TS channels in tsA-201 cells. Voltage-activated currents were never recorded in untransfected tsA-201 cells. As in neonatal myocytes, the amplitude of the elementary Ca^{2+} currents activated by a voltage pulse to -30 mV was similar (0.49 ± 0.01 pA) to that in neonatal ventricular myocytes (0.53 ± 0.01 pA; $p > 0.05$). This gives further support to the view that $Ca_V1.2$ channels produced the currents recorded in neonatal myocytes. Consistent with our Ca^{2+} sparklet studies, we recorded a number of Ca^{2+} currents resulting from the simultaneous opening and closing (i.e. coupled gating) of channels in cells expressing $Ca_V1.2$-TS than WT $Ca_V1.2$ (Figure 2.5G).

Increased L-type Ca^{2+} channel activity in arterial myocytes has been implicated in the chain of events that leads to vascular dysfunction during hypertension (Nieves-Cintrón, Amberg, Navedo, Molkentin, & Santana, 2008; Pesic, Madden, Pesic, & Rusch, 2004). In hypertensive arterial myocytes, higher $Ca_V1.2$ channel activity is due, at least in part, to increased local PKCα activity. We found a higher frequency of coupled $Ca_V1.2$ channel gating events both in arterial myocytes from an animal

model of angiotensin II-induced hypertension and in tsA-201 cells expressing $Ca_V1.2$-TS channels (Figure 2.5H).

We investigated whether, as with WT $Ca_V1.2$ channels, the higher frequency of coupled gating events of $Ca_V1.2$-TS channels was associated with dislocation of CaM from the IQ domain in the C terminal of these channels. Accordingly, FRET between $Ca_V1.2$-TS-EGFP and CaM-tRFP was undetectable (n = 13 cells; Figure 2.5I). These data suggest that coupled gating of $Ca_V1.2$ channels is associated with displacement of CaM from the IQ domain in the C-terminal tail and contributes to enhanced channel function and Ca^{2+} influx during hypertension and TS.

2.4.8 AKAP150 increases the probability of coupled gating between $Ca_V1.2$ channels

The scaffolding protein AKAP150 targets PKCα to the cell membrane and interacts with the C-tail of $Ca_V1.2$ channels (Gao et al., 1997; Klauck et al., 1996; Oliveria et al., 2007). Therefore, we tested the hypothesis that PKCα activation and its targeting to the membrane by AKAP150 is necessary to induce coupled gating of $Ca_V1.2$ channels during CaM inhibition (Figure 2.7). Application of W7 increased the number of coupled $Ca_V1.2$ channel events in PKCα null ($PKC\alpha^{-/-}$; n = 5 cells), but not in AKAP150 null myocytes ($AKAP150^{-/-}$; n = 9 cells; $p < 0.05$). Because the expression of PKCα is similar in WT and $AKAP150^{-/-}$ myocytes, the lack of effect of W7 on $Ca_V1.2$ channels in $AKAP150^{-/-}$ was not due to decreased PKCα expression

(Navedo et al., 2008). These data suggest that CaM antagonists work downstream of PKCα and that AKAP150 participates in the molecular events that facilitate coupled gating of $Ca_V1.2$ channels.

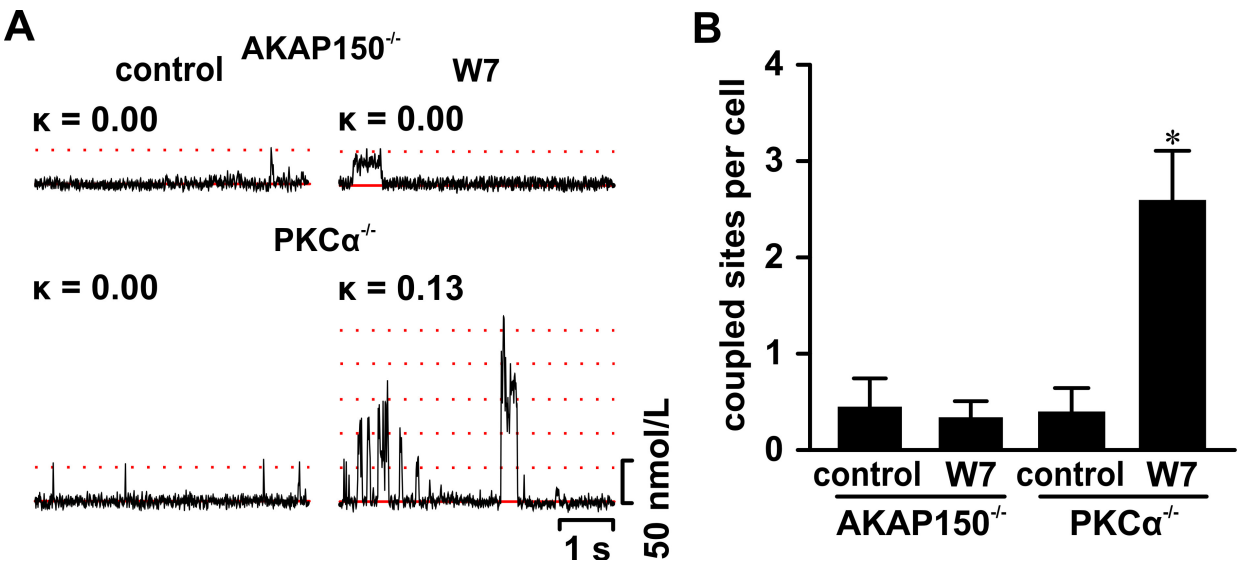

Figure 2.7. AKAP150, but not PKCα, is required for coupled gating of $Ca_V1.2$ channels. (A) Representative $\Delta[Ca^{2+}]_i$ records from Ca^{2+} sparklet sites in AKAP150$^{-/-}$ and PKCα smooth muscle cells under control conditions (right) and after exposure to 100 μmol/L W7. The coupling coefficient (κ) of these Cav1.2 channels is shown above each trace. Dotted lines show the amplitude of quantal levels. (B) Bar plot of the mean number of coupled sites per cell.

2.4.9 Coupling of $Ca_V1.2$ channels involves interactions between neighboring channels via their C-termini

We investigated the role of the C-terminal of $Ca_V1.2$ channels in coupled gating. To do this, a $Ca_V1.2$ construct lacking amino acids 1670-2171 (CaV1.2Δ1670X), which

eliminates a large section of the C-terminal tail, was expressed in tsA-201 cells (Figure 2.8A). These channels lack the putative AKAP-binding region. Unlike WT channels, $Ca_V1.2\Delta1670X$ channels showed no coupled gating activity under either control conditions or after the application of W7 (n = 5 cells), indicating that residues 1670-2171 of $Ca_V1.2$ are critical for coupled gating activity.

The C-termini of $Ca_V1.2$ channels could be involved in coupled gating by coming into close proximity. To examine this possibility, we expressed WT and TS $Ca_V1.2$ channels with EGFP or tRFP fused to their C-temini and determined FRET between channels (Figure 2.8B). Under control conditions, FRET between WT $Ca_V1.2$-EGFP and $Ca_V1.2$-tRFP was low (0.02 ± 0.02; n = 10 cells). This is consistent with the observation of a relatively low frequency of coupled $Ca_V1.2$ events under these experimental conditions (see Figure 2.1 above). Application of W7 or PDBu, which increases coupled gating of $Ca_V1.2$ channels, increased FRET between WT $Ca_V1.2$-EGFP and $Ca_V1.2$-tRFP channels to 0.16 ± 0.02 (n = 8 cells) and 0.23 ± 0.03 (n = 10 cells), respectively ($p < 0.05$). Interestingly, under control conditions, FRET was higher in cells expressing tRFP- and EGFP-tagged $Ca_V1.2$-TS channels (0.10 ± 0.01; n = 10 cells) than between WT $Ca_V1.2$ channels ($p < 0.05$; Figure 2.8B). These data suggest that the C-termini of $Ca_V1.2$ channels come into close proximity under conditions that favor coupled gating.

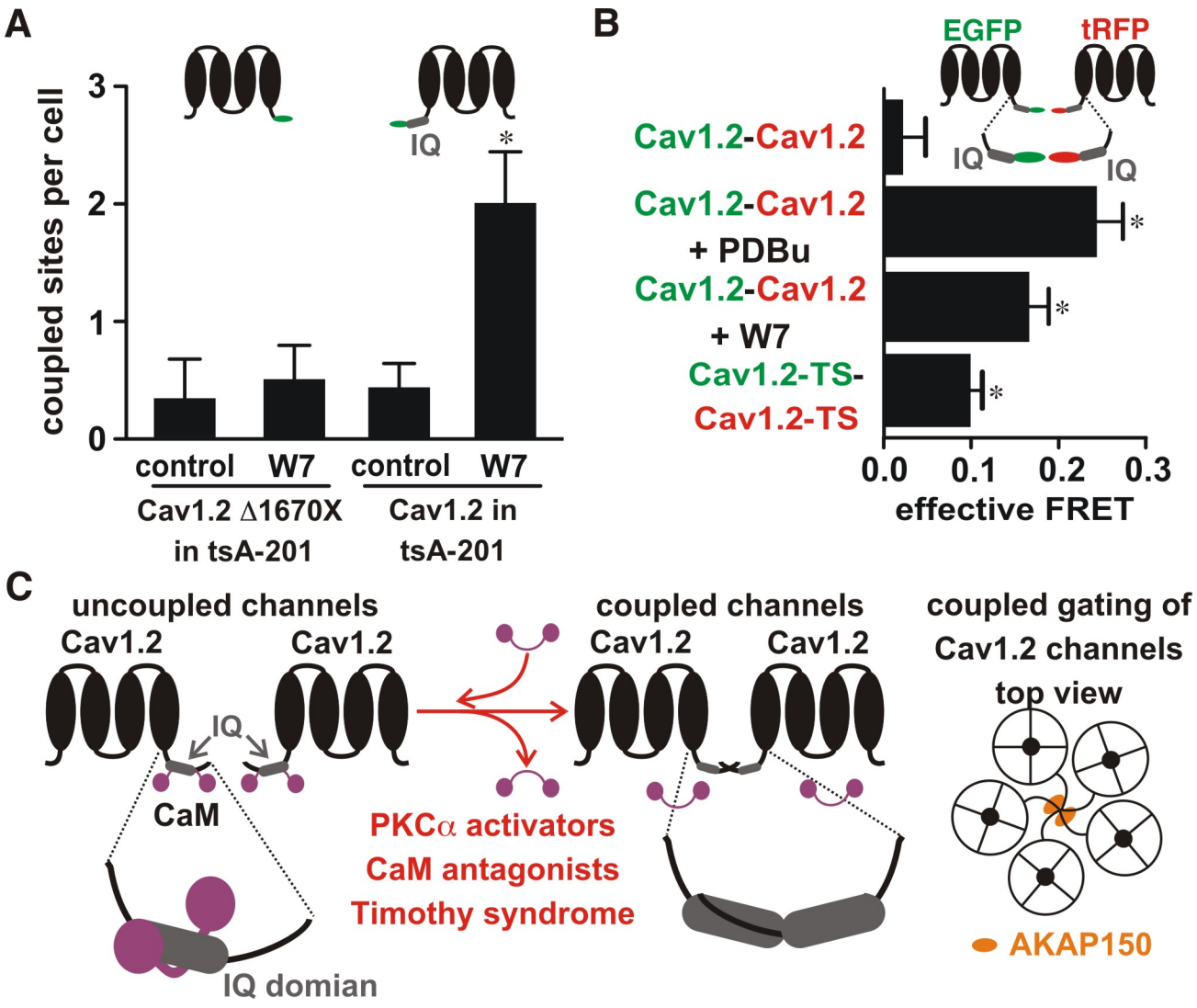

Figure 2.8. Coupled gating involves the C-tail of $Ca_V1.2$ channels.
A) Bar plot of number of sites showing coupling of Cav1.2 channels in cells expressing a truncated Cav1.2 channel (Cav1.2Δ1670X) or WT Cav1.2 channels before and after application of 100 µmol/L W7. (B) Bar plot of effective FRET between Cav1.2-TS-EGFP and Cav1.2-TS-tRFP or WT Cav1.2-EGFP and Cav1.2-tRFP before and after PDBu or W7. The inset shows a cartoon of Cav1.2-EGFP and Cav1.2-tRFP. (C) Proposed model for coupled gating of Cav1.2 channels.

2.5 Discussion

In this study, we demonstrated that a cluster of $Ca_V1.2$ channel proteins could be organized to facilitate their coordinated opening and closing. A cartoon of the proposed model for coupled gating of $Ca_V1.2$ channels is shown in Figure 2.8C. Our data suggest that CaM antagonists (e.g. W7 and CaM inhibitory peptide), activators of PKCα, or a specific $Ca_V1.2$ channel mutation (e.g. Timothy syndrome), that move CaM away from the IQ domain in the C-terminal tail of the channel promote coupled gating between $Ca_V1.2$ channels. Although at present the exact mechanisms underlying coupled gating between CaV1.2 are unclear, our FRET analysis of EGFP- and tRFP-tagged $Ca_V1.2$ channels suggests the possibility that coupled gating between these channels may involve transient interactions between a variable number (2-6) of adjacent channels via their C-termini. A recent report suggesting that the C-terminal of $Ca_V1.2$ channels dimerizes *in vitro* and another study using electron microscopy suggesting that $Ca_V1.2$ channels exist as dimers give additional credence to this view (Fallon et al., 2009; M.-C. Wang, Collins, et al., 2004).

An important feature of our model is that AKAP150 increases the probability of coupled gating presumably by facilitating interactions between the C-termini of $Ca_V1.2$. As introduced in Chapter 1, AKAP150 interacts with the C-termini $Ca_V1.2$ channels via mutual leucine zipper (LZ) domains (Oliveria et al., 2007).

Interestingly, AKAP150 also exists as dimers (Gold et al., 2011). Because AKAP150 interacts with only a subpopulation of $Ca_V1.2$ channels, this scaffolding protein promotes coupled gating in a fraction of channels, resulting in subcellular variations in $Ca_V1.2$ activity (Navedo et al., 2008). This represents a novel function of AKAP150 that is independent of its ability to target proteins to specific regions of the cell.

An important implication of our model is that the level of expression of AKAP150 is a critical determinant of coupled $Ca_V1.2$ channel activity in cardiac and smooth muscle cells for multiple reasons. We demonstrated that PKCα increases the frequency of coupled gating events. Interestingly, in the Timothy syndrome, the Gly-436-Arg substitution in $Ca_V1.2$ creates a putative phosphorylation site for CaM-dependent kinase II (CaMKII) (Erxleben et al., 2006). The actions of PKCα and CaMKII on WT and $Ca_V1.2$-TS are opposed by the Ca^{2+}/CaM-dependent phosphatase calcineurin. Note, however, that AKAP150 targets PKCα and calcineurin to the surface membrane. Accordingly, the level of coupled gating events between $Ca_V1.2$ channels may not be simply limited by AKAP150 expression, but also by the relative activities of nearby calcineurin, CaMKII, and PKCα.

These conditions for coupled gating between $Ca_V1.2$ channels impose technical challenges for the recording and analysis of the molecular mechanisms underlying these events. For example, since only a subpopulation of $Ca_V1.2$ channels could undergo coupled gating, the use of patch-clamp approaches to record currents from

relatively small areas of the membrane is likely to yield limited results in terms of the number of couple gating events per trial. However, our study suggests that optical recordings of $Ca_V1.2$ channels from relatively large portions of the surface may represent a more efficient approach to study coupled gating between these channels. For the same reasons, conventional biochemical approaches (e.g. co-IP) broadly used to examine direct, stable protein-protein interactions could be difficult to implement to study the molecular mechanisms of coupled gating between $Ca_V1.2$ channels. FRET could be used to circumvent these limitations. However, although powerful, this technique has its limitations because it reports the proximity of two fluorescent proteins (in our case EGFP and tRFP) and not necessarily the specific sections of the channel to which they are fused. Thus, currently, whether coupled gating between $Ca_V1.2$ channels involves direct physical interactions between the C-tails of adjacent channels or to an intermediary protein such as AKAP150 and how this translates into the simultaneous opening and closing of their pores is unclear. Future experiments should address this critical issue.

Our data provide insights into the mechanisms by which PKCα could induce coupled gating between $Ca_V1.2$ channels. We found that PKC activation moves CaM away from the IQ domain of $Ca_V1.2$ channels. Yet, although PKCα increases coupled $Ca_V1.2$ channel activity, this kinase was not required for the induction of coupled activity since application of W7 induced coupled gating of $Ca_V1.2$ channels in $PKC\alpha^{-/-}$ arterial myocytes. Together, these findings suggest that PKCα activation promotes coupled gating between $Ca_V1.2$ channels by inducing the movement of CaM away

from the IQ domain in the C-tail of $Ca_V1.2$. However, our data indicate that phosphorylation of $Ca_V1.2$ channel by this kinase *per se* is not necessary to induce coupled gating. Subsequent studies should examine if a similar mechanism is involved in coupled gating between $Ca_V1.2$-TS channels.

An intriguing observation in this study is that coupling between $Ca_V1.2$ channels is transient, with the number of channels opening and closing simultaneously varying with time and between sites. In many instances, we saw sets of 2, 3, 4, 5 and 6 channels opening and closing together. We did not detect a particular pattern in terms of the number of channels undergoing coupled gating. This coupling mechanism is fundamentally different from that of ryanodine receptors (RyRs) in cardiac muscle, in which tetramers of tightly coupled (i.e. $\kappa \approx 1$) channels undergo stable openings under physiological conditions (Marx et al., 2001). At present, the precise mechanisms that control the coupling strength between $Ca_V1.2$ channels and how it changes under physiological (e.g. changes in membrane potential) and pathological conditions is unclear.

Although the effects of coupled gating of $Ca_V1.2$ channels on excitation-contraction (EC) coupling in cardiac and smooth muscle were not examined in this study, previous studies suggest coupling of these channels could have important implications in this process. As previously introduced in Chapter 1, in ventricular myocytes, $Ca_V1.2$ channels and RyRs in nearby junctional sarcoplasmic reticulum (jSR) form a functional unit called a “couplon” (Franzini-Armstrong et al., 1999).

Ca^{2+} influx via $Ca_V1.2$ activates small clusters of RyRs via the mechanism of Ca^{2+}-induced Ca^{2+} release, producing Ca^{2+} sparks. In these cells, activation of multiple couplons during an action potential results in a cell-wide increase in $[Ca^{2+}]_i$ that activates contraction. Because the probability of Ca^{2+} spark occurrence (P_{Spark}) is proportional to the $Ca_V1.2$ current and local $[Ca^{2+}]_i^2$, it is intriguing to speculate that P_{Spark} is likely to be higher in couplons with coupled $Ca_V1.2$ channels than in couplons with independently gating channels (L.F. Santana et al., 1996). An important physiological observation by Inuoe and Bridge that suggested at the phase II plateau phase of the cardiac AP, the opening ~10-15 $Ca_V1.2$ channels is necessary to reach the high Ca^{2+} spark activation probability of >0.9 also tantalizingly suggests that, even with the transient nature of coupled gating observed in WT $Ca_V1.2$ channels, coupled gating may be physiologically important at modulating EC coupling (Inoue & Bridge, 2003). Given that the open probability of a single $Ca_V1.2$ channel at the AP plateau voltage of +50 mV is ~0.5, the role of positive cooperativity brought about by coupled gating may in fact be necessary for the maintenance of fidelity in EC coupling (Dixon, Yuan, Cheng, Navedo, & Santana, 2012; M Rubart et al., 1996). Unlike ventricular myocytes, in smooth muscle, $Ca_V1.2$ channels and RyRs are not tightly coupled. In these cells, activation of $Ca_V1.2$ channels results in an increase in $[Ca^{2+}]_i$ that directly activates contractile proteins. Thus, an increase in coupled gating of $Ca_V1.2$ channels could result in an increase in Ca^{2+} influx and thus global $[Ca^{2+}]_i$. Subsequent studies should examine the test these intriguing hypotheses.

To conclude, we propose that coupled gating of $Ca_V1.2$ channels could translate into a larger increase in L-type Ca^{2+} channel activity than by an increase in independent gating activity. The simultaneous activation of a small cluster of channels would enhance Ca^{2+} influx per gating event. Under physiological conditions, this could increase the activation probability of Ca^{2+}-dependent proteins involved in contraction, excitability, memory, and gene expression. In TS, coupled gating of $Ca_V1.2$ channels could increase the probability of Ca^{2+}-dependent arrhythmias and increase Ca^{2+}-dependent neurotoxicity. In hypertensive smooth muscle, coupled gating of $Ca_V1.2$ channels could increase myogenic tone and hence blood pressure. We propose that coupled gating of $Ca_V1.2$ channels may represent a general mechanism that contributes to Ca^{2+} influx and excitability under physiological and pathological conditions.

Chapter 3: Restoration of normal L-type Ca^{2+} channel function during Timothy syndrome by ablation of an anchoring protein

3.1 Summary

As was introduced in Chapter 1, L-type Ca^{2+} ($Ca_V1.2$) channels shape the cardiac action potential waveform and are essential for excitation-contraction coupling in the heart. A gain-of-function G406R mutation in a cytoplasmic loop of $Ca_V1.2$ channels causes long QT syndrome 8 (LQT8), a disease also known as Timothy syndrome. However, the mechanisms by which this mutation enhances $Ca_V1.2$-LQT8 currents and generates lethal arrhythmias are unclear. As was covered in the previous chapter, AKAP150 is necessary in the mechanism of coupled gating, and the frequency of coupled gating was increased in heterologously expressed $Ca_V1.2$-LQT8 channels in tsA-201 cells. We wanted to test the hypothesis that the anchoring protein AKAP150 modulates $Ca_V1.2$-LQT8 channel gating in ventricular myocytes. Using a combination of molecular, imaging, and electrophysiological approaches, we discovered that $Ca_V1.2$-LQT8 channels are abnormally coupled to AKAP150. A pathophysiological consequence of forming this aberrant ion channel-anchoring protein complex is enhanced $Ca_V1.2$-LQT8 currents. This occurs through

a mechanism whereby the anchoring protein functions like a subunit of $Ca_V1.2$-LQT8 channels that stabilizes the open conformation and augments the probability of coordinated openings of these channels. Ablation of AKAP150 restores normal gating in $Ca_V1.2$-LQT8 channels and protects the heart from arrhythmias. Importantly, we found that CaMKII inhibition does not restore normal gating in $Ca_V1.2$-LQT8 channels. In conclusion, we propose that AKAP150-dependent changes in $Ca_V1.2$-LQT8 channel gating may constitute a novel general mechanism for $Ca_V1.2$-driven arrhythmias.

3.1.1 Abbreviations

AKAP150 = A-kinase anchoring protein 150
AP = action potential
$[Ca^{2+}]_i$ = intracellular Ca^{2+} concentration
CaM = calmodulin
CaMKII = Ca^{2+}/calmodulin-dependent kinase II
$Ca_V1.2$-LQT8 = $Ca_V1.2$ channels with the long QT syndrome mutation
$Ca_V1.2$-WT = wild type $Ca_V1.2$ channels
EC coupling= excitation-contraction coupling
ECG = electrocardiogram
LQT8 = long QT syndrome 8 (Timothy syndrome)
LZ = leuzine zipper
MEF = mouse embryonic fibroblast
TdP= Torsades de pointes
tRFP = tag red fluorescent protein
WT = wild type

3.2 Introduction

After uncovering evidence in the previous chapter that strongly suggest that a subpopulation of L-type Ca^{2+} ($Ca_V1.2$) channels undergo a novel coupled gating modality, which involves the association of a subpopulation $Ca_V1.2$ channels with AKAP150 (rodent ortholog of AKAP79/150) as a part of its mechanism. Interestingly, we also observed an increase in coupled gating in $Ca_V1.2$-LQT8 channels bearing the single amino acid substitution (G406R) that causes Timothy syndrome, also known LQT8, when heterologously expressed in tsA-201 cells (Splawski et al., 2004, 2005). As was introduced in Chapter 1, Timothy syndrome is a multisystem disease characterized by gain-of-function in $Ca_V1.2$-LQT8 channels (Splawski et al., 2004). $Ca_V1.2$ channels are expressed in the sarcolemma of atrial and ventricular myocytes where they play a critical role in activating Ca^{2+} release from the sarcoplasmic reticulum (SR) during excitation-contraction (EC) coupling, which was covered in great detail in Chapter 1. The magnitude and time course of the $Ca_V1.2$ current determines the waveform of the cardiac action potential (AP) (Luo & Rudy, 1991). Thus, changes in $Ca_V1.2$ channel function can have profound effects on cardiac EC coupling and excitability. Accordingly, Timothy syndrome is characterized by prolongation of the electrocardiogram (ECG) QT interval and lethal arrhythmias, which is why it is also known as long QT syndrome 8 (LQT8). Interest in the mechanisms of LQT8 has been intense because it is a multisystem disease, with many patients also afflicted by autism. Thus, a single amino acid mutation in

$Ca_V1.2$ causes clinically significant disorders in the cardiac and central nervous systems.

Electrophysiological and imaging studies introduced in the two previous chapters have revealed two distinctive features of LQT8 mutant $Ca_V1.2$ channels ($Ca_V1.2$-LQT8). *First*, these channels inactivate at a slower rate than wild type (WT) channels (Barrett & Tsien, 2008; Splawski et al., 2004; Thiel et al., 2008). *Second*, small clusters of $Ca_V1.2$-LQT8 channels have a higher probability of undergoing coordinated openings and closings ("coupled gating") than WT channels (Navedo et al., 2010). Although recent reports suggested that the G406R substitution in $Ca_V1.2$ creates a new phosphorylation site for the Ca^{2+}/calmodulin-dependent kinase II (CaMKII), which contributes to an increase in the open probability (P_o) of $Ca_V1.2$-LQT8 channels, others suggested that phosphorylation by CaMKII is *not* necessary for their slower rate of inactivation (Erxleben et al., 2006; Thiel et al., 2008; Viktor Yarotskyy et al., 2009). Thus, the mechanism by which the activity of $Ca_V1.2$-LQT8 channels is coordinated to generate irregular cardiac rhythm remained unclear.

A potential mechanism regulating the activity of $Ca_V1.2$-LQT8 channels involves the anchoring protein AKAP150. AKAP150 targets specific protein kinases and phosphatases to regions near $Ca_V1.2$ channels in ventricular myocytes and neurons (Coghlan et al., 1995; Nichols et al., 2010). Furthermore, AKAP150 binds to the carboxyl tail of $Ca_V1.2$ channels via leucine zipper (LZ) motifs in these two proteins, facilitating physical interactions between $Ca_V1.2$ carboxyl tails (Oliveria et al., 2007).

AKAP150 increases the probability of long openings and coupled gating events between $Ca_V1.2$ channels (Navedo et al., 2010). At present, however, whether the interaction with AKAP150 modulates the abnormal $Ca_V1.2$-LQT8 channel activity is unknown.

Here, we employed a combination of cellular, molecular, imaging, and electrophysiological approaches to investigate this important issue *in situ* in cardiac myocytes from a transgenic mouse model of LQT8, which we generated for this study. We discovered that AKAP150 is required for abnormal gating of $Ca_V1.2$-LQT8 channels. Importantly, our data indicate that ablation of AKAP150 corrects arrhythmogenic $Ca_V1.2$-LQT8 channel activity in ventricular myocytes.

3.3 Materials and Methods

3.3.1 Generation of LQT8 mice

pcDNA3 plasmids encoding WT rabbit $Ca_V1.2$ Ca^{2+} channels (NCBI Reference Sequence: NC_013676.1) were provided by Dr. Diane Lipscombe. We generated the rabbit homolog of the human LQT8 (Timothy syndrome) $Ca_V1.2$ (G436R, Rabbit; G406R Human) (Erxleben et al., 2006). tRFP was fused to the carboxyl terminal of $Ca_V1.2$ by fusion PCR cloning (BPS Bioscience). Then, the $Ca_V1.2$-tRFP was cut out by HindIII and cloned into the vector pBS-αMHC-hGH, a generous gift from Dr. Jeffrey Robbins (University of Cincinnati, Ohio). The construct was linearized by NotI, and the transgene was purified from vector backbone by QIAEX II Gel Extraction Kit (Qiagen). The 13kb transgene was microinjected into pronuclei of fertilized single-cell C57BL/6 × C3H mouse embyos. After injection, the eggs are surgically transferred to the oviducts of time-mated pseudopregnant foster mothers. A combination of PCR and Southern blotting of genomic DNAs identified the founders. The cardiac-specific expression of the transgene was confirmed by RT-PCR and biotinylation Western blot (Figure 3.3 A-B).

3.3.2 Isolation of ventricular myocytes

Mice (WT littermates, LQT8, and LQT8/AKAP150$^{-/-}$) were euthanized with a lethal dose of sodium pentobarbital (100 mg/kg) administered intraperitoneally as approved by the University of Washington Institutional Animal Care and Use Committee. Ventricular myocytes were isolated using a Langendorff perfusion apparatus as previously described (Rossow et al., 2009; Shioya, 2007). The isolated ventricular myocytes were kept at room temperature (22-25^{o}C) in Tyrode's solution with the following constituents (mmol/L): 140 NaCl, 5 KCl, 10 HEPES, 10 glucose, 2 $CaCl_2$, and 1 $MgCl_2$; pH 7.4 and used 0.5-6 hours after isolation.

3.3.3 $Ca_V1.2$ constructs and their expression in mouse embryonic fibroblasts (MEFs)

pcDNA3 plasmids encoding calcium channel accessory subunits (Ca_V-β_{2a}, GenBank accession number: M88751, and Ca_V-$\alpha_2\delta_1$, GenBank accession number: AF286488) were provided by Dr. Diane Lipscombe. Plasmids for the enhanced green fluorescent protein (EGFP) was purchased from Invitrogen. EGFP was fused to the C-terminus of $Ca_V1.2$ and $Ca_V1.2$-LQT8, yielding $Ca_V1.2$-LQT8-EGFP and $Ca_V1.2$-EGFP. Cultures of MEF cells were maintained in Dulbecco's Modified Eagle Medium supplemented with 10% fetal bovine serum, L-glutamine (2 mmol/L), 1% streptomycin and penicillin solution, 1% Modified Eagle Medium non-essential amino acids, and 100 nmol/L 2-mercaptoethanol. Cells were transiently transfected with

the pcDNA3 clones of $Ca_V1.2$-WT-EGFP or $Ca_v1.2$-LQT8-EGFP, Ca_V-β_{2a}, and Ca_V-$\alpha_2\delta_1$ using JetPEI (Polyplus). Successfully transfected cells were identified on the basis of EGFP fluorescence.

3.3.4 Coupled Markov chain model

Membrane currents were analyzed using a binary coupled Markov chain model originally described by Chung and Kennedy to simulate and fit independent records of partially coupled channels (Chung & Kennedy, 1996; Navedo et al., 2010). The program was written in Matlab® language, and the full code is given in Appendix A. Channel openings were identified using a half-amplitude protocol, with the quantal level for a unitary event set at 0.50 pA for currents. The activity of $Ca_v1.2$ channels during a patch-membrane recorded I_{Ca} time course was modeled as a first order, discrete Markov chain, and the Markovian transition matrix was estimated from the current and their corresponding channel opening time courses using the built-in Hidden Markov parameter estimation function in Matlab®. The estimated transition matrix was modeled as a partially coupled Markov chain where a dimensionless parameter (κ) is the coupling coefficient between fully uncoupled and fully coupled cases. In addition to the coupling coefficient (κ), the model has two additional parameters: the channel open-to-open probability (ρ) and the channel closed-to-closed probability (ς), and together they fully describe the contribution from the fully uncoupled case to the transition matrix. For each record, the optimum set of

parameters (κ, ρ, ς) for the partially coupled Markov chain model was fitted using a gradient descent algorithm.

The utility of this model is that it is a “lumped” model, where the channels switch between the binary observable states of either “open” or “closed,” and therefore, instead of trying to deduce the gating kinetics of multiple channels, which involves many free parameters, our model has only three free parameters, including the coupling coefficient (κ). It does not completely describe the actual kinetics of the channel and consequently the transition probabilities obtained from this lumped model are not interpreted as rate constants.

3.3.5 Electrophysiology

All electrophysiological recordings were performed while cells were superfused with saline solutions at room temperature (≈ 22 ˚C). For whole-cell L-type Ca^{2+} currents (I_{Ca}), membrane potential was controlled via the patch-clamp technique using an EPC10 (HEKA) or an Axopatch 200B amplifier (Molecular Devices). Data were acquired at 10 kHz and low-pass filtered at 5 kHz. Ventricular myocytes and MEFs were continuously superfused with Tyrode’s solution. Once whole-cell configuration has been successfully established in myocytes, a solution with the following constituents (mmol/L) was exchanged: 140 N-methyl d-glucamine (NMDG), 5 $CsCl_2$, 2 $CaCl_2$, 1 $MgCl_2$, 10 glucose, 10 HEPES, adjusted to pH 7.4 with HCl, and 50 μmol/L of tetracaine was added to block SR Ca^{2+} induced Ca^{2+} release. For MEFs

experiments, this solution was exchanged for a solution containing a similar composition except that $CaCl_2$ was 20 mmol/L, NMDG concentration was 120 mmol/L, and no tetracaine was added. Pipettes for whole-cell patch-clamp were pulled using a Flaming-Brown type puller (Sutter Instruments) with nominal resistance of 1-2 MΩ and filled with a solution composed of (mmol/L): 87 Cs-aspartate, 20 CsCl, 1 $MgCl_2$, 5 MgATP, 10 EGTA, 10 HEPES, and 4.7 $CaCl_2$, adjusted to pH 7.2 with CsOH. The free [Ca^{2+}] was 150 nmol/L, as calculated using the MaxChelator program (Patton, Thompson, & Epel, 2004). I_{Ca} was evoked from both myocytes and MEFs by 200 ms long depolarization pulses from -80 mV to -40 to +50 mV. For myocytes, an additional 100 ms long voltage step to -40 mV immediately preceded the depolarization pulses as to inactivate Ca^{2+} conductance through voltage-gated Na^+ channels. For experiments involving treatments with the chemical inhibitors Rp-cAMP, Ht31, and KN-93, the inhibitors were dissolved in the appropriate external solution for whole-cell I_{Ca} recordings to the appropriate concentration (100 µmol/L for Rp-cAMP, 10 µmol/L Ht31, and 5 µmol/L for KN-93). We recorded post-treatment I_{Ca} 10 minutes after starting superfusion with the inhibitor solution.

For action potential (AP) recordings in ventricular myocytes, we used the whole-cell current clamp mode of the Axopatch 200B amplifier. Cells were continuously superfused with Tyrode's solution. Pipettes for AP recordings had nominal resistance of 1-2 MΩ and filled with a solution composed of (mmol/L): 30 KCl, 110 K-aspartate, 10 HEPES, 10 NaCl, 5 MgATP, adjusted to pH 7.2 with KOH. APs were

excited by 5 ms long current injections of 7 nA occurring every 1 s. This relatively slow stimulation rate and low solution temperature (≈ 22 ˚C) likely prolonged the action potential of ventricular myocytes. Membrane voltage records were sampled at 10 kHz and low-pass filtered at 2 kHz. Early afterdepolarizations (EADs) were visually identified as spontaneous depolarizations in membrane voltage during phases II and III of the cardiac AP, while delayed afterdepolarizations (DADs) were visually identified as spontaneous depolarizations in membrane voltage during phase IV of the cardiac AP.

We also recorded L-type Ca^{2+} channel currents from cell-attached patches in ventricular myocytes. Data were acquired using an Axopatch 200B amplifier at 10 kHz and low-pass filtered at 2 kHz. The patch pipettes were pulled using a Flaming-Brown type puller and heat polished using a microforge (Narishige) with a nominal resistance of 2-3 MΩ. The pipette solution contained (mmol/L): 20 $CaCl_2$ (charge carrier), 130 TEA, and 10^{-3} tetrodotoxin (TTX), adjusted to pH = 7.2 with HCl. Voltage gated Na^+ channels were blocked with TTX, while voltage gated K^+ channels were blocked with TEA. The L-type Ca^{2+} channel agonist BayK-8644 (500 nM) was included in the pipette solution to increase the mean open time and P_o of these channels. Currents were recorded while cells were exposed to a solution containing (mmol/L): 145 KCl, 10 HEPES, and 10 NaCl (pH = 7.4). L-type Ca^{2+} channel currents were evoked by a 1 s step depolarization to -30 mV from the holding potential of -80 mV. Membrane currents were analyzed using pCLAMP 10

(Molecular Devices). All experiments were performed at room temperature (22-25^{o}C).

3.3.6 Confocal imaging of Ca^{2+} signals

Ventricular myocytes were loaded with the membrane-permeable acetoxymethyl-ester form of Fluo-4 (Fluo-4 AM, Invitrogen) for measurement of $[Ca^{2+}]_i$ as previously described (Nichols et al., 2010). Cells were placed in a perfusion chamber and incubated with normal Tyrode at 22 –25 °C. Field stimulation was performed with two platinum wires (0.5 cm separation) placed at the bottom of the perfusion chamber. An IonOptix Myopacer (IonOptix Corp) stimulator was used to deliver square voltage pulses (4 ms duration) with amplitude of 35 volts at a frequency of 1 Hz. We imaged temporal fluorescence fluctuations caused by $[Ca^{2+}]$ transients using the line-scan mode (2 ms/line) of our Olympus Fluo View 1000 confocal microscope with an Olympus APON (60X, NA = 1.49) oil-immersion lens. Fluo-4 was excited with a 473 nm solid-state laser. Line-scan images were analyzed using ImageJ. Background subtracted fluorescence signals were normalized by dividing fluorescence at each point (F) with the baseline fluorescence (F_0). Spontaneous Ca^{2+} release (SCR) events were identified manually as increases in fluorescence that were not elicited by stimulation.

3.3.7 Analysis of the spatial distribution of $Ca_V1.2$-WT and tRFP-tagged $Ca_V1.2$-LQT8 channels

We used immunofluorescence approaches to determine the spatial distribution of $Ca_V1.2$-WT in WT and AKAP150$^{-/-}$ myocytes. To do this, myocytes were plated on BD Cell-Tak coated cover slips. Cells were allowed to attach for 4 hours. Cells were then fixed in a solution containing 2% paraformaldehyde, 75 mmol/L Lysine and 10 mmol/L sodium periodate in phosphate buffer (McLean & Nakane, 1974). Cells were washed three times in phosphate buffered saline (PBS), and permeabilized with 0.075% Triton X-100/PBS and incubated for 30 minutes in blocking buffer containing 2% donkey serum, 20% goat serum, and 1% bovine serum albumin in pearmeabilization solution. Specific L-type $Ca_V1.2$ channel α-1C subunit (Sigma) antibody was used for immunolabeling of L-type $Ca_V1.2$ channels. Cells were extensively washed in PBS and incubated for 2 hours with donkey anti-rabbit Alexa Fluor 488-conjugated (5 mg/mL) antibody (Molecular Probes). Cells were visualized using an Olympus Fluo View 1000 confocal laser-scanning microscope equipped with an UPLSAPO 60X water lens (NA = 1.2) and a zoom of 1.9 (pixel size = 0.19 µm).

The same confocal microscope was used to image tRFP-tagged $Ca_V1.2$-LQT8 in living, freshly dissociated LQT8 and LQT8/AKAP150$^{-/-}$ myocytes. tRFP was excited with a 559 nm laser. To quantify the number of tRFP-tagged $Ca_v1.2$-LQT8 clusters

in ventricular myocytes, maximum intensity projections were generated from Z-stacks. Clusters were counted and measured using ImageJ software (National Institute of Health). In brief, projected images were loaded into ImageJ. A threshold range that enabled segmentation of clusters from the background was set and the image was converted to a binary form. The number of clusters and their feret diameter was then obtained. For an example of this analysis see Figure 3.1 below.

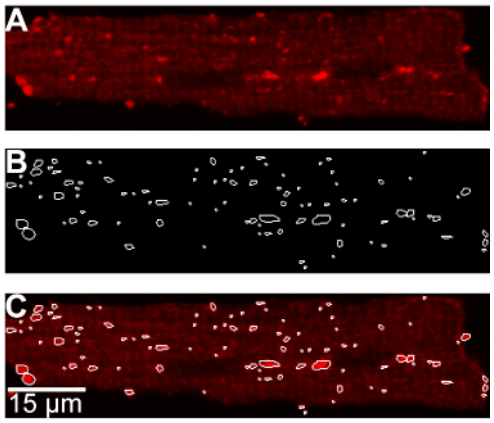

Figure 3.1: Quantification of $Ca_V1.2$-LQT8 channel clusters in LQT8 myocytes.
(A) A typical confocal image of a $Ca_V1.2$-LQT8 cardiomyocyte. **(B)** Outlines of clusters obtained using the particle analysis tool in ImageJ. **(C)** Confocal image shown in **(A)** with an overlay of the outlined clusters shown in **(B)**.

3.3.8 Electrocardiogram (ECG) Telemetry

Ambulatory telemetry recordings were performed in WT littermate, LQT8, AKAP150$^{-/-}$, and LQT8/AKAP150$^{-/-}$ mice. Radiotelemetry ECG monitors (Data Sciences International) were implanted intraperitoneally, with the electrode leads sutured in place subcutaneously over the chest wall and assuming a lead II configuration. The

mice were under isoflurane anesthesia during surgery, and they were given buprenorphine for analgesia for 24 hours post-surgery. A week after the surgery the mice were acclimatized to the treadmill exercise regimen. The exercise treadmill (Columbus Instruments) was started at 5 m/minute and the shock grid turned on, and the speed was increased by 1 m/minute every minute. The mice were exercised for 15 minutes per session or until they reached exhaustion, which was defined as greater than 5 seconds spent resting on the shock grid, at which time the shock grid was turned off. After acclimatization, the mice were exercised according to the regimen, during which their ECGs were recorded. The ECG records were analyzed using the ECG Analysis software (DSI), which automatically detected the QT intervals and arrhythmic events. The software used Bazett's formula to calculate the heart rate corrected QT interval (QT_C):

$$QT_c = \frac{QT}{\sqrt{RR}},$$

where QT is the uncorrected QT interval and RR is the RR interval (Vincent, Timothy, Leppert, & Keating, 1992).

3.3.9 Western blots

For these experiments, we used acutely dissociated ventricular myocytes from WT littermates, LQT8, AKAP150$^{-/-}$, and LQT8/AKAP150$^{-/-}$ mice. Western blots were

performed as recently described (Bannister et al., 2009). Briefly, myocytes were washed 3 times with ice-cold PBS and subsequently incubated with PBS containing 1.0 mg/mL EZ-Link Sulfo-NHS-LC-LC-biotin (Thermo Scientific) for 60 minutes at 4°C. After labeling, the cells were washed 3 times in ice-cold PBS containing 100 mmol/L glycine to quench and remove excess biotin reagent and by-products. Biotinylated myocytes were homogenized in radio-immunoprecipitation assay (RIPA) buffer and cellular debris removed by centrifugation. Total protein was then determined by bicinchoninic acid (BCA) analysis. 480 μg proteins were mixed with 120μl NeutrAvidin agarose resin (Thermo Scientific) and incubated overnight for avidin pull-down of biotinylated surface proteins. Following pull down, the supernatant comprised the non-biotinylated (cytosolic) protein fraction, while surface proteins remained bound to the avidin beads. Proteins were eluted from beads by boiling in SDS-PAGE sample buffer and analyzed by Western blotting using standard techniques. We also performed Western blotting on crude cell homogenates, proteins pulled down by avidin, and the leftover supernatant against GAPDH, a cytosolic protein, as quality control to ensure the specificity of the biotinylation reaction against membrane proteins (Figure 3.2). Anti-$Ca_V1.2$ antibody was purchased from Alomone Labs (Cat# ACC-003). Anti-GAPDH antibody was purchased from Sigma-Aldrich (Cat# G8795).

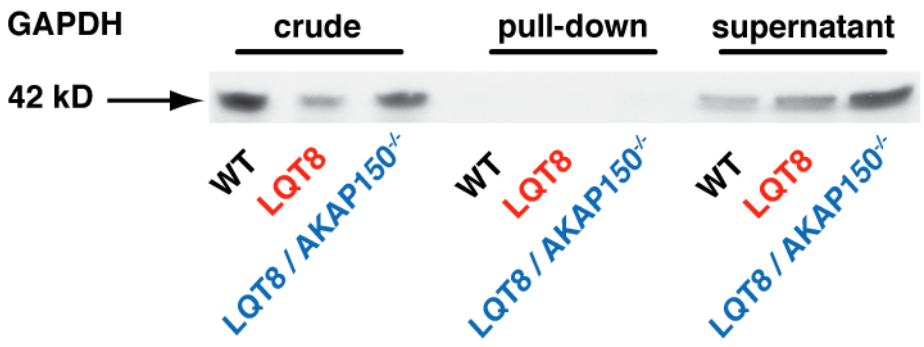

Figure 3.2: Avidin pull-down of biotinylated protein is specific for sarcolemmal proteins.
A Western blot showing GAPDH from crude cell homogenate (crude), proteins pulled down by avidin (pull-down), and the remaining supernatant from WT, LQT8, and LQT8/AKAP150$^{-/-}$ ventricular myocytes. GAPDH, a cytosolic protein, is absent from the avidin bound proteins.

3.3.10 Statistics

Data are presented as mean ± SEM. Two-sample comparisons were made using a student's T-test. A *p* value of less than 0.05 was considered significant. The asterisk (*) symbol is used in the figures to illustrate a significant difference between groups ($p<0.05$).

3.4 Results

	WT	LQT8	AKAP150$^{-/-}$	LQT8/ AKAP150$^{-/-}$
Western blot				
% $Ca_V1.2$-LQT8	0	41 ± 5	0	43 ± 4
Whole –cell I_{Ca}				
r_{50} at +10 mV	0.21 ± 0.05	0.39 ± 0.03*	0.22 ± 0.03	0.24 ± 0.02
Maximum amplitude (pA/pF)	-3.98 ± 0.99	-5.12 ± 0.60	-3.59 ± 0.23	-4.27 ± 0.36
On-cell I_{Ca}				
NP_o	0.0121 ± 0.002	0.110 ± 0.042*	n.d.**	0.017 ± 0.007
Coupling coefficient (κ)	0.029 ± 0.005	0.134 ± 0.015*	n.d.	0.033 ± 0.013
Fraction coupled	0.08 ± 0.04	0.43 ± 0.10*	n.d.	0.10 ± 0.06
τ_{short} (ms)	0.8	1.3	n.d.	0.6
τ_{long} (ms)	-	9.4	n.d.	-
$[Ca^{2+}]_i$ transient				
Amplitude (F/F_0)	3.5 ± 0.2	4.8 ± 0.4*	2.5 ± 0.5	3.3 ± 0.1
Amplitude + 100 nM ISO (F/F_0)	5.5 ± 0.4*	7.1 ± 0.2*	2.7 ± 0.4	3.4 ± 0.1
AP				
APD_{90} (ms)	30 ± 5	253 ± 41*	56 ± 5	71 ± 6
(EAD or DAD) / s	0.06 ± 0.04	1.02 ± 0.08*	0	0.10 ± 0.03
ECG and arrhythmia				
Resting HR (beats/min)	694 ± 27	692 ± 23	677 ± 4	695 ± 18
Exercise HR (beats/min)	748 ± 3	757 ± 3	744 ± 4	755 ± 1
Arrhythmia frequency (% animals w/ tachyarrhythmia)	0	60%	0%	0%
QT_c Bazet (ms)	97 ± 1	116 ± 1*	105 ± 1	108 ± 1
Hypertrophy				
Heart weight/Body weight (mg/g)	4.75 ± 0.32	6.62 ± 0.65*	4.86 ± 0.36	5.07 ± 0.15
Cardiac myocyte length (μm)	107.2 ± 7.5	137.2 ± 8.9*	105.5 ± 4.3	103.2 ± 3.6
Cardiac myocyte width (μm)	25.8 ± 1.6	34.3 ± 2.0*	29.8 ± 5.5	24.6 ± 1.5
Contractility				
% Maximum fractional shortening	96 ± 2	91 ± 3	96 ± 2	96 ± 3
% Maximum fractional shortening + 100 nmol/L ISO	89 ± 3	84 ± 3	97 ± 2*	95 ± 2

3.4.1 Phenotypic characteristics of LQT8 mice.

*p<0.05 **n.d.=not determined

Table 3.1. Phenotypic characteristics of LQT8 mice.

3.4.2 Ablation of AKAP150 protects against cardiac hypertrophy during LQT8

We generated a transgenic mouse that expresses $Ca_V1.2$-LQT8 channels fused to the tag-red fluorescent protein (tRFP) solely in cardiac myocytes (LQT8; Figure 3.3A) and crossed them with AKAP150 null mice (LQT8/AKAP150$^{-/-}$) (Tunquist et al., 2008). Table 3.1 summarizes 21 different anatomical and functional features of these mice. We found that the heart-to-body weight ratio of LQT8 hearts was larger than that of WT, AKAP150$^{-/-}$, and LQT8/AKAP150$^{-/-}$ mice. Indeed, LQT8 myocytes were longer and wider than WT, AKAP150$^{-/-}$, and LQT8/AKAP150$^{-/-}$ myocytes. These findings suggest that expression of $Ca_V1.2$-LQT8 promotes cardiac hypertrophy and loss of AKAP150 protects LQT8 mice against it.

3.4.3 AKAP150 is not required for the expression or spatial organization of $Ca_V1.2$-LQT8 channels in adult ventricular myocytes

Western blot analysis of biotinylated endogenous WT $Ca_V1.2$ ($Ca_V1.2$-WT) and $Ca_V1.2$-LQT8 indicated that sarcolemmal $Ca_V1.2$-WT expression was similar in WT, LQT8, AKAP150$^{-/-}$, and LQT8/AKAP150$^{-/-}$ myocytes (Figure 3.3B). $Ca_V1.2$-LQT8 channels comprised 41 ± 5 (n = 6 mice) and 43 ± 4% (n = 6 mice) of the total sarcolemmal $Ca_V1.2$ population in LQT8 and LQT8/AKAP150$^{-/-}$ myocytes, respectively. Like $Ca_V1.2$-WT channels in WT and AKAP150$^{-/-}$ myocytes, $Ca_V1.2$-LQT8 channels were prominently expressed along the transverse tubules (T-

tubules) of LQT8 and LQT8/AKAP150$^{-/-}$ myocytes. However, unlike Ca_V1.2-WT channels, Ca_V1.2-LQT8 channels were also expressed in the intercalated discs and seemed to form multiple clusters in the sarcolemma and near the nuclear envelope of LQT8 and LQT8/AKAP150$^{-/-}$ cells (Figure 3.3C). The number of Ca_V1.2-LQT8 clusters were similar in LQT8 (Figure 3.2, 154 ± 7 clusters/cell, n = 7) and LQT8/AKAP150$^{-/-}$ cells (142 ± 68 clusters/cell, n = 5; p >0.05) (see Methods and Materials for a description of this analysis). Collectively, these data suggest that Ca_V1.2-LQT8 and CaV1.2-WT channels are differentially expressed in ventricular myocytes, but that AKAP150 does not regulate the expression or distribution of these channels in these myocytes.

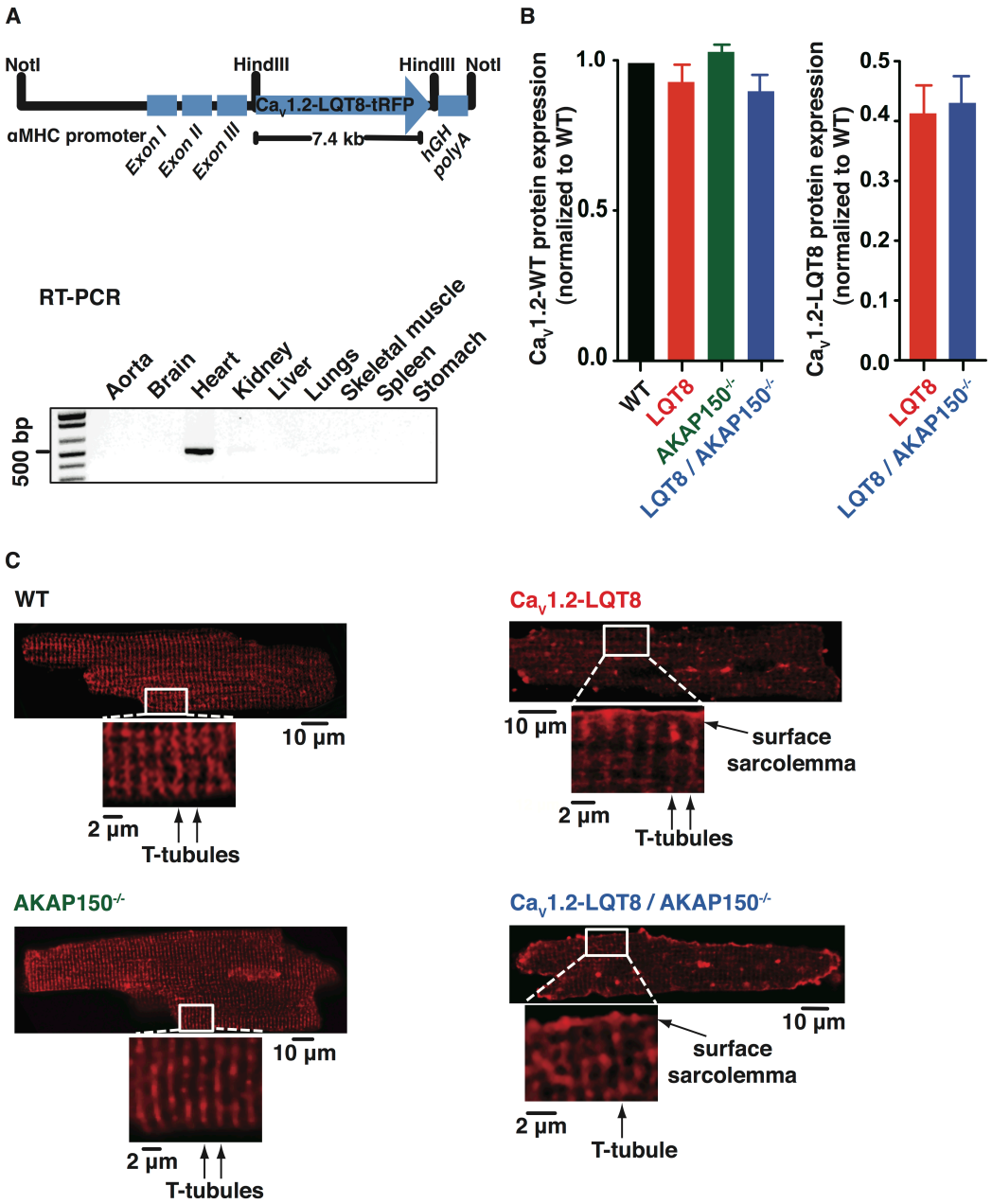

Figure 3.3. AKAP150 is not required for the expression and spatial distribution of $Ca_V1.2$-LQT8 channels in ventricular myocytes.
(A) Cardiac-specific expression of $Ca_V1.2$-LQT8 channels was achieved by using the α-myosin heavy chain (αMHC) promoter. The lower panel shows that expression of $Ca_V1.2$-LQT8 transcript was cardiac specific in LQT8 mice. **(B)** Sarcolemmal WT and LQT8 $Ca_V1.2$ protein expression in WT, LQT8, AKAP150$^{-/-}$, and LQT8/AKAP150$^{-/-}$ myocytes. **C)** Confocal images of WT or LQT8 $Ca_V1.2$ channel-associated fluorescence in WT (immunofluorescence), LQT8 (tRFP fluorescence), AKAP150 (immunofluorescence), and LQT8/AKAP150$^{-/-}$ myocytes (tRFP fluorescence). Below each image, the section of the cell contained within the white rectangles is shown at higher magnification.

3.4.4 Estimation of the relative number of $Ca_V1.2$-WT and $Ca_V1.2$-LQT8 channels in LQT8 myocytes

We determined the relative number of $Ca_V1.2$-WT and $Ca_V1.2$-LQT8 channels in LQT8 myocytes from macroscopic Ca^{2+} currents (I_{Ca}) in these cells (Figure 3.4) as follows. Note that, in LQT8 myocytes, the macroscopic Ca^{2+} current is defined by the following equation:

$$I_{Ca} = I_{Ca,WT} + I_{Ca,LQT8},$$

where $I_{Ca,\,WT}$ and $I_{Ca,\,LQT8}$ are the currents produced by WT and LQT8 channels, respectively. At +10 mV, I_{Ca} records from WT myocytes suggest that $I_{Ca,WT}$ fully inactivates (i.e., $I_{Ca,\,WT}$ = 0 pA) at 200 ms. However, our data show that in LQT8 myocytes, I_{Ca} at 200 ms into a voltage step to +10 mV is ~1/3 that of the peak I_{Ca}. For a typical myocyte with a membrane capacitance of 100 pF, and assuming a peak current density of 3 pA/pF (recorded range 2.5-6.0 pA/pF) at +10 mV, the peak I_{Ca}=(100pF)(3 pA/PF)=300 pA. At 200 ms into a voltage step to +10 mV, I_{Ca}=(1/3)(300 pA)=100 pA. Thus, 200 ms into a voltage step to +10mV,

$$I_{Ca} = (NP_oR_{200}i_{Ca})_{LQT8} = 100\,pA,$$

where N is the number of channels, P_o is the open probability, R_{200} is the fraction current remaining at 200 ms due to Ca^{2+} dependent inactivation only, and i_{Ca} is the unitary current of LQT8 channels. Our data suggest that WT and LQT8 channels have similar i_{Ca}. Although i_{Ca} in the presence of physiological 2 mmol/L Ca^{2+} at +10 mV is too small to measure, we used published values and fit them with the Goldman, Hodgkin, and Katz (GHK) constant field equation (M Rubart et al., 1996). This gave a predicted i_{Ca} value of 0.05 pA at +10 mV. Assuming a maximum P_o value for $Ca_V1.2$-LQT8 channels of 0.5 and using the published value of 0.75 for R_{200}, then (Barrett & Tsien, 2008)-

$$N_{LQT8} \approx \frac{100\,pA}{(0.5*0.7*0.05pA)} = 5714\,.$$

Because at +10 mV, the P_o of $Ca_V1.2$-WT channels is 0.3, we estimated the number of Cav1.2-WT channels at peak I_{Ca} as follows (Josephson et al., 2010):

$$N_{WT} = \frac{I_{Ca} - (N_{LQT8}P_{o,LQT8}i_{Ca})}{(P_{o,WT}i_{Ca})} \approx \frac{300\,pA - \left(7143*0.5*0.05pA\right)}{0.3*0.05pA} = 12381\,.$$

Thus, LQT8 channels account for ≈32% of the total number of channels in this exemplar LQT8 myocyte, a value that is in close agreement with our Western blot data (i.e., $Ca_V1.2$-LQT8 = 41 ± 5% of the total sarcolemmal $Ca_V1.2$ protein) in Figure 3.3B.

3.4.5 Loss of AKAP150 restores normal inactivation of I_{Ca} in LQT8 myocytes

We recorded macroscopic $Ca_V1.2$ currents (I_{Ca}) from WT, AKAP150$^{-/-}$, LQT8, and LQT8/AKAP150$^{-/-}$ ventricular myocytes. Although the amplitude of I_{Ca} was similar in WT, AKAP150$^{-/-}$, LQT8, and LQT8/AKAP150$^{-/-}$ ventricular myocytes ($p > 0.05$), there were striking differences in the rate of inactivation of these currents (Figure 3.4 A-B and Table 3.1). Indeed, the fraction of I_{Ca} remaining 50 ms (r_{50}) after the onset of depolarization to +10 mV from LQT8 myocytes was larger (n = 8) than in WT (n = 9) and AKAP150$^{-/-}$ myocytes (n = 5; $p < 0.05$), suggesting expression of functional $Ca_V1.2$-LQT8 channels in LQT8 myocytes. Indeed, from these I_{Ca} currents, we determined that $Ca_V1.2$-LQT8 channels account for ≈32% of the total $Ca_V1.2$ channel population in LQT8 myocytes. Interestingly, the r_{50} of I_{Ca} in LQT8/AKAP150$^{-/-}$ (n = 9) was similar to that of WT and AKAP150$^{-/-}$. These data suggest that loss of AKAP150 restores normal I_{Ca} inactivation in LQT8 myocytes.

Our I_{Ca} data raise an important question: is AKAP150 required for the expression of functional $Ca_V1.2$-LQT8 channels? To address this question, we expressed these channels in WT and AKAP150$^{-/-}$ mouse embryonic fibroblasts (MEFs). As shown in Figure 2C, we recorded robust I_{Ca} (1-3 pA/pF) only in cells transfected with $Ca_V1.2$-WT or $Ca_V1.2$-LQT8. In WT MEFs (Figure 3.4 C-D and Table 3.1), $Ca_V1.2$-LQT8 currents (r_{50} = 0.73 ± 0.10, n = 5) inactivated at a much slower rate than $Ca_V1.2$-WT

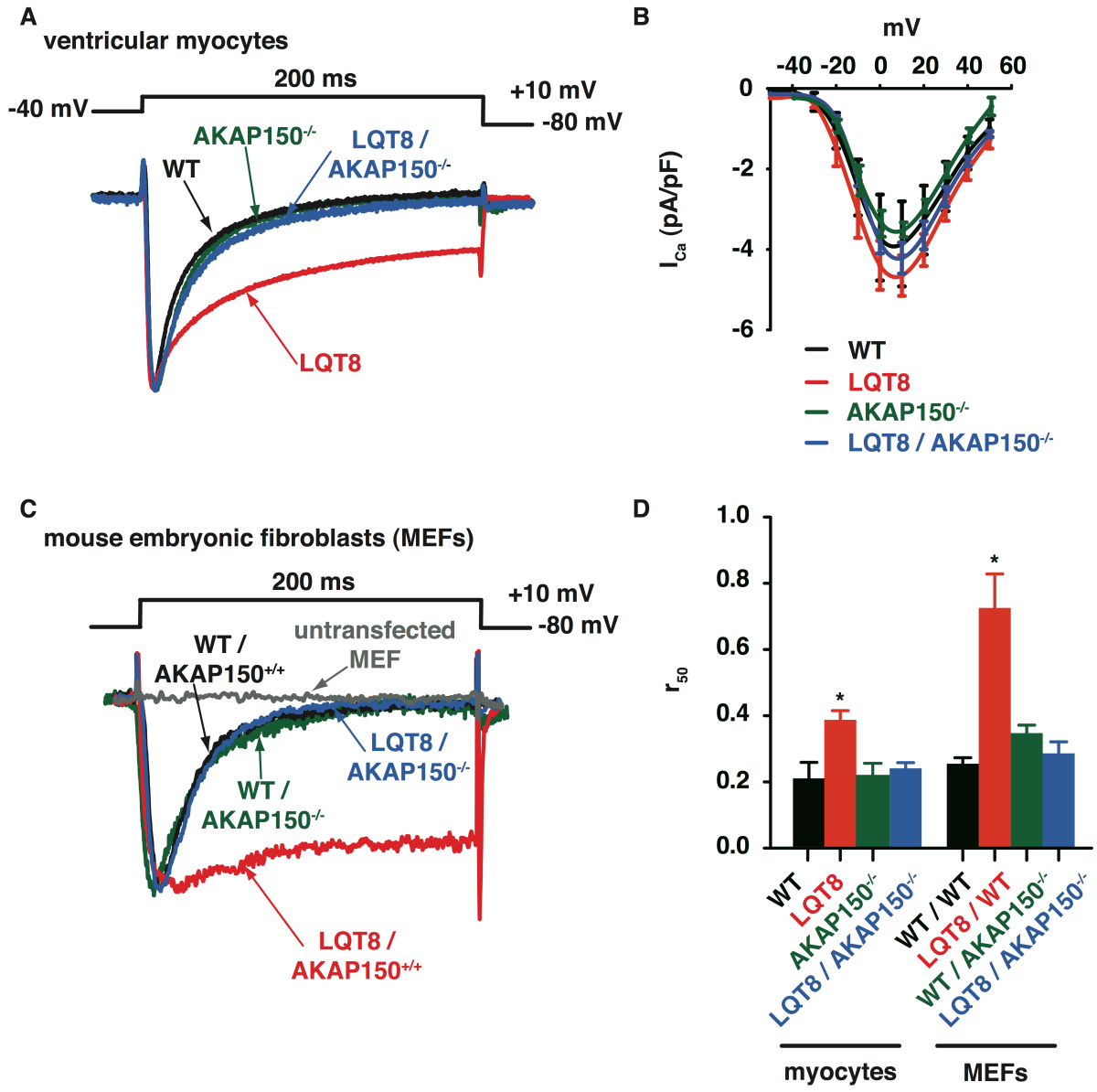

Figure 3.4. Loss of AKAP150 restores normal inactivation of I_{Ca} in LQT8 myocytes. **(A)** Normalized I_{Ca} records from representative WT, LQT8, AKAP150$^{-/-}$, and LQT8/AKAP150$^{-/-}$ ventricular myocytes. **(B)** Current-voltage relationship of I_{Ca} in WT, LQT8, AKAP150$^{-/-}$, and LQT8/AKAP150$^{-/-}$ myocytes. **(C)** I_{Ca} records from WT and AKAP150$^{-/-}$ MEFs expressing either WT or LQT8 $Ca_V1.2$ channels. A current record from an untransfected MEF is also shown. (**D**) Bar plot of the fraction r_{50} in ventricular myocytes or MEFs.

currents at +10 mV (r_{50} = 0.25 ± 0.02, n = 6; $p < 0.05$). However, in AKAP150$^{-/-}$ MEFs, $Ca_V1.2$-LQT8 channels (r_{50} = 0.28 ± 0.03, n = 5) produced currents with a similar time course to that of $Ca_V1.2$-WT channels (r_{50} = 0.35 ± 0.03 at +10 mV; n = 5 cells; $p > 0.05$). Thus, although AKAP150 is not necessary for the expression of functional WT or LQT8 $Ca_V1.2$ channels, it is required for defective inactivation of $Ca_V1.2$-LQT8 channels.

3.4.6 PKA or CaMKII do not modulate the rate of inactivation of I_{Ca} in LQT8 myocytes

A potential mechanism by which AKAP150 could promote a slow rate of inactivation of $Ca_V1.2$-LQT8 currents is by acting as an anchor for protein kinase A (PKA) (Nichols et al., 2010; Oliveria et al., 2007). Another possibility is that the effects of AKAP150 on $Ca_V1.2$-LQT8 channel inactivation depend on CaMKII activity (Erxleben et al., 2006). We tested the hypothesis that AKAP150 modulates $Ca_V1.2$-LQT8 channel function independent of its ability to target PKA activity to specific regions of the ventricular myocyte. To do this, we recorded I_{Ca} in LQT8 myocytes before and after the application of 100 µmol/L of the PKA inhibitor Rp-cAMP or 10 µmol/L of the PKA-AKAP interaction inhibitor Ht31 (Figure 3.5) (Van Haastert et al., 1984; Vijayaraghavan, Goueli, Davey, & Carr, 1997). Consistent with our hypothesis, application of either Rp-cAMP or Ht31 did not change the r_{50} of I_{Ca} in LQT8

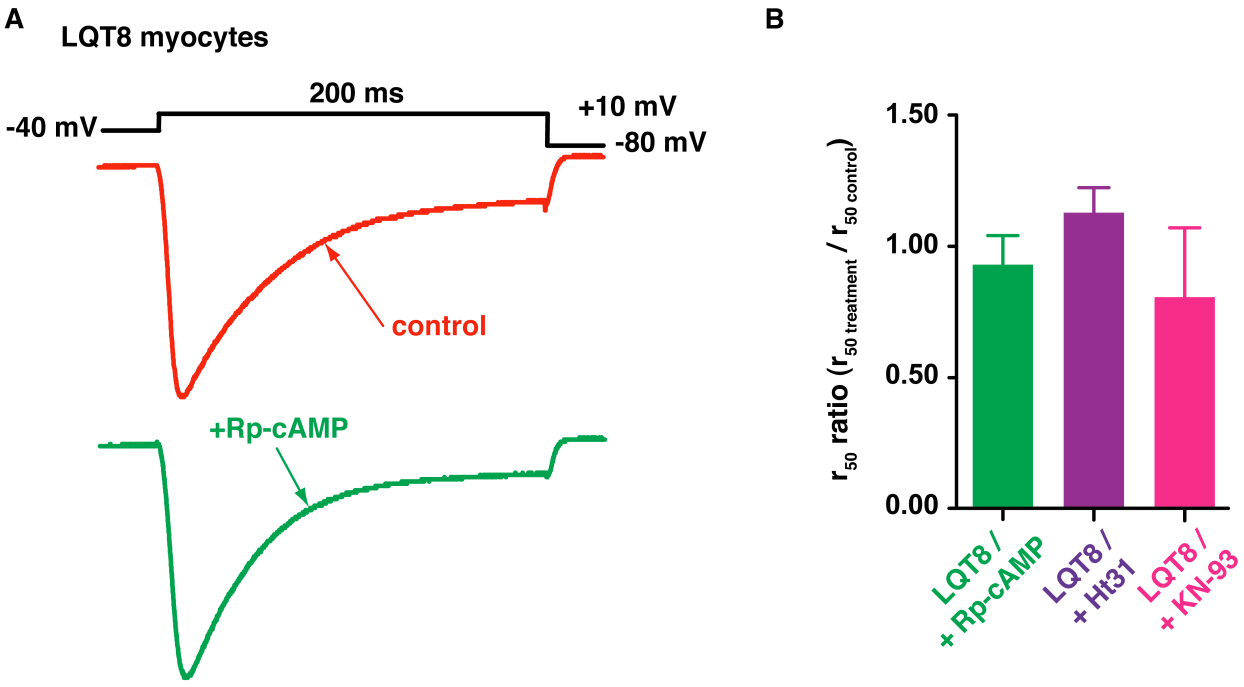

Figure 3.5: CaMKII and PKA do not modulate the rate of inactivation of I_{Ca} in LQT8 myocytes. **(A)** Representative normalized I_{Ca} records from a LQT8 ventricular myocyte before and after the application of Rp-cAMP. I_{Ca} was activated by a 200 ms depolarization to +10 mV from -80 mV. **(B)** Bar plot of the fraction of I_{Ca} remaining 50 ms (r_{50}) into a depolarization pulse to +10 mV in LQT8 ventricular myocytes before and after the application of Rp-cAMP, ht31, or KN-93.

myocytes ($p > 0.05$), suggesting that PKA is not responsible for the potentiation of I_{Ca} during LQT8. We also test the hypothesis that phosphorylation of $Ca_V1.2$-LQT8 by CaMKII causes delayed inactivation in these channels. Application of 5 μmol/L of KN-93, a CaMKII inhibitor, did not restore r_{50} of I_{Ca} in LQT8 myocytes to WT levels, suggesting CaMKII activity is not required for slow I_{Ca} inactivation in these cells (Figure 3.5, $p > 0.05$) (Sumi et al., 1991).

Furthermore, these data support the view that the necessity of AKAP150 for decreased $Ca_V1.2$-LQT8 channel inactivation is not dependent on CaMKII activity or its ability to target PKA locally.

3.4.7 AKAP150 is required for increased $Ca_V1.2$ channel activity and coupled gating seen in LQT8 myocytes

To test the hypothesis that ablation of AKAP150 decreases the P_o, open time, and frequency of coupled gating events by $Ca_V1.2$ channels in LQT8 myocytes, we recorded the *in situ* activity of $Ca_V1.2$ channels in WT, LQT8, and LQT8/AKAP150$^{-/-}$ myocytes using the cell-attached configuration of the patch clamp technique (Figure 3.6A and Table 3.1). AKAP150$^{-/-}$ myocytes were not included in these experiments because the amplitude, rate of inactivation, and voltage-dependence of I_{Ca} in these cells is similar to that of WT cells and LQT8/AKAP150$^{-/-}$ cells. Thus, it is unlikely that single $Ca_V1.2$ channel activity in AKAP150 null myocytes would be different to that of WT and LQT8/AKAP150$^{-/-}$ cells.

The amplitudes of elementary Ca^{2+} currents were similar in WT (0.55 ± 0.10 pA, n = 8 cells), LQT8 (0.60 ± 0.11 pA, n = 12 cells), and LQT8/AKAP150$^{-/-}$ (0.58 ± 0.12 pA,

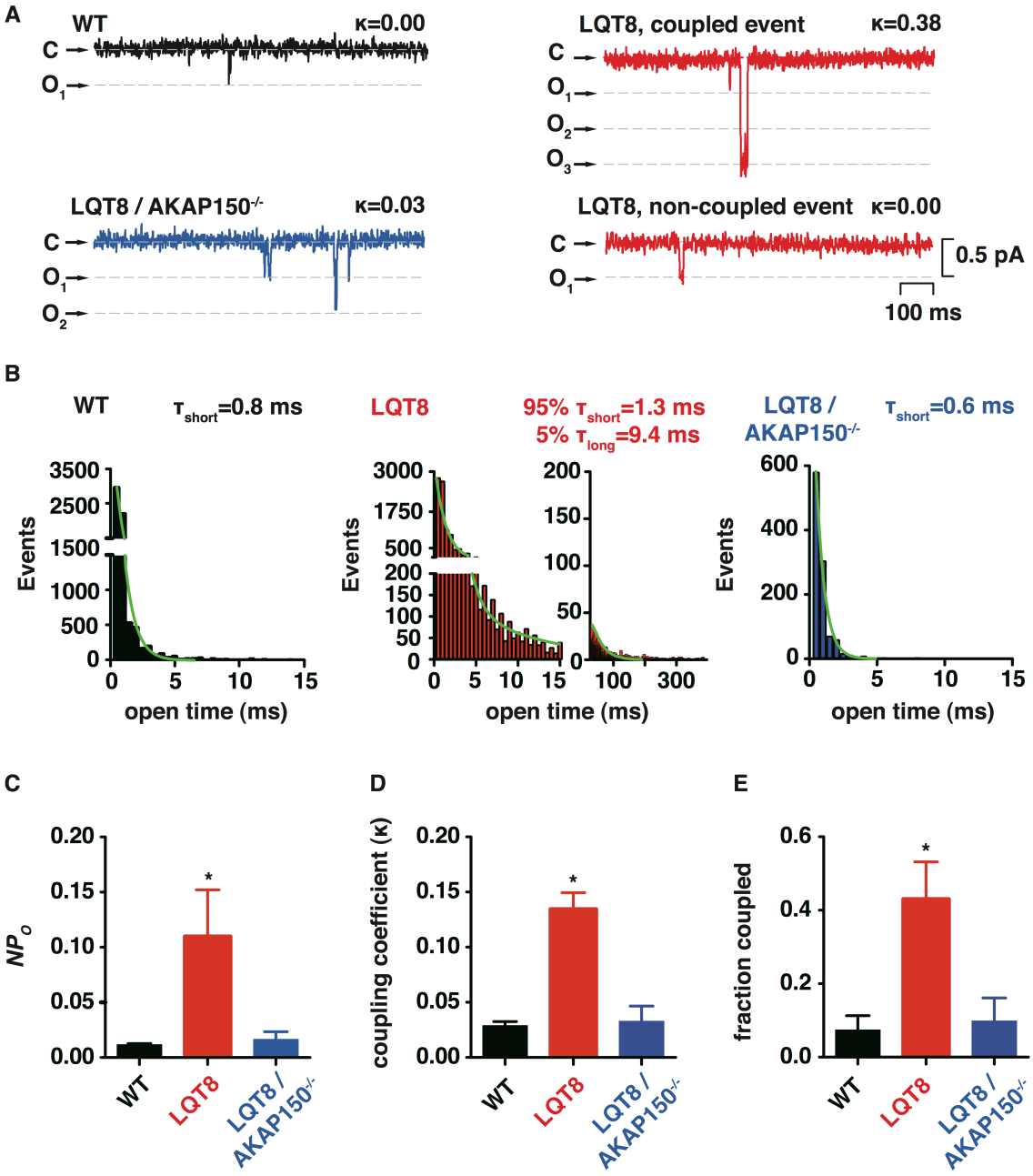

Figure 3.6. AKAP150 is required for increased in $Ca_V1.2$ channel activity and coupled gating seen in LQT8 myocytes.
(A) Exemplar cell-attached $Ca_V1.2$ channel currents from membrane patches recorded during a step depolarization to -30 mV from -80 mV, with various coupling coefficients (κ) from WT, LQT8, and LQT8/AKAP150$^{-/-}$ ventricular myocytes. The 0 pA current level is marked by C. Dashed grey lines show the amplitude of opening for 1 (O_1), 2 (O_2), or 3 (O_3) channels. **(B)** Open dwell time histograms of $Ca_V1.2$ channel openings in WT (n = 8 cells, 1 patch/cell), LQT8 (n = 12 cells), and LQT8/AKAP150$^{-/-}$ (n = 10 cells) myocytes. The time constants (τ) of exponential function fits (green line) of these histograms are shown. In LQT8 patches, a two-term exponential fit with a τ_{short} and τ_{long} of 1.3 and 9.4 ms represent 95% and 5% of the entire population is optimal. Bar plots of the NP_O, κ, and the fraction of records with κ values > 0.05 are shown in panels **C**, **D**, and **E**, respectively.

n = 10 cells) myocytes at -30 mV ($p > 0.05$). Consistent with our I_{Ca} data, the activity (i.e., NP_o where N is the number of channels and P_o is the open probability) of $Ca_V1.2$ channels in LQT8 myocytes (0.11 ± 0.04) was ≈10-fold higher than in WT (0.01 ± 0.01) and LQT8/AKAP150$^{-/-}$ (0.02 ± 0.01) myocytes ($p < 0.05$; Figure 3.6B). Furthermore, analysis of the open dwell times from $Ca_V1.2$ channels revealed that a larger proportion of channel openings are long openings in LQT8 myocytes than those recorded from LQT8/AKAP150$^{-/-}$ and WT myocytes. The open time histograms from WT and LQT8/AKAP150$^{-/-}$ myocytes could be fit with a single exponential function with a time constant (τ_{short}) of 0.8 ms and 0.6 ms, while the open time histogram of $Ca_V1.2$ channels in LQT8 myocytes could be fit with the sum of two exponential functions with τ_{short} of 1.3 ms and τ_{long} of 9.4 ms, which accounted for 95% and 5% of the channel openings, respectively (Figure 3.6B). The time constants from LQT8 myocytes likely represents a mixed population of WT and LQT8 $Ca_V1.2$ channels operating in two gating modalities in LQT8 myocytes. By contrast, the long $Ca_V1.2$ channel openings observed in LQT8 myocytes were completely absent in LQT8/AKAP150$^{-/-}$ cells. Collectively, these data suggest that AKAP150 is required for long openings of $Ca_V1.2$ channels in LQT8 myocytes.

To test the hypothesis that $Ca_V1.2$-LQT8 channels have a higher probability of coupled gating than $Ca_V1.2$-WT channels in ventricular myocytes, we implemented a coupled Markov chain model to determine the coupling coefficient (κ) among $Ca_V1.2$ channels (Chung & Kennedy, 1996; Navedo et al., 2010). The mean coupling coefficient was 0.13 ± 0.03 for Ca^{2+} channels in LQT8 myocytes and 0.03 ± 0.01 for

WT and 0.03 ± 0.01 for LQT8/AKAP$^{-/-}$ cells (Figure 3.6D). Indeed, the frequency of coupled gating events (κ > 0.1) was higher in LQT8 (43 ± 10%) myocytes than in WT (8 ± 4%) and LQT8/AKAP150$^{-/-}$ (10 ± 6%) myocytes ($p < 0.05$; Figure 3.6E).

3.4.8 Loss of AKAP150 restores normal $[Ca^{2+}]_i$, AP waveform, and cardiac rhythm in LQT8 mice

We recorded AP-evoked $[Ca^{2+}]_i$ transients in WT, LQT8, AKAP150$^{-/-}$, and LQT8/AKAP150$^{-/-}$ myocytes (Figure 3.7A and Table 3.1). The amplitudes of the AP-evoked $[Ca^{2+}]_i$ transient in WT myocytes (n = 7), AKAP150$^{-/-}$ (n = 7), and LQT8/AKAP150$^{-/-}$ myocytes (n = 9) were similar ($p > 0.05$). The $[Ca^{2+}]_i$ transient was larger in LQT8 myocytes (n = 9) than in these myocytes ($p < 0.05$). Furthermore, although 56% of LQT8 myocytes had spontaneous Ca^{2+} release (SCR) events under control conditions, none was detected in WT, AKAP150$^{-/-}$, or LQT8/AKAP150$^{-/-}$ myocytes under similar experimental conditions. Because AKAP150 is required for β-adrenergic induced increases in the amplitude of the AP-evoked $[Ca^{2+}]_i$ transient in ventricular myocytes, we examined the effects of the β-adrenergic agonist isoproterenol (ISO, 100 nM) on WT, LQT8, AKAP150$^{-/-}$, and LQT8/AKAP150$^{-/-}$ myocytes (Figure 3.7A and Table 3.1) (Nichols et al., 2010). We found that ISO increased the amplitude of the AP-evoked $[Ca^{2+}]_i$ in WT and LQT8, but not in AKAP150$^{-/-}$ or LQT8/AKAP150$^{-/-}$ myocytes, providing functional confirmation of the loss of AKAP150 in these cells ($p < 0.05$).

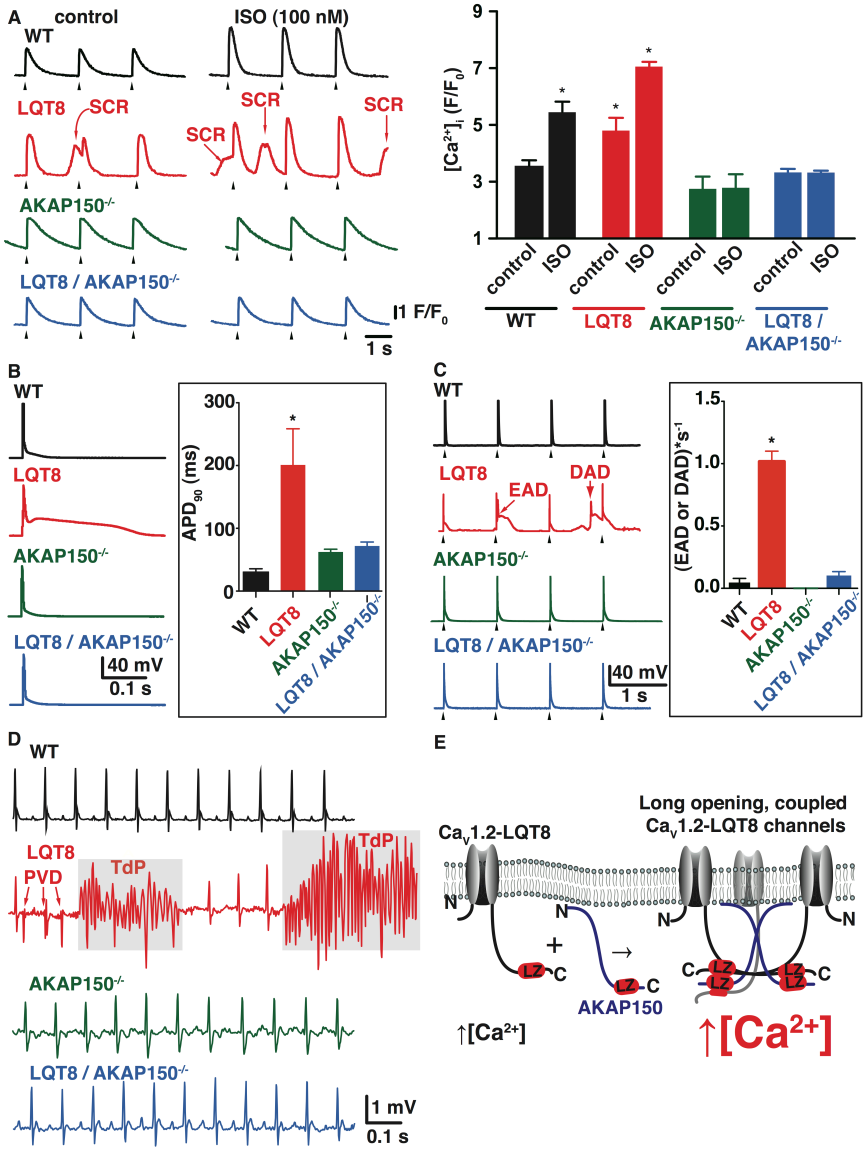

Figure 3.7. Loss of AKAP150 restores normal $[Ca^{2+}]_i$, AP waveform, and cardiac rhythm in LQT8 mice.
(A) $[Ca^{2+}]_i$ transients from representative WT, LQT8, and LQT8/AKAP150$^{-/-}$ myocytes before and after the application of 100 nM ISO. Spontaneous Ca^{2+} release events (SCR) in LQT8 myocytes are indicated. Arrowheads below indicate external stimuli. Bar plot represents the $[Ca^{2+}]_i$ transient amplitudes. **(B)** APs from WT, LQT8, and LQT8/AKAP150$^{-/-}$ myocytes. (*Inset*) Bar plot of APD_{90}. **(C)** Trains of APs recorded from WT, LQT8, AKAP150$^{-/-}$ and LQT8/AKAP150$^{-/-}$ myocytes. EAD and DAD are indicated. Arrowheads below indicate current injection. The inset shows a bar plot of the rate of EADs or DADs in WT, LQT8, AKAP150$^{-/-}$, and LQT8/AKAP150$^{-/-}$ myocytes. **(D)** ECG traces from WT, LQT8, and LQT8/AKAP150$^{-/-}$ mice. PVDs in the LQT8 trace are marked by arrows. The gray box highlights TdP in this LQT8 mouse. **(E)** Proposed model of how AKAP150 binds to the C-terminal tail of $Ca_V1.2$-LQT8 channels, facilitating longer channel openings and interaction between multiple $Ca_V1.2$-LQT8 channels, which increases the frequency of coupled gating and greater Ca^{2+} influx, leading to arrhythmias.

ISO also increased the number of spontaneous Ca^{2+} release events in $Ca_V1.2$-LQT8 cells from 40 to 85%, but not in WT, AKAP150$^{-/-}$, and LQT8/AKAP150$^{-/-}$ myocytes. We investigated whether restoration of normal inactivation of I_{Ca} in LQT8/AKAP150$^{-/-}$ myocytes translated to changes in AP waveform in these cells. Consistent with our I_{Ca} data, the duration of the AP at 90% repolarization (APD_{90}) was longer in LQT8 (n = 10) than in WT (n = 5), AKAP150$^{-/-}$ (n = 5), and LQT8/AKAP150$^{-/-}$ (n = 11) myocytes ($p < 0.05$; Figure 3.7B and Table 3.1). In addition, analysis of records with trains of APs revealed that LQT8 myocytes had a higher frequency of early (EADs) and delayed afterdepolarizations (DADs) than WT, AKAP150$^{-/-}$, and LQT8/AKAP150$^{/-}$ myocytes (Figure 3.7C and Table 3.1).

To determine the electrophysiological phenotype of WT, LQT8, AKAP150$^{-/-}$, and LQT8/AKAP150$^{-/-}$ mice, we implanted telemetric ECG transmitters (Figure 3.7D and Table 3.1) (Mitchell, Jeron, & Koren, 1998). Heart rate was similar in WT (n = 6), LQT8 (n = 5), AKAP150$^{-/-}$ (n = 6), and LQT8/AKAP150$^{-/-}$ at rest (n = 6) or during mild exercise ($p > 0.05$). However, consistent with our I_{Ca} and AP data, the QT interval — corrected for heart rate using Bazett's formula (i.e., QT_c) — of LQT8 mice (116 ± 1 ms) is longer than that of WT (97 ± 1 ms), AKAP150$^{-/-}$ (98 ± 1), and LQT8/AKAP150$^{-/-}$ mice (108 ± 1 ms; $p < 0.05$). During exercise, although multiple premature ventricular depolarizations (PVDs) and epiodes of *torsades de pointes* (TdPs, a hallmark of LQT) were observed in LQT8 mice, none was recorded from WT, AKAP150$^{-/-}$, and LQT8/AKAP150$^{-/-}$ mice (Figure 3.7D and Table 3.1). Thus, loss of AKAP150 was protective against arrhythmias in mice expressing $Ca_V1.2$-LQT8.

3.5 Discussion

Our findings suggest a new model of $Ca_V1.2$-LQT8 channel dysfunction during Timothy syndrome (Figure 3.7E). In this model, the anchoring protein AKAP150 and $Ca_V1.2$-LQT8 form a complex that is necessary for aberrant $Ca_V1.2$-LQT8 channel gating and arrhythmias. $Ca_V1.2$-LQT8 channels likely interact with AKAP150 via LZ motifs in the carboxyl tails of both proteins (Oliveria et al., 2007). We propose that AKAP150 functions like an allosteric modulator of $Ca_V1.2$-LQT8 channels, increasing $Ca_V1.2$-LQT8 currents by stabilizing the open conformation and increasing the probability of coupled gating between $Ca_V1.2$-LQT8 channels. This leads to increased Ca^{2+} influx, AP prolongation, cardiac hypertrophy, and arrhythmias. Coupled gating of $Ca_V1.2$-LQT8 channels presumably occurs because AKAP150 promotes physical interactions of adjacent channels via their carboxyl tails (Gold et al., 2011; Navedo et al., 2010; Oliveria et al., 2007). While this mechanism may superficially resemble the role of the AKAP protein Yotiao in LQT1, specifically Yotiao's role in targeting PKA and protein phosphatase 1 (PP1) to KCNQ1-KCNE1 K^+ channels, an important feature and key difference of our model implicates AKAP150 in LQT8 arrhythmogenesis that is completely independent of its as a kinase and phosphatase scaffold, which is a completely novel role for this scaffolding protein (Marx et al., 2002).

While our model of AKAP150 as an allosteric modulator of $Ca_V1.2$-LQT8 may also

bring into the question of whether AKAP150 functions like a true subunit of $Ca_V1.2$, the answer to this question is more ambiguous. Our data suggest that the association of AKAP150 with the carboxy terminal of $Ca_V1.2$-LQT8 channel directly modulates gating like a $Ca_V1.2$ subunit, independent of its role as a scaffold for kinases, resulting in significantly increased coupled gating and prolonged opening time that translate macroscopically into delayed inactivation of I_{Ca}. However, does AKAP150 behave similarly in WT cardiac myocytes not under βAR stimulation? A previous study by Nichols et al. showed that AKAP150 does not have a significant effect on the whole cell I_{Ca} and the basal level of EC coupling in WT cardiac myocytes not under βAR stimulation (Colecraft et al., 2002; Dai et al., 2009; Nichols et al., 2010). In Chapter 2 of this dissertation, we found that AKAP150 is necessary for a low-level of transient coupled gating when associated with a subpopulation of $Ca_V1.2$-WT channels; however, it would be extremely difficult to resolve the contribution of coupled gating from this small subpopulation of $Ca_V1.2$-WT channels under normal physiology on a macroscopic level (Navedo et al., 2010). Therefore, the subunit-like effect of AKAP150 on macroscopic I_{Ca} kinetics is only significant in $Ca_V1.2$-LQT8 channels, and importantly it is not significant in $Ca_V1.2$-WT channels.

Another important function of $Ca_V1.2$ subunits is their role as chaperones in the membrane trafficking of ion channels, such as the role of the β subunit in enhancing $Ca_V1.2$ membrane trafficking and the γ subunit in the trafficking of AMAPA-R (Chen, El-Husseini, Tomita, Bredt, & Nicoll, 2003; Yamaguchi et al., 1998). Our data suggest that AKAP150 does not fulfill this role. $Ca_V1.2$-LQT8 channels are

expressed in the sarcolemma of cardiac myocytes at the same level in AKAP150$^{-/-}$ background as in WT background. Just as importantly, we find that $Ca_V1.2$-LQT8 channels are properly expressed in AKAP150$^{-/-}$ MEFs.

How important is the role of coupled gating of $Ca_V1.2$-LQT8 in the pathophysiology of LQT8? Our data and model suggest that 2 to 6 $Ca_V1.2$-LQT8 channels transiently undergo coupled gating. The very transient nature and variable stoichiometry of this interaction pose a challenge for future computer models examining the physiological effects of coupled gating. However, we hypothesized that coupled gating would lead to an increase in the positive cooperativity of the voltage-dependence of activation in $Ca_V1.2$ channels on EC coupling. Also, coupled gating's effect on EC coupling would be a highly non-linear process given the derivation in Chapter 1 that the probability of Ca^{2+} spark activation P_{spark} is proportional to $[Ca^{2+}]_i^2$ (L.F. Santana et al., 1996). A recent follow-up study from our group artificially increased coupled gating frequency between pairs of $Ca_V1.2$-WT-GI/$Ca_V1.2$-WT-FKF1 channels via the photodimerization of the FLAVIN-BINDING, KELCH REPEAT, F BOX 1 (FKF1) and GIGANTEA (GI) plant proteins expressed on the carboxy termini of these channels (Dixon et al., 2012). In this study, we observed increases in whole-cell I_{Ca} by up to ~100% and increases in the cooperativity of the Boltzmann function fit of the voltage-dependence of normalized $Ca_V1.2$ conductance. Since the thermodynamic equilibrium of photodimerization has to be less than 100%, and we still observed *transient* coupled gating behavior after photodimerization, the large potentiation seen in I_{Ca} can only be attributed to the non-linear increase in cooperativity seen in

the voltage-dependence of activation. The increase in I_{Ca} after photodimerization was mirrored by a similar increase in [Ca^{2+}] transient and cell-shortening, illustrating the potentiating effect of coupled gating on EC coupling. And what is even more interesting, we observed that when dimerized to $Ca_V1.2$-LQT8-FKF1 channels, $Ca_V1.2$-WT-GI channels begin to assume kinetic characteristics of the $Ca_V1.2$-LQT8 channels, further implicating coupled gating as a highly cooperative behavior that could magnify the effect of the minority ~32-41% of total $Ca_V1.2$ channels being $Ca_V1.2$-LQT8 in LQT8 ventricular myocytes. Interestingly, another group created a knock-in mouse model of Timothy syndrome as a mouse model for the study of autism, and they observed a highly non-linear dose-dependent effect of the mutant gene (Bader et al., 2011).

Our data, from the study of $Ca_V1.2$ at the single channel level to ECG telemetry from whole animals, provide insights into the cellular mechanisms by which $Ca_V1.2$-LQT8 channels increase the probability of arrhythmias. We found that expression of $Ca_V1.2$-LQT8 channels increased the frequency of arrhythmogenic EADs and DADs. EADs are produced by reactivation of $Ca_V1.2$ channels during the long APs of LQT8 myocytes, and EADs can also share the same mechanism as DADs: SCR due to SR Ca^{2+} overload, triggering local depolarizing NCX current (Choi et al., 2002; Michael Rubart & Zipes, 2005). The convergent mechanism of both EADs and DADs fits well of our observation of both EADs and DADs contained within one AP recording. On the whole organism level, EADs are associated with TdP, especially in LQT syndromes, which we observed in our ECG telemetry records in the LQT8 mice

(Choi et al., 2002; Volders et al., 2000). EADs initiate TdP via the mechanism of "triggered activity," when a cluster of rogue myocytes undergo EAD, forming an abnormal cluster of automaticity (Michael Rubart & Zipes, 2005; Weiss et al., 2011). It is intriguing to speculate that the larger Ca^{2+} influx associated with $Ca_V1.2$-LQT8 channels leads to SR Ca^{2+} overload and thus to SCR events and DADs in LQT8 myocytes (Lukyanenko et al., 2001). Since the mechanism of EC coupling is dependent on the local trans-sarcolemmal Ca^{2+} current, future experiments should examine in detail the relationship between Ca^{2+} influx via $Ca_V1.2$-LQT8 and EADs and DADs in these cells (M. Cannell et al., 1995; Stern, 1992).

Ablation of AKAP150 corrects pathological $Ca_V1.2$-LQT8 channel gating and arrhythmias and prevents hypertrophy of LQT8 hearts presumably by decreasing Ca^{2+} influx via $Ca_V1.2$-LQT8 channels. Because AKAP150 does not bind CaMKII, loss of this scaffolding protein is not expected to affect CaMKII-dependent modulation of $Ca_V1.2$-LQT8 channels in ventricular myocytes (Erxleben et al., 2006; Thiel et al., 2008). Our data do not suggest that CaMKII plays a role in the altered I_{Ca} kinetics seen in LQT8. However, our data suggest that AKAP150 is required for any potential CaMKII-induced changes in EC coupling in LQT8 myocytes due to I_{Ca} facilitation (Thiel et al., 2008). Thus, we propose that disrupting the interaction between AKAP150 and $Ca_V1.2$-LQT8 is a potential target for novel therapeutics for treating the broad spectrum of Timothy syndrome's symptoms, including lethal arrhythmias and autism.

Chapter 4: Heart failure- the final frontier for biophysics in cardiovascular medicine?

4.1 Introduction

With our recent discovery of coupled gating of L-type Ca^{2+} channels and persistent Ca^{2+} sparklets, our laboratory has demonstrated using advanced biophysical techniques that spatial heterogeneity in microdomains of Ca^{2+} signaling could play critical roles in the pathophysiology of disease (E. P. Cheng et al., 2011; Navedo et al., 2008, 2010, 2005). Ever since the days of William Harvey, the science of cardiovascular biology has been on a gradual movement from the descriptive to the quantitative. With greater elucidation of the biophysics behind both normal cardiac physiology and the pathophysiology of relatively straightforward "classic" disease models, such as channelopathies, heart failure remains a field where descriptive and qualitative models far outweigh the biophysical and the quantitative. However, we stand on the exciting precipice in heart failure biology, as all the biophysical tools that have been recently developed are at the ready to be applied in this critical field of translational research.

Heart failure is the final clinical manifestation of almost all cardiac diseases, including congenital heart disease. For the United States, with a rising incidence of

over 600,000 cases per year and a prevalence of 5.3 million people afflicted, heart failure is a disease with an enormous cost in lives and resources (Rosamond, Flegal, & Furie, 2008). However, because of its sheer complexity and multiple etiologies, most studies in heart failure are focused on further unraveling the complex signaling network involved employing traditional biochemical assays. Fundamentally, heart failure is the inability for the heart to provide sufficient output to meet its metabolic demands, commonly called systolic failure, or the inability to provide sufficient cardiac output without abnormally high filling pressure, commonly called diastolic failure (Shah & Fifer, 2007). The myocardium in the failing heart has reduced contractility, and it compensates mechanically by hypertrophy, which increases the chamber size, or preload, and increased preload preserves stroke volume via the Frank-Starling law, the cardiac analogy of the length-tension relationship in skeletal muscle (Kemp & Conte, 2012). Since cardiac output = stroke volume × heart rate, preservation of stroke volume is the primary driving force for the pathophysiological remodeling during heart failure. Hypertrophy, especially under conditions of increased afterload (i.e. hypertension, aortic stenosis), also causes eccentric hypertrophy of the myocardium, increasing wall thickness and decreasing its passive mechanical compliance, contributing to diastolic failure (Shah & Fifer, 2007).

Neurohormonal change during heart failure is a double-edged sword; it plays an important role to help preserve cardiac output as well as in the pathophysiology of heart failure. The adrenergic system goes into overdrive to help the myocardium

maintain contractility, but chronically elevated adrenergic signaling is detrimental to the myocardium and contractility (Xiao, 2001). β-blockers are the first line drugs clinically for the treatment of heart failure (Shah & Fifer, 2007). Heart failure also activates the renin-angiotensin-aldosterone (RAA) axis, which reduces the kidneys' salt excretion, to increase preload, resulting in volume overload and the associated symptoms of edema and pulmonary congestion. Diuretic are also commonly used for symptomatic relieve in heart failure.

A growing body of evidence suggests that intracellular compartmentalization in signaling plays an important role in the disease process of heart failure, and may offer novel therapeutic targets. For example, although chronically elevated β-adrenergic signaling is part of the pathophysiology of heart failure, closer examination of β-adrenergic receptors (β-ARs) in cardiac myocytes shows the β2 receptors, which make up ~25% of the population of β-adrenergic receptors in cardiac myocytes, can be coupled to G_i and activate the anti-apoptotic Akt signaling pathway (Talan, Ahmet, Xiao, & Lakatta, 2011; Xiao, 2001). However, most investigators studying molecular interactions and signaling complexes in heart failure still rely on traditional biochemical techniques like co-immunoprecipitation. It is rather ironic that by employing biochemical techniques, one is removing the very spatiotemporal specificity that one aims to investigate. Previously, patch-clamp electrophysiology was the only biophysical method available for the study of single-proteins in cardiac myocytes; however, advances in modern imaging techniques, such as confocal microscopy, Fluorescence Resonance Energy Transfer (FRET),

Scanning Ion Conductance Microscopy (SICM), and Total Internal Reflection Fluorescence microscopy (TIRF) offer the advantage of quantitatively querying protein activity and interaction on the molecular level in living cells.

4.2 FRETing about microdomains of β-AR signaling during heart failure

Recent studies have combined the use of bioengineered PKA and cAMP FRET reporters in the study of β-AR signaling in both normal physiology and pathophysiology during heart failure (S. Liu, Zhang, & Xiang, 2011; Nikolaev et al., 2010; Y. K. Xiang, 2011). FRET is the technique that optically probes molecular interaction when a donor and acceptor fluorescent proteins are within the Förster's radius as to allow dipole-dipole radiationless energy transfer from the donor, typically excited with a laser, to the acceptor, and its efficiency described by the following equation (Haugland, Yguerabide, & Stryer, 1969):

$$E = \frac{1}{1 + \left({}^{r}/_{R_0}\right)^6},$$

where R_0 is the Förster's radius, which is a function of the overlap of the acceptor absorption and donor emission spectra and the relative orientation of the molecular dipoles, described by the following equation (Haugland et al., 1969):

$$R_0^6 = \frac{9Q_0 \ln(10)\kappa^2 J}{128\pi^5 n^4 N_A},$$

where Q_0 is the quantum yield of the donor; κ^2 is the dipole orientation factor; n is the index of refraction of the medium; N_A is Avogadro's number; and J is the spectral overlap integral given by (Haugland et al., 1969):

$$J = \int f_D(\lambda)\epsilon_A(\lambda)\lambda^4 d\lambda,$$

where f_D is the normalized donor emission spectrum; and ϵ_A is the acceptor molar extinction coefficient.

A recent study by Liu et al. cleverly employed SR-targeted PKA FRET reporter SR-AKAR3 to study the level of PKA activity at the SR membrane during β-AR stimulation with 10 μmol/L ISO (S. Liu et al., 2011). The AKAR3 FRET reporter consists of a PKA substrate in series with a phospholamino binding domain, flanked on either side by CFP and YFP (Allen & Zhang, 2006). When phosphorylated by PKA, the intramolecular binding of the phospholamino domain to the phosphorylated PKA substrate allows FRET between CFP and YFP. Liu et al. showed that the level of FRET increase after ISO stimulation agreed well with PLN phosphorylation level assayed using Western blot (S. Liu et al., 2011). The activation of PKA during heart failure at the SR surface can causes hyperphosphorylation of RyR2 and PLN (George, Sabbah, Xu, Wang, & Wang, 2011; Marks, 2001). Therefore, the propagation of the β-AR signal from the sarcolemma to the SR surface via freely

diffusing cAMP is of great interest to the study of both the spatiotemporal regulation of normal β-AR signaling and the aberrant β-AR signaling during heart failure. On the sarcolemma of cardiac myocytes, a recent work by Nichols et al. showed that the AKAP79/150 scaffolding recruits a critical macromolecular signaling complex containing all the adrenergic signaling components: β-AR, caveolin-3, adenylate cyclase 5/6 (AC5/6), calcineurin (PP2B), PKA, and very importantly, $Ca_V1.2$ (Nichols et al., 2010). The targeting of AKAP79/150 is via a LZ domain was demonstrated via FRET (Oliveria et al., 2007). Interestingly, Nichols et al. found using both electrophysiology and confocal microscopy of the whole-cell $[Ca^{2+}]$ transient that in AKAP150$^{-/-}$ cardiac myocytes, where this β-AR signaling complex associated around $Ca_V1.2$ is disrupted, 10^{-7} mol/L ISO stimulation still increases $Ca_V1.2$ current but paradoxically not the whole-cell $[Ca^{2+}]$ transient, a seemingly de-coupling of β-AR modulation between the sarcolemma and the SR (Nichols et al., 2010).

Another study from the Xiang group using live neonatal cardiac myocytes from either WT, β1-AR KO, or β2-AR KO mice found a potential answer to the conundrum that β-AR signaling in the sarcolemma can become decoupled from the SR, and in this study the authors found a regulation mechanism for the spatiotemporal propagation of β-AR signaling to the SR surface from the sarcolemma under ISO stimulation (De Arcangelis et al., 2010). The authors found that there is an ISO dose-dependent, temporally biphasic, increase in FRET from the cAMP reporter ICUE3 and the PKA reporter AKAR3 (De Arcangelis et al., 2010). While we just learned about AKAR3, ICUE3 was designed around a fragment of the cAMP binding protein Epac

sandwiched between CFP and YFP (De Arcangelis et al., 2010; DiPilato, Cheng, & Zhang, 2004). Binding of cAMP onto the Epac fragment within ICUE3 causes a conformational change that increases the FRET between CFP and YFP (DiPilato et al., 2004). By taking the increase in YFP:CFP emission ratio to obtain either the increases in [cAMP] or PKA activity, De Arcangelis et al. found that the positive ISO dose-dependence on β-AR signaling response produces progressively larger transient elevations in [cAMP] and PKA activity until reaching the saturating ISO concentration, at 10^{-8} mol/L ISO in WT and β2 KO cardiac myocytes, or at 10^{-5} mol/L ISO in β1 KO cardiac myocytes (De Arcangelis et al., 2010). Beyond saturation, there is a positive dose-dependent increase in the amplitude of steady-state [cAMP] and PKA activity elevation. From these results, the authors concluded that β1-AR signaling, via the dominant receptor subtype in cardiac myocytes, is much more global, and β2 is much more spatiotemporally restricted. The authors found that transient [cAMP] elevations produced by sub-saturating ISO concentrations do not functionally translate into increased contractility, which occurs only when the [cAMP] elevation reaches steady state at and above the saturating ISO concentration. Unsurprisingly, the authors also found that the temporal duration of transient [cAMP] elevations as reported by FRET was a function of both AC and PDE4 activation. AC is the “limiting-reagent” in β-AR signaling, with many more β-ARs present than ACs, and AC inhibition at supra-saturation doses of ISO reduces [cAMP] elevation back to being transient (De Arcangelis et al., 2010). On the other hand, PDE4 inhibition with rolipram completely abolished the transient nature of [cAMP] elevation at sub-saturation doses of ISO ($<10^{-8}$ mol/L). PDE4 is pre-associated with β1 AR, and it

dissociates from the receptor in an agonist dependent manner, shifting the [cAMP] elevation from transient to steady-state (De Arcangelis et al., 2010; Y. K. Xiang, 2011). PDE4 hydrolysis of cAMP is thought to be the competing “brake” in controlling the extent of the spatiotemporal domain of cAMP signaling after β1-AR activation because the rate of diffusion for cAMP is too fast to establish any meaningful microdomain in signaling without the “brake” (De Arcangelis et al., 2010; DiPilato et al., 2004). The biphasic, agonist dose dependent nature of the spatiotemporal reach of β-AR signaling, caused by the tug-of-war between AC and PDE4, may explain how chronic β-AR signaling during heart failure can lead to dysfunctions in EC coupling (Gómez et al., 1997). In fact, a previous study by Lehnart et al. showed that PDE4D deficiency leads to heart failure and arrhythmogenesis (Lehnart et al., 2005).

4.3 The grand SICM behind the compartmentalization of β2-AR signaling

In another study using advanced optical techniques to elucidate the compartmentalized nature β-AR signaling in live cardiac myocytes, Nikolaev et al. ingeniously combined the use of cAMP FRET reporter and SICM to show conclusively the compartmentalization of β-AR signaling in adult rat and mouse cardiac myocytes (Nikolaev et al., 2010). SICM employs a very fine (~100 nm diameter) glass nanopipette filled with an electrolyte (Korchev, Negulyaev, Edwards, Vodyanoy, & Lab, 2000). Variation in the current flow out of the nanopipette tip

reflects the relative Z-distance of the tip over a surface, and it can allow us to read the morphology of the surface underneath with the resolution of the size of the nanopipette tip; for example, Nikolaev et al. successfully resolved T-tubules on the surface of cardiac myocytes (Nikolaev et al., 2010). The authors also used the nanopipette to puff 10^{-6} mol/L ISO locally as the agonist, in the presence of either β1 or β2-AR selective pharmacologic blockers in the superfusing solution, to selectively stimulate either local β1 or β2-AR signaling. For FRET imaging of [cAMP], the authors used the EPAC2-camp FRET reporter, which linearizes upon cAMP binding to the EPAC2 domain, and consequently cAMP elevation decreases the FRET between the YFP and CFP located at either end of the reporter (Nikolaev et al., 2010). In this study, FRET was recorded using an epifluorescence microscope, equipped with a beam-splitter to separate the CFP and YFP emission wavelengths. Although the epifluorescence microscope does not have sufficient resolution to visualize myocyte ultrastructure like T-tubules, the FRET intensity was superimposed on the super-resolution "image" of the sarcolemma obtained from SICM, which allowed the authors to correlate FRET and structural data. In agreement with De Arcangelis et al, Nikolaev et al. found, via the decrease in the FRET of EPAC2-camp, that β1-AR signaling is much more global than β2-AR; however, in this study the spatial compartmentalization of β-AR signaling is truly observed and not inferred from observations in the temporal domain as in the previous study (De Arcangelis et al., 2010; Nikolaev et al., 2010). Nikolaev et al. found that β2-selective stimulation only evoked locally restricted [cAMP] elevation when applied near T-tubules, but not near cell crests (Nikolaev et al., 2010). On the

other hand, β1-selective stimulation provoked robust cell-wide [cAMP] elevation when locally stimulated anywhere on the sarcolemma, on either T-tubules or cell crests. However, unlike the previous study by De Arcangelis et al., application of a PDE inhibitor IBMX failed to “rescue” β2-AR response over the cell crests in healthy cardiac myocytes, which suggest that is where β2-ARs are sequestered spatially. However, application of rolipram, a PDE4 specific inhibitor, changed β2-AR induced [cAMP] from local to global, like β1-AR signaling. The same spatial restriction in β2-AR signaling existed even in cardiac myocytes from the β1-AR KO mice, suggesting the two β-AR subtypes are not exchangeable in healthy myocytes.

Given the evidence for spatial compartmentalization of β2-AR signaling in normal physiology, its implications in heart failure is elucidated by cardiac myocytes from a rat model of myocardial infarction induced heart failure, which showed a loss of the spatial sequestration of β2-AR signaling (Nikolaev et al., 2010). The author showed via SICM that heart failure rat cardiac myocytes had undergone extensive T-tubular remodeling, resulting in an extensive loss of T-tubules, which Lyon et al. also identified in both human and rat heart failure cardiac myocytes using both SICM and confocal microscopy of di-8-ANEPPS membrane staining (Marx et al., 2001). Whereas β1-AR signaling remained unmolested in heart failure rat cardiac myocytes, β2-AR signaling lost its spatial restriction, and it could be evoked anywhere on the sarcolemma (Nikolaev et al., 2010). The authors buttressed their findings that the loss of T-tubules lead to a redistribution of β2-AR by reproducing the same loss in spatial restriction for β2-AR signaling in β1-AR KO mouse cardiac

myocytes de-tubulated with formamide. In addition to losing its spatial specificity in localization, stimulation β2-AR in cell crests in heart failure rat cardiac myocytes resulted in global [cAMP] elevation, just like β1-AR. Because from IHC staining of PKA in human heart failure cardiac myocytes showed delocalization from the Z-lines, the authors then tested the hypothesis whether PKA, which is colocalized with β2-AR, AC, caveolin 3, and $Ca_V1.2$ within caveolae in T-tubules via the scaffold protein AKAP150, was buffering the cAMP produced by local β2-AR stimulation in cardiac myocytes by disrupting the interaction between AKAP150 and PKA with the Ht31 peptide (Nichols et al., 2010; Nikolaev et al., 2010). Confirming their hypothesis, Ht31 caused β2-AR stimulation at T-tubules to cause a global [cAMP] transient, demonstrating once again the importance of the supramolecular signaling complex organized around AKAP150 in β-AR signaling in heart failure (Nikolaev et al., 2010). The authors tested another hypothesis that the β2-ARs are localized in cholesterol-rich lipid rafts, or caveolae, in T-tubules. Caveolae are miniature flask-shaped invaginations in the sarcolemma enriched in cholesterol, and they are thought to form around caveolins (Richter et al., 2008). Coincidentally, Nichols et al. showed by co-IP that caveolin-3 is a component of the AKAP150 signaling complex in cardiac myocytes (Nichols et al., 2010). In another affirmation, β2-AR signaling in healthy cardiac myocytes treated with a detergent to deplete membrane cholesterol became delocalized, just as in heart failure cardiac myocytes (Nikolaev et al., 2010). The results of this study suggest that β2-AR, when associated with the AKAP79/150 based signaling complex within caveolae in T-tubules may be cardioprotective in

normal physiology, and the loss of its spatiotemporal restriction contributes to the pathophysiology of heart failure.

4.4 Caveolae and heart disease: The Lipid Raft of the Medusa?

There is growing body of biophysical evidence for the important role caveolae play in the pathophysiology of heart diseases. Whereas Nikolaev et al. indirectly inferred the role of caveolae in the localization of β2-AR to T-tubules; Ianoul et al. used a very advanced super-resolution imaging technique of near-field scanning microscopy (NSOM) to show the colocalization of β2-AR and caveolin-3 (Ianoul et al., 2005; Nikolaev et al., 2010). NSOM is a very interesting imaging technique as it combines features of atomic force microscopy and near-field light microscopy, giving us a resolution of ~50 nm (Ianoul et al., 2005; Lewis et al., 2003). NSOM has the advantage of specificity for only surface features on a cell and not what lies on the inside (Ianoul et al., 2005). Ianoul et al. used NSOM to image cultured H9C2 cells that had been stained with an anti-β2-AR primary antibody and a fluorescent secondary antibody then fixed. They found that β2-ARs are found in discrete, variably sized clusters (~60-300 nm), at a density of roughly to 30-50 receptors/μm^2, which are uniformly distributed across the cell membrane (H9C2 cells have no T-tubules). The packing density of β2-AR in these clusters is much less than that found for rhodopsin in rods (Ianoul et al., 2005). NSOM imaging of fixed H9C2 cells and neonatal cardiac myocytes stained for caveolin-3 found clusters approximately

twice as large as those clusters of β2-AR, and these presumed caveolae agree well in size with previous studies using electron microscopy. In H9C2 cells and neonatal cardiac myocytes doubly-stained for both β2-AR and caveolin-3, Ianoul et al. found using both NSOM and conventional confocal microscopy that these two proteins colocalize in a subpopulation of clusters. Their clustering and colocalization is not altered by ISO treatment of the cells before they were fixed, suggesting that the localization of β2-AR in caveolae is physiological in β2-AR signaling. However, the observation of β2-AR outside of caveolae suggest that there is a non-pathological role for β2-AR signaling outside of caveolae as well (Ianoul et al., 2005).

Although caveolin-3's role in β2-AR signaling may be an important part of the pathophysiology of heart failure, mutations in caveolin-3 itself have been recently identified as the etiology for a novel form of congenital long QT syndrome (Vatta et al., 2006). Vatta et al. found that two caveolin-3 mutations, F97C and S141R, cause a significant increase in the late, non-inactivating component of the $Na_V1.5$ whole-cell Na^+ current, which presumably delays repolarization and cause QT prolongation. Immunohistochemistry of human ventricular myocytes showed that $Na_V1.5$ and cavolin-3 colocalize in the sarcolemma, and these novel mutations do not affect caveolin-3 coimmunoprecipitating with $Na_V1.5$ (Vatta et al., 2006). Currently, the specific molecular interactions between the mutant caveolin-3 that cause the alteration to $Na_V1.5$ inactivation is yet identified.

4.5 On the TIRF of Ca^{2+} microdomains and heart failure

Another important biophysical tool that is used to study microdomains in cardiac signaling near the sarcolemma is TIRF microscopy, which offers extremely high signal to noise ratio for the study of signaling events that occur within its evanescent field of ~100 nm thick (Navedo et al., 2005). Ca^{2+} is possibly the most basic and important signaling molecule in cardiac myocytes, and the available of low-affinity Ca^{2+} indicators allow us to image fast [Ca^{2+}] fluctuations. In our laboratory, we use TIRF in the study of microdomains of Ca^{2+} signaling called Ca^{2+} sparklets, which are the fluorescence increase of Ca^{2+} indicators like fluo-5F and rhod-2 caused by the opening of surface membrane Ca^{2+} channels (Navedo et al., 2006). Snell's law describes the theory of operation behind TIRF. When light traveling from a substrate with a higher index of refraction is incident upon an interface into a medium with a lower index of refraction, it will totally reflect if the incident angle is sharper than the critical angle, θ_C,

$$\theta_C = \sin^{-1} {}^{n_2}/_{n_1},$$

where n_1 and n_2 are the higher and lower indices of refraction, respectively. On the other side of the interface, there exists an "evanescent" electric field with an intensity that decays exponentially with distance away from the interface (Axelrod, Burghardt, & Thompson, 1984):

$$I(z) = I_0 e^{-\frac{z}{d}}.$$

Where *z* is the distance away from the interface, and *d* is:

$$d = \frac{\lambda_0}{4\pi}[n_1^2 \sin^2\theta - n_2^2]^{-1/2},$$

where λ_0 is the wavelength of the incident light. $d < \lambda_0$ typically, with a typical useful evanescent field of ~100 nm thick above the coverslip (Axelrod et al., 1984; Navedo et al., 2005). The thin "optical slice" offered by the evanescent field gives us superior signal-to-noise compared to confocal microscopy, provided that the signalome that we seek to visualize is close to the cell membrane.

In our Ca^{2+} sparklet studies, conducted near the diastolic potential of -70 mV to maximize the Ca^{2+} driving force, the Ca^{2+} sparklets were recorded by a high-speed CCD camera at ~10 Hz, with sufficient temporal resolution to visualize the flickering on and off of the Ca^{2+} channels with good signal-to-noise ratio. We converted the background subtracted fluorescence ratio values into $[Ca^{2+}]$ using the F_{max} equation, and we consistently obtained the identical "quantal" value for $\Delta[Ca^{2+}]$ by a single $Ca_V1.2$ channel opening of ~38 nmol/L (Maravall et al., 2000; Navedo et al., 2005). These studies reveal that increased spatial heterogeneity in sparklet activity under conditions analogous to those associated with heart failure. For example, our Ca^{2+} sparklet data show that PKCα activation produces persistent Ca^{2+} sparklets and facilitates $Ca_V1.2$ channels to underdo coupled gating (Navedo et al., 2010). PKCα

activation leads to heart failure, and its inhibition is protective against it (Ladage et al., 2011). Furthermore, data from AKAP150$^{-/-}$ myocytes show that the scaffolding protein AKAP150 is required for targeting PKCα to $Ca_V1.2$ channels to facilitate both persistent and coupled Ca^{2+} sparklets, and consequently we imaged using confocal microscopy the difference in the level of translocation of the nuclear transcription factor NFAT into the nucleus in AKAP150$^{-/-}$ myocytes (Navedo et al., 2008, 2010; Nieves-Cintrón et al., 2008). Calcineurin (PP2B) is also targeted to $Ca_V1.2$ by AKAP150, and it is activated by increases in AKAP150-dependent Ca^{2+} sparklet activity (Nieves-Cintrón et al., 2008). Activated calcineurin dephoshorylates NFAT, triggering its translocation into the nucleus (Nieves-Cintrón et al., 2008). Coincidentally, using classic biochemical methods, Liu et al. showed that NFAT plays a role in hypertrophy and pathologic remodeling during heart failure (Q. Liu, Chen, Auger-Messier, & Molkentin, 2012). NFAT signaling also acts on a much shorter timescale in arrhythmogenesis at 48 hours after a myocardial infarction, causing the down-regulation of the phase 1 repolarizing transient outward K^+ current (I_{to}) (Rossow, Minami, Chase, Murry, & Santana, 2004).

By being a scaffold for PKCα, PKA, and calcineurin (PP2B), AKAP150 is truly the Swiss army knife of scaffolding proteins (Scott & Santana, 2010). And as we learned from multiple studies, its role in organizing β2-AR in caveolae signaling may play an important role in the pathophysiology of heart failure (Ianoul et al., 2005; Nichols et al., 2010; Nikolaev et al., 2010). From our Ca^{2+} sparklets recorded using TIRF microscopy, we found that its interaction with $Ca_V1.2$ is required for coupled

gating (Navedo et al., 2010). We found that coupled gating plays a critical role in the pathophysiology of Timothy syndrome (LQT8), a congenital long QT syndrome that can cause hypertrophy in both human patients and our LQT8 transgenic mouse model (E. P. Cheng et al., 2011; Navedo et al., 2010; Splawski et al., 2004). Importantly, we completely rescued WT phenotype in LQT8/AKAP150$^{-/-}$ mice, and we showed that AKAP150 interaction with mutant $Ca_V1.2$-LQT8 channels is responsible for the LQT8 phenotype (E. P. Cheng et al., 2011).

A question that has perplexed our group is to be able to visualize what we hypothesize to be a variable stoichiometry of AKAP150 mediated coupling between $Ca_V1.2$ channels, as traditional co-IP studies are both too harsh and not quantitative. A recent technique pioneered by Jain et al., using TIRF microscopy to image single-molecule pull-downs in order to study single molecular protein-protein interactions, offers an intriguing option for our group, as well as others, who want to directly visualize protein complexes at the single-molecule level (Jain, Liu, Xiang, & Ha, 2012). As a proof of concept for this exciting new technique, Jain et al. used AKAP, immobilized on polyethyleneglycol coated quartz coverslips by anti-AKAP antibodies bound to the coverslip by avidin, as the bait molecule to pull down PKA as the prey molecule. The molecular complex was incubated in an anti-PKA antibody conjugated to YFP. Jain et al. was able to visualize individual AKAP-PKA complexes using TIRF microscopy with good signal-to-noise level (Jain et al., 2012). This study shows how a hybrid technique between biophysics and biochemistry can

gives us direct quantitative results at the single molecule level not previously possible with traditional co-IP.

4.6 Shining the light on signaling pathways at the single molecular level

Another TIRF-based technique that we can use to resolve molecular stoichiometry in heart failure signaling is single-molecule stepwise photobleaching. An elegant recent study by He et al. employs TIRF in single-molecule stepwise photobleaching to visualize the dimerization of transforming growth factor β (TGF-β) receptors in the sarcolemma of neonatal ventricular myocytes undergoing hypertrophy (He et al., 2011). They observed more frequent dimers, which were activated TGF-β receptors, in cardiac myocytes treated with either angiotensin II or phenylephrine to induce hypertrophy. The EMCCD camera acquired TIRF movies had good temporal resolution at 10 Hz, and after processing the raw movies by subtracting the averaged background and integrating the fluorescence in regions of interest, the resultant records clearly showed sharp, step-wise single molecular photobleaching steps that had good signal-to-noise, which allowed them to clearly differentiate dimers from monomers. They also verified the imaging results with a traditional Western blot, and it showed an increased level of activated (phosphorylated) nuclear transcription factor Smad3, which is downstream in the TGF-β signaling cascade. Their data agree well with previous studies that show TGF-β signaling via the activation and nuclear translocation of Smads to play a key role in cardiac

remodeling post-MI that leads to heart failure (Bujak & Frangogiannis, 2007). However, another previous study, using a different heart failure induction protocol, found that during hypertrophic cardiac remodeling caused by pressure overload, TGF-β signaling is transduced via TAK1 and p38, instead of through Smad2/3/4 (D. Zhang et al., 2000). Such conundrum is a common frustration for those trying to decipher the labyrinthine signaling networks of heart failure that appear to have multiple choices of interaction partners at every turn.

A recent study from the field of developmental biology employing bimolecular fluorescence complementation (BiFC) gives us another potential biophysical tool to untangle the "conflicting" signaling pathways in live cells (Saka, Hagemann, Piepenburg, & Smith, 2007). Saka et al. fused N- and C- terminal halves of the fluorescent protein VENUS onto Smad2 and Smad4, respectively. When activated, Smad2 and Smad4 bind to each other and accumulate in the nucleus, and Saka et al. were able to visualize the formation of Smad2/4 complex after midblastula transition and Smad2/4 nuclear accumulation using a conventional epifluorescence microscope as an increase in VENUS fluorescence in the *Xenopus* oocyte nucleus. The advantage of BiFC over the more widely used optical method for the study of bimolecular interaction, FRET, is that the resultant signal much brighter per molecule, so the signal-to-noise ratio is much less of an issue especially for proteins not naturally expressed in high concentrations. Similar technique could be applied in the study of TGFβ pathway in heart failure to elucidate whether Smad2/4 complex indeed contributes to TGF-β mediated signaling in phenylephrine and angiotensin II

induced hypertrophy, or if TGF-β signaling cascades exclusively through the TAK1 pathway in heart failure. BiFC gives us another tool to complement FRET in resolving single-molecular interactions in cardiac signaling pathways.

4.7 Epilogue

Application of novel biophysical techniques in the study of local signaling pathways that participate in heart failure allows us to dissect more finely the complicated Gordian Knot of heart failure. Because heart failure is the final convergent pathway for multiple disease processes, caution must be observed in not over-generalizing any novel drug target identified in heart failure. For example, even though our group has demonstrated in multiple studies how an abnormal elevation in $Ca_V1.2$ channel activity due to coupled gating is pathologic; however, a recent study found that in mice with one copy of the $Ca_V1.2$ gene knocked out, resulting in significantly decreased trans-sarcolemmal Ca^{2+} current, heart failure develops because of excessive β-AR signaling as a compensatory mechanism (E. P. Cheng et al., 2011; Dixon et al., 2012; Goonasekera et al., 2012; Navedo et al., 2010). The Goldilocks' Rule seems to apply in medicine: not too hot, not too cold. One of the hopes with using biophysical techniques in the study of heart failure is that by understanding signaling at a higher spatiotemporal resolution, we would not seek to employ the pharmacologic equivalent of a sledgehammer in the treatment of heart failure, when a more civil alternative could be had.

Chapter 5: Concluding remarks

In this dissertation, I make the case for AKAP79/150 mediated coupled gating of a subpopulation of L-type $Ca_V1.2$ channels, occurring in both normal $Ca_V1.2$ physiology and during pathophysiology, such as in hypertension and Timothy syndrome, which is a paradigm shift in how we think of both scaffolding proteins and voltage-gated ion channels should behave. Coupled gating of $Ca_V1.2$ may appear to be too deterministic to fit into our Markovian view of ion channels; however, given that ~10-15 $Ca_V1.2$ channels need to be simultaneously open in order to achieve the high Ca^{2+} spark activation probability during the phase II plateau of the cardiac AP, when the open probability of $Ca_V1.2$ is ~0.5 at the membrane voltage of +50 mV, the improbably low probability of 0.5^{10}-0.5^{15} speaks for itself (Dixon et al., 2012).

In Chapter 2, I present the study of how we initially characterized coupled gating of $Ca_V1.2$ channels. We first observed via Ca^{2+} sparklets using TIRF microscopy that spatially heterogeneous clusters of 2 to 6 $Ca_V1.2$ channels can transiently undergo concerted openings and closings. We then hypothesized that $Ca_V1.2$ channels undergo coupled gating. As an objective measure of "coupled-ness," I chose to use a lumped parameter partially coupled Markov model to fit our Ca^{2+} sparklet and cell-attached current records and to provide us with the coupling coefficient (κ) (Chung & Kennedy, 1996). We found that in the presence of AKAP79/150, we could increase

the probability of 2-6 channels to undergo coupled gating by PKCα activation and CaM inhibition, giving us mechanistic insight. We also found that $Ca_V1.2$-TS (Timothy syndrome) channels undergo more frequent coupled gating. Yet, future studies need to investigate fully the questions of stoichiometry and voltage dependence in the coupled gating mechanism. We showed using FRET that under conditions that favored coupled gating, there is increased interaction between the carboxy tails of neighboring channels, and there is also decrease in interaction between CaM and the IQ domain. Future studies need to answer the questions that via which domain in the carboxy tail do these channels interact, and how does $[Ca^{2+}]$ feed back into CaM dislodgement from the IQ domain?

In Chapter 3, I foray deeper into the role of coupled gating and AKAP150 in arrhythmogenesis in LQT8, the principal cardiac manifestation of Timothy syndrome, by characterizing the LQT8 transgenic mouse and the LQT8/ $AKAP150^{-/-}$ cross mouse. Compared to wild-type (WT) and LQT8/ $AKAP150^{-/-}$ ventricular myocytes, LQT8 ventricular myocytes have delayed inactivation in whole-cell $Ca_V1.2$ current, and there is increased frequency in coupled gating and open time in our cell-attached current records. Importantly, $AKAP150^{-/-}$ completely restored WT I_{Ca} inactivation and frequency of coupled gating in mice expressing $Ca_V1.2$-LQT8 channels, while inhibition of CaMKII does not. LQT8 myocytes also have prolonged action potential duration and arrhythmogenic voltage fluctuations, such as early and delayed afterdepolarizations, when compared to both WT and LQT8/ $AKAP150^{-/-}$. With respect to EC coupling, LQT8 ventricular myocytes have increased $[Ca^{2+}]$

transient amplitudes and more frequent arrhythmogenic spontaneous Ca^{2+} releases when compared to both WT and LQT8/ AKAP150$^{-/-}$. On the whole animal level, when we recorded ECG telemetry during exercise, LQT8 mice have prolonged QT_C interval and more frequent incidence of Torsades de Pointes (TdP) ventricular tachycardia than WT and LQT8/ AKAP150$^{-/-}$. I believe this study conclusively demonstrate that association between $Ca_V1.2$-LQT8 channels and AKAP150 is necessary for the expression of the LQT8 phenotype, and coupled gating of $Ca_V1.2$-LQT8 channels plays a central role in the pathophysiology and arrhythmogenesis in TS. However, even though the frequency of coupled gating is highly elevated in $Ca_V1.2$-LQT8 channels, it is still transient phenomenon. Future studies should attempt to combine optical and electrophysiological techniques to characterize the fraction of $Ca_V1.2$-LQT8 channels that undergo coupled gating and the lifetime of these transient oligomers of $Ca_V1.2$-LQT8 channels. Future studies should also attempt to simultaneously image coupled Ca^{2+} sparklets and Ca^{2+} sparks in LQT8 ventricular myocytes to establish the local effect of coupled gating on the probability of Ca^{2+} spark activation, thereby conclusively establishing the role of coupled gating in the local control of EC coupling.

In conclusion, AKAP79/150 mediated coupled gating occur in a spatially and temporally heterogeneous subpopulation of $Ca_V1.2$ channels, and increased frequency in coupled gating plays a central role in the pathophysiology of LQT8, causing perturbations of EC coupling that lead to arrhythmogenesis. I found that In trying to understand the secrets of coupled gating and the arrhythmogenic

mechanisms of Timothy syndrome I have become philosophically intrigued by how alterations to the probability of quasi-stochastic events can lead to very deterministic outcomes due to the large signal amplification built into a signal transduction cascade such as EC coupling. In Timothy syndrome, for example, the interaction between $Ca_V1.2$-LQT8 and AKAP79/150 increases the frequency of coupled gating and longer openings. Yet, I am amazed by how such seemingly transient shifts in kinetics in oligomers of $Ca_V1.2$ channels translate into severely disturbed EC coupling and arrhythmias. Future studies should try to answer this question: does a threshold for arrhythmogenesis triggered by coupled gating of $Ca_V1.2$ channels exist, and if it does, how much coupled gating is pathophysiological? If coupled gating is part of the normal physiology of EC coupling by helping to maintain the synchrony of EC coupling during the AP plateau, then the point of no return must exists before the positive feedback from locally enhanced EC coupling becomes pathophysiological. I hope the discovery of coupled gating in $Ca_V1.2$ channels and its role in arrhythmogenesis in LQT8 contributes to our understanding of the local control of EC coupling, especially its spatial and temporal heterogeneity, and how perturbations to this mechanism can lead to arrhythmias.

Bibliography

Abiria, S. A., & Colbran, R. J. (2010). CaMKII associates with CaV1.2 L-type calcium channels via selected β subunits to enhance regulatory phosphorylation. *Journal of Neurochemistry*, *112*(1), 150–161. doi:10.1111/j.1471-4159.2009.06436.x

Allen, M. D., & Zhang, J. (2006). Subcellular dynamics of protein kinase A activity visualized by FRET-based reporters. *Biochemical and Biophysical Research Communications*, *348*(2), 716–721. doi:10.1016/j.bbrc.2006.07.136

Arikkath, J., & Campbell, K. P. (2003). Auxiliary subunits: essential components of the voltage-gated calcium channel complex. *Current Opinion in Neurobiology*, *13*(3), 298–307. doi:10.1016/S0959-4388(03)00066-7

Axelrod, D., Burghardt, T. P., & Thompson, N. L. (1984). Total Internal Reflection Fluorescence. *Annu. Rev. Biophys. Bioeng.*, *13*(1), 247–268. doi:10.1146/annurev.bb.13.060184.001335

Baddeley, D., Jayasinghe, I. D., Lam, L., Rossberger, S., Cannell, M. B., & Soeller, C. (2009). Optical single-channel resolution imaging of the ryanodine receptor distribution in rat cardiac myocytes. *Proceedings of the National Academy of Sciences*, *106*(52), 22275 –22280. doi:10.1073/pnas.0908971106

Bader, P. L., Faizi, M., Kim, L. H., Owen, S. F., Tadross, M. R., Alfa, R. W., Bett, G. C. L., et al. (2011). Mouse model of Timothy syndrome recapitulates triad of

autistic traits. *Proceedings of the National Academy of Sciences*, *108*(37), 15432 –15437. doi:10.1073/pnas.1112667108

Bannister, J. P., Adebiyi, A., Zhao, G., Narayanan, D., Thomas, C. M., Feng, J. Y., & Jaggar, J. H. (2009). Smooth Muscle Cell α2δ-1 Subunits Are Essential for Vasoregulation by CaV1.2 Channels. *Circulation Research*, *105*(10), 948 – 955. doi:10.1161/CIRCRESAHA.109.203620

Barrett, C. F., & Tsien, R. W. (2008). The Timothy syndrome mutation differentially affects voltage- and calcium-dependent inactivation of CaV1.2 L-type calcium channels. *Proceedings of the National Academy of Sciences*, *105*(6), 2157 – 2162. doi:10.1073/pnas.0710501105

Bauman, A. L., Michel, J. J. C., Henson, E., Dodge-Kafka, K. L., & Kapiloff, M. S. (2007). The mAKAP signalosome and cardiac myocyte hypertrophy. *IUBMB Life*, *59*(3), 163–169. doi:10.1080/15216540701358593

Bean, B. P., Nowycky, M. C., & Tsien, R. W. (1984). [beta]-Adrenergic modulation of calcium channels in frog ventricular heart cells. *Nature*, *307*(5949), 371–375. doi:10.1038/307371a0

Berne, R. M., Spreelakis, N., & Geiger, S. R. (Eds.). (1979). *Handbook of Physiology: The Cardiovascular System*. Bethesda, MD: American Physiological Society.

Bezanilla, F. (2000). The Voltage Sensor in Voltage-Dependent Ion Channels. *Physiological Reviews*, *80*(2), 555 –592.

Blayney, L. M., & Lai, F. A. (2009). Ryanodine receptor-mediated arrhythmias and sudden cardiac death. *Pharmacology & Therapeutics*, *123*(2), 151–177. doi:10.1016/j.pharmthera.2009.03.006

Bolte, S., & Cordelières, F. P. (2006). A guided tour into subcellular colocalization analysis in light microscopy. *Journal of Microscopy*, *224*(3), 213–232. doi:10.1111/j.1365-2818.2006.01706.x

Brehm, P., & Eckert, R. (1978). Calcium entry leads to inactivation of calcium channel in Paramecium. *Science*, *202*(4373), 1203 –1206. doi:10.1126/science.103199

Bujak, M., & Frangogiannis, N. G. (2007). The role of TGF-β signaling in myocardial infarction and cardiac remodeling. *Cardiovascular Research*, *74*(2), 184 –195. doi:10.1016/j.cardiores.2006.10.002

Cannell, M. B., & Kong, C. H. T. (2012). Local control in cardiac E–C coupling. *Journal of Molecular and Cellular Cardiology*, *52*(2), 298–303. doi:10.1016/j.yjmcc.2011.04.014

Cannell, M., Berlin, & Lederer, W. (1987). Effect of membrane potential changes on the calcium transient in single rat cardiac muscle cells. *Science*, *238*(4832), 1419 –1423. doi:10.1126/science.2446391

Cannell, M., Cheng, H., & Lederer, W. (1995). The control of calcium release in heart muscle. *Science*, *268*(5213), 1045 –1049. doi:10.1126/science.7754384

Catterall, W. A. (2000). STRUCTURE AND REGULATION OF VOLTAGE-GATED Ca2+ CHANNELS. *Annu. Rev. Cell Dev. Biol.*, *16*(1), 521–555. doi:10.1146/annurev.cellbio.16.1.521

Catterall, W. A. (2011). Voltage-Gated Calcium Channels. *Cold Spring Harbor Perspectives in Biology*, *3*(8). doi:10.1101/cshperspect.a003947

Cens, T., Rousset, M., Leyris, J.-P., Fesquet, P., & Charnet, P. (2006). Voltage- and calcium-dependent inactivation in high voltage-gated Ca2+ channels. *Progress in Biophysics and Molecular Biology*, *90*(1–3), 104–117. doi:10.1016/j.pbiomolbio.2005.05.013

Chen, L., El-Husseini, A., Tomita, S., Bredt, D. S., & Nicoll, R. A. (2003). Stargazin Differentially Controls the Trafficking of α-Amino-3-hydroxyl-5-methyl-4-isoxazolepropionate and Kainate Receptors. *Molecular Pharmacology*, *64*(3), 703 –706. doi:10.1124/mol.64.3.703

Cheng, E. P., Yuan, C., Navedo, M. F., Dixon, R. E., Nieves-Cintrón, M., Scott, J. D., & Santana, L. F. (2011). Restoration of Normal L-Type Ca2+ Channel Function During Timothy Syndrome by Ablation of an Anchoring Protein / Novelty and Significance. *Circulation Research*, *109*(3), 255 –261. doi:10.1161/CIRCRESAHA.111.248252

Cheng, H, Lederer, W., & Cannell, M. (1993). Calcium sparks: elementary events underlying excitation-contraction coupling in heart muscle. *Science*, *262*(5134), 740 –744. doi:10.1126/science.8235594

Cheng, Heping, & Lederer, W. J. (2008). Calcium Sparks. *Physiological Reviews*, *88*(4), 1491–1545. doi:10.1152/physrev.00030.2007

Cheng, Heping, Song, L.-S., Shirokova, N., González, A., Lakatta, E. G., Ríos, E., & Stern, M. D. (1999). Amplitude Distribution of Calcium Sparks in Confocal

Images: Theory and Studies with an Automatic Detection Method. *Biophysical Journal*, *76*(2), 606–617. doi:10.1016/S0006-3495(99)77229-2

Cheng, Heping, & Wang, S. Q. (2002). Calcium signaling between sarcolemmal calcium cahnnels and ryanodine receptors in heart cells. *Frontiers in Bioscience*, *7*, 1867–1878.

Chien, A. J., Zhao, X., Shirokov, R. E., Puri, T. S., Chang, C. F., Sun, D., Rios, E., et al. (1995). Roles of a Membrane-localized Subunit in the Formation and Targeting of Functional L-type Ca Channels. *Journal of Biological Chemistry*, *270*(50), 30036 –30044. doi:10.1074/jbc.270.50.30036

Choi, B.-R., Burton, F., & Salama, G. (2002). Cytosolic Ca2+ triggers early afterdepolarizations and torsade de pointes in rabbit hearts with type 2 long QT syndrome. *The Journal of Physiology*, *543*(2), 615 –631. doi:10.1113/jphysiol.2002.024570

Chung, S.-H., & Kennedy, R. A. (1996). Coupled Markov chain model: Characterization of membrane channel currents with multiple conductance sublevels as partially coupled elementary pores. *Mathematical Biosciences*, *133*(2), 111–137. doi:10.1016/0025-5564(95)00084-4

Coghlan, V., Perrino, B., Howard, M., Langeberg, L., Hicks, J., Gallatin, W., & Scott, J. (1995). Association of protein kinase A and protein phosphatase 2B with a common anchoring protein. *Science*, *267*(5194), 108 –111. doi:10.1126/science.7528941

Colecraft, H. M., Alseikhan, B., Takahashi, S. X., Chaudhuri, D., Mittman, S., Yegnasubramanian, V., Alvania, R. S., et al. (2002). Novel functional

properties of Ca2+ channel β subunits revealed by their expression in adult rat heart cells. *The Journal of Physiology*, *541*(2), 435 –452. doi:10.1113/jphysiol.2002.018515

Cooper, P. J., Soeller, C., & Cannell, M. B. (2010). Excitation–contraction coupling in human heart failure examined by action potential clamp in rat cardiac myocytes. *Journal of Molecular and Cellular Cardiology*, *49*(6), 911–917. doi:10.1016/j.yjmcc.2010.04.012

Couchonnal, L. F., & Anderson, M. E. (2008). The Role of Calmodulin Kinase II in Myocardial Physiology and Disease. *Physiology*, *23*(3), 151 –159. doi:10.1152/physiol.00043.2007

Dai, S., Hall, D. D., & Hell, J. W. (2009). Supramolecular Assemblies and Localized Regulation of Voltage-Gated Ion Channels. *Physiological Reviews*, *89*(2), 411 –452. doi:10.1152/physrev.00029.2007

Day, R. N., Voss, T. C., Enwright, J. F., Booker, C. F., Periasamy, A., & Schaufele, F. (2003). Imaging the Localized Protein Interactions Between Pit-1 and the CCAAT/Enhancer Binding Protein α in the Living Pituitary Cell Nucleus. *Molecular Endocrinology*, *17*(3), 333 –345. doi:10.1210/me.2002-0136

Dayal, A., Schredelseker, J., Franzini-Armstrong, C., & Grabner, M. (2010). Skeletal muscle excitation–contraction coupling is independent of a conserved heptad repeat motif in the C-terminus of the DHPRβ1a subunit. *Cell Calcium*, *47*(6), 500–506. doi:10.1016/j.ceca.2010.04.003

De Arcangelis, V., Liu, S., Zhang, D., Soto, D., & Xiang, Y. K. (2010). Equilibrium between Adenylyl Cyclase and Phosphodiesterase Patterns Adrenergic

Agonist Dose-Dependent Spatiotemporal cAMP/Protein Kinase A Activities in Cardiomyocytes. *Molecular Pharmacology*, *78*(3), 340 –349. doi:10.1124/mol.110.064444

De Jongh, K. S., Murphy, B. J., Colvin, A. A., Hell, J. W., Takahashi, M., & Catterall, W. A. (1996). Specific Phosphorylation of a Site in the Full-Length Form of the α1 Subunit of the Cardiac L-Type Calcium Channel by Adenosine 3‘,5‘-Cyclic Monophosphate- Dependent Protein Kinase†. *Biochemistry*, *35*(32), 10392–10402. doi:10.1021/bi953023c

De Waard, M., Gurnett, C. A., & Campbell, K. P. (1996). Structural and functional diversity of voltage-activated calcium channels. *Ion Channels*, *4*, 41–87.

Demuro, A., & Parker, I. (2004). Imaging the Activity and Localization of Single Voltage-Gated Ca2+ Channels by Total Internal Reflection Fluorescence Microscopy. *Biophysical Journal*, *86*(5), 3250–3259. doi:10.1016/S0006-3495(04)74373-8

Demuro, A., & Parker, I. (2005). “Optical Patch-clamping.” *The Journal of General Physiology*, *126*(3), 179 –192. doi:10.1085/jgp.200509331

Devic, E., Xiang, Y., Gould, D., & Kobilka, B. (2001). β-Adrenergic Receptor Subtype-Specific Signaling in Cardiac Myocytes from β1 and β2 Adrenoceptor Knockout Mice. *Molecular Pharmacology*, *60*(3), 577 –583.

di Barletta, M. R., Viatchenko-Karpinski, S., Nori, A., Memmi, M., Terentyev, D., Turcato, F., Valle, G., et al. (2006). Clinical Phenotype and Functional Characterization of CASQ2 Mutations Associated With Catecholaminergic

Polymorphic Ventricular Tachycardia. *Circulation*, *114*(10), 1012 –1019. doi:10.1161/CIRCULATIONAHA.106.623793

Díaz, M. E., O'Neill, S. C., & Eisner, D. A. (2004). Sarcoplasmic Reticulum Calcium Content Fluctuation Is the Key to Cardiac Alternans. *Circulation Research*, *94*(5), 650 –656. doi:10.1161/01.RES.0000119923.64774.72

DiPilato, L. M., Cheng, X., & Zhang, J. (2004). Fluorescent indicators of cAMP and Epac activation reveal differential dynamics of cAMP signaling within discrete subcellular compartments. *Proceedings of the National Academy of Sciences of the United States of America*, *101*(47), 16513 –16518. doi:10.1073/pnas.0405973101

Dixon, R. E., Yuan, C., Cheng, E. P., Navedo, M. F., & Santana, L. F. (2012). Ca2+ signaling amplification by oligomerization of L-type Cav1.2 channels. *Proceedings of the National Academy of Sciences*, *109*(5), 1749 –1754. doi:10.1073/pnas.1116731109

Dodge, K. L., Khouangsathiene, S., Kapiloff, M. S., Mouton, R., Hill, E. V., Houslay, M. D., Langeberg, L. K., et al. (2001). mAKAP assembles a protein kinase A/PDE4 phosphodiesterase cAMP signaling module. *EMBO J*, *20*(8), 1921–1930. doi:10.1093/emboj/20.8.1921

Doupnik, C. A., Davidson, N., & Lester, H. A. (1995). The inward rectifier potassium channel family. *Curr Opin Neurobiol*, *5*(3), 268–277.

Drake, R. L., Vogl, W., & Mitchell, A. W. M. (2005). *Anatomy for Students*. Philadelphia: Churchill Livingstone.

Dressler, W., & Jonas, S. (1964). Observations in patients with implanted pacemaker: II. Effective refractory period and full recovery time of the ventricular myocardium calculated from clinical tracings. *American Heart Journal*, *67*(6), 724–733. doi:10.1016/0002-8703(64)90173-5

Erickson, M. G., Alseikhan, B. A., Peterson, B. Z., & Yue, D. T. (2001). Preassociation of Calmodulin with Voltage-Gated Ca2+ Channels Revealed by FRET in Single Living Cells. *Neuron*, *31*(6), 973–985. doi:10.1016/S0896-6273(01)00438-X

Erxleben, C., Liao, Y., Gentile, S., Chin, D., Gomez-Alegria, C., Mori, Y., Birnbaumer, L., et al. (2006). Cyclosporin and Timothy syndrome increase mode 2 gating of CaV1.2 calcium channels through aberrant phosphorylation of S6 helices. *Proceedings of the National Academy of Sciences of the United States of America*, *103*(10), 3932 –3937. doi:10.1073/pnas.0511322103

Fabiato, A. (1985). Rapid ionic modifications during the aequorin-detected calcium transient in a skinned canine cardiac Purkinje cell. *The Journal of General Physiology*, *85*(2), 189 –246. doi:10.1085/jgp.85.2.189

Fallon, J. L., Baker, M. R., Xiong, L., Loy, R. E., Yang, G., Dirksen, R. T., Hamilton, S. L., et al. (2009). Crystal structure of dimeric cardiac L-type calcium channel regulatory domains bridged by Ca2+·calmodulins. *Proceedings of the National Academy of Sciences*, *106*(13), 5135 –5140. doi:10.1073/pnas.0807487106

Findlay, I. (2004). Physiological modulation of inactivation in L-type Ca2+ channels: one switch. *The Journal of Physiology*, *554*(2), 275 –283. doi:10.1113/jphysiol.2003.047902

Fourcaudot, E., Gambino, F., Casassus, G., Poulain, B., Humeau, Y., & Luthi, A. (2009). L-type voltage-dependent Ca2+ channels mediate expression of presynaptic LTP in amygdala. *Nat Neurosci*, *12*(9), 1093–1095. doi:10.1038/nn.2378

Franzini-Armstrong, C., Protasi, F., & Ramesh, V. (1999). Shape, Size, and Distribution of Ca2+ Release Units and Couplons in Skeletal and Cardiac Muscles. *Biophysical Journal*, *77*(3), 1528–1539. doi:10.1016/S0006-3495(99)77000-1

Fuller, M. D., Emrick, M. A., Sadilek, M., Scheuer, T., & Catterall, W. A. (2010). Molecular Mechanism of Calcium Channel Regulation in the Fight-or-Flight Response. *Science Signaling*, *3*(141), ra70. doi:10.1126/scisignal.2001152

Gao, T., Yatani, A., Dell'Acqua, M. L., Sako, H., Green, S. A., Dascal, N., Scott, J. D., et al. (1997). cAMP-Dependent Regulation of Cardiac L-Type Ca2+ Channels Requires Membrane Targeting of PKA and Phosphorylation of Channel Subunits. *Neuron*, *19*(1), 185–196. doi:10.1016/S0896-6273(00)80358-X

Garibyan, L., & Lilly, L. S. (2007). Chapter 4: The Electrocardiogram. *Pathophysiology of Heart Disease* (4th ed.). Philadelphia: Lippincott Williams & Wilkins.

George, I., Sabbah, H. N., Xu, K., Wang, N., & Wang, J. (2011). β-Adrenergic receptor blockade reduces endoplasmic reticulum stress and normalizes calcium handling in a coronary embolization model of heart failure in canines. *Cardiovascular Research*, *91*(3), 447 –455. doi:10.1093/cvr/cvr106

Gold, M. G., Stengel, F., Nygren, P. J., Weisbrod, C. R., Bruce, J. E., Robinson, C. V., Barford, D., et al. (2011). Architecture and dynamics of an A-kinase anchoring protein 79 (AKAP79) signaling complex. *Proceedings of the National Academy of Sciences*, *108*(16), 6426 –6431. doi:10.1073/pnas.1014400108

Goldman, D. E. (1943). POTENTIAL, IMPEDANCE, AND RECTIFICATION IN MEMBRANES. *The Journal of General Physiology*, *27*(1), 37 –60. doi:10.1085/jgp.27.1.37

Gómez, A. M., Valdivia, H. H., Cheng, H., Lederer, M. R., Santana, L. F., Cannell, M. B., McCune, S. A., et al. (1997). Defective Excitation-Contraction Coupling in Experimental Cardiac Hypertrophy and Heart Failure. *Science*, *276*(5313), 800 –806. doi:10.1126/science.276.5313.800

Gomez-Ospina, N., Tsuruta, F., Barreto-Chang, O., Hu, L., & Dolmetsch, R. (2006). The C Terminus of the L-Type Voltage-Gated Calcium Channel CaV1.2 Encodes a Transcription Factor. *Cell*, *127*(3), 591–606. doi:10.1016/j.cell.2006.10.017

Goonasekera, S. A., Hammer, K., Auger-Messier, M., Bodi, I., Chen, X., Zhang, H., Reiken, S., et al. (2012). Decreased cardiac L-type Ca2+ channel activity

induces hypertrophy and heart failure in mice. *The Journal of Clinical Investigation*, *122*(1), 280–290.

Guatimosim, C., Hull, C., Von Gersdorff, H., & Prado, M. A. M. (2002). Okadaic acid disrupts synaptic vesicle trafficking in a ribbon-type synapse. *Journal of Neurochemistry*, *82*(5), 1047–1057. doi:10.1046/j.1471-4159.2002.01029.x

Györke, I., Hester, N., Jones, L. R., & Györke, S. (2004). The Role of Calsequestrin, Triadin, and Junctin in Conferring Cardiac Ryanodine Receptor Responsiveness to Luminal Calcium. *Biophysical Journal*, *86*(4), 2121–2128. doi:10.1016/S0006-3495(04)74271-X

Harris, D. M., Mills, G. D., Chen, X., Kubo, H., Berretta, R. M., Votaw, V. S., Santana, L. F., et al. (2005). Alterations in Early Action Potential Repolarization Causes Localized Failure of Sarcoplasmic Reticulum Ca2+ Release. *Circulation Research*, *96*(5), 543 –550. doi:10.1161/01.RES.0000158966.58380.37

Haugland, R. P., Yguerabide, J., & Stryer, L. (1969). DEPENDENCE OF THE KINETICS OF SINGLET-SINGLET ENERGY TRANSFER ON SPECTRAL OVERLAP. *Proceedings of the National Academy of Sciences*, *63*(1), 23–30.

Hayashi, T., Martone, M. E., Yu, Z., Thor, A., Doi, M., Holst, M. J., Ellisman, M. H., et al. (2009). Three-dimensional electron microscopy reveals new details of membrane systems for Ca2+ signaling in the heart. *Journal of Cell Science*, *122*(7), 1005 –1013. doi:10.1242/jcs.028175

He, K., Fu, Y., Zhang, W., Yuan, J., Li, Z., Lv, Z., Zhang, Y., et al. (2011). Single-molecule imaging revealed enhanced dimerization of transforming growth

factor β type II receptors in hypertrophic cardiomyocytes. *Biochemical and Biophysical Research Communications*, *407*(2), 313–317. doi:10.1016/j.bbrc.2011.03.008

Hecht, H. H. (1961). Some observations and theories concerning the electrical behavior of heart muscle. *The American Journal of Medicine*, *30*(5), 720–746. doi:10.1016/0002-9343(61)90210-8

Heinemann, S. H., Terlau, H., Stuhmer, W., Imoto, K., & Numa, S. (1992). Calcium channel characteristics conferred on the sodium channel by single mutations. *Nature*, *356*(6368), 441–443. doi:10.1038/356441a0

Hess, P., & Tsien, R. W. (1984). Mechanism of ion permeation through calcium channels. *Nature*, *309*(5967), 453–456. doi:10.1038/309453a0

Hicks, M., Shigekawa, M., & Katz, A. (1979). Mechanism by which cyclic adenosine 3':5'-monophosphate-dependent protein kinase stimulates calcium transport in cardiac sarcoplasmic reticulum. *Circulation Research*, *44*(3), 384 –391. doi:10.1161/01.RES.44.3.384

Huffaker, R., Lamp, S. T., Weiss, J. N., & Kogan, B. (2004). Intracellular calcium cycling, early afterdepolarizations, and reentry in simulated long QT syndrome. *Heart Rhythm*, *1*(4), 441–448. doi:10.1016/j.hrthm.2004.06.005

Hulme, J. T., Lin, T. W.-C., Westenbroek, R. E., Scheuer, T., & Catterall, W. A. (2003). β-Adrenergic regulation requires direct anchoring of PKA to cardiac CaV1.2 channels via a leucine zipper interaction with A kinase-anchoring protein 15. *Proceedings of the National Academy of Sciences*, *100*(22), 13093 –13098. doi:10.1073/pnas.2135335100

Huxley, A. F., & Niedergerke, R. (1954). Structural Changes in Muscle During Contraction: Interference Microscopy of Living Muscle Fibres. *Nature*, *173*(4412), 971–973. doi:10.1038/173971a0

Huxley, H., & Hanson, J. (1954). Changes in the Cross-Striations of Muscle during Contraction and Stretch and their Structural Interpretation. *Nature*, *173*(4412), 973–976. doi:10.1038/173973a0

Ianoul, A., Grant, D. D., Rouleau, Y., Bani-Yaghoub, M., Johnston, L. J., & Pezacki, J. P. (2005). Imaging nanometer domains of β-adrenergic receptor complexes on the surface of cardiac myocytes. *Nature Chemical Biology*, *1*(4), 196–202. doi:Article

Imredy, J. P., & Yue, D. T. (1994). Mechanism of Ca2+-sensitive inactivation of L-type Ca2+ channels. *Neuron*, *12*(6), 1301–1318. doi:10.1016/0896-6273(94)90446-4

Inoue, M., & Bridge, J. H. B. (2003). Ca2+ Sparks in Rabbit Ventricular Myocytes Evoked by Action Potentials. *Circulation Research*, *92*(5), 532 –538. doi:10.1161/01.RES.0000064175.70693.EC

Iyer, V., Edelman, E. R., & Lilly, L. S. (2007). Chapter 1: Basic Cardiac Structure and Function. *Pathophysiology of Heart Disease* (4th ed.). Philadelphia: Lippincott Williams & Wilkins.

Izu, L. T., Bányász, T., Balke, C. W., & Chen-Izu, Y. (2007). Eavesdropping on the Social Lives of Ca2+ Sparks. *Biophysical Journal*, *93*(10), 3408–3420. doi:10.1529/biophysj.107.112466

Jain, A., Liu, R., Xiang, Y. K., & Ha, T. (2012). Single-molecule pull-down for studying protein interactions. *Nat. Protocols*, *7*(3), 445–452. doi:10.1038/nprot.2011.452

Josephson, I. R., Guia, A., Sobie, E. A., Lederer, W. J., Lakatta, E. G., & Stern, M. D. (2010). Physiologic gating properties of unitary cardiac L-type Ca2+ channels. *Biochemical and Biophysical Research Communications*, *396*(3), 763–766. doi:10.1016/j.bbrc.2010.05.016

Kaufman, E. S. (2009). Mechanisms and clinical management of inherited channelopathies: Long QT syndrome, Brugada syndrome, catecholaminergic polymorphic ventricular tachycardia, and short QT syndrome. *Heart Rhythm*, *6*(8, Supplement), S51–S55. doi:10.1016/j.hrthm.2009.02.009

Kemp, C. D., & Conte, J. V. (2012). The pathophysiology of heart failure. *Cardiovasc Pathol*. Retrieved from http://www.hubmed.org/display.cgi?uids=22227365

Klauck, T. M., Faux, M. C., Labudda, K., Langeberg, L. K., Jaken, S., & Scott, J. D. (1996). Coordination of Three Signaling Enzymes by AKAP79, a Mammalian Scaffold Protein. *Science*, *271*(5255), 1589 –1592. doi:10.1126/science.271.5255.1589

Korchev, Y. E., Negulyaev, Y. A., Edwards, C. R. W., Vodyanoy, I., & Lab, M. J. (2000). Functional localization of single active ion channels on the surface of a living cell. *Nat Cell Biol*, *2*(9), 616–619. doi:10.1038/35023563

Lacerda, A. E., Kim, H. S., Ruth, P., Perez-Reyes, E., Flockerzi, V., Hofmann, F., Birnbaumer, L., et al. (1991). Normalization of current kinetics by interaction between the [alpha]1and [beta] subunits of the skeletal muscle

dihydropyridine-sensitive Ca2+ channel. *Nature*, *352*(6335), 527–530. doi:10.1038/352527a0

Ladage, D., Tilemann, L., Ishikawa, K., Correll, R. N., Kawase, Y., Houser, S. R., Molkentin, J. D., et al. (2011). Inhibition of PKCα/β With Ruboxistaurin Antagonizes Heart Failure in Pigs After Myocardial Infarction Injury / Novelty and Significance. *Circulation Research*, *109*(12), 1396 –1400. doi:10.1161/CIRCRESAHA.111.255687

Lakatta, E. G., Maltsev, V. A., & Vinogradova, T. M. (2010). A Coupled SYSTEM of Intracellular Ca2+ Clocks and Surface Membrane Voltage Clocks Controls the Timekeeping Mechanism of the Heart's Pacemaker. *Circulation Research*, *106*(4), 659 –673. doi:10.1161/CIRCRESAHA.109.206078

Langer, G. A., & Peskoff, A. (1996). Calcium concentration and movement in the diadic cleft space of the cardiac ventricular cell. *Biophysical Journal*, *70*(3), 1169–1182. doi:10.1016/S0006-3495(96)79677-7

Lehnart, S. E., Wehrens, X. H. T., Reiken, S., Warrier, S., Belevych, A. E., Harvey, R. D., Richter, W., et al. (2005). Phosphodiesterase 4D Deficiency in the Ryanodine-Receptor Complex Promotes Heart Failure and Arrhythmias. *Cell*, *123*(1), 25–35. doi:10.1016/j.cell.2005.07.030

Lewis, A., Taha, H., Strinkovski, A., Manevitch, A., Khatchatouriants, A., Dekhter, R., & Ammann, E. (2003). Near-field optics: from subwavelength illumination to nanometric shadowing. *Nat Biotech*, *21*(11), 1378–1386. doi:10.1038/nbt898

Liao, P., & Soong, T. (2010). $Ca_V1.2$ channelopathies: from arrhythmias to autism, bipolar disorder, and immunodeficiency. *Pflügers Archiv European Journal of Physiology*, *460*(2), 353–359. doi:10.1007/s00424-009-0753-0

Liao, Z., Lockhead, D., Larson, E. D., & Proenza, C. (2010). Phosphorylation and modulation of hyperpolarization-activated HCN4 channels by protein kinase A in the mouse sinoatrial node. *The Journal of General Physiology*, *136*(3), 247 –258. doi:10.1085/jgp.201010488

Liberles, S. D., Diver, S. T., Austin, D. J., & Schreiber, S. L. (1997). Inducible gene expression and protein translocation using nontoxic ligands identified by a mammalian three-hybrid screen. *Proceedings of the National Academy of Sciences*, *94*(15), 7825 –7830.

Liu, Q., Chen, Y., Auger-Messier, M., & Molkentin, J. D. (2012). Interaction Between NFκB and NFAT Coordinates Cardiac Hypertrophy and Pathological Remodeling. *Circulation Research*. doi:10.1161/CIRCRESAHA.111.260729

Liu, S., Zhang, J., & Xiang, Y. K. (2011). FRET-based direct detection of dynamic protein kinase A activity on the sarcoplasmic reticulum in cardiomyocytes. *Biochemical and Biophysical Research Communications*, *404*(2), 581–586. doi:10.1016/j.bbrc.2010.11.116

Lukyanenko, V., & Györke, S. (1999). Ca2+ sparks and Ca2+ waves in saponin-permeabilized rat ventricular myocytes. *The Journal of Physiology*, *521*(3), 575 –585. doi:10.1111/j.1469-7793.1999.00575.x

Lukyanenko, V., Viatchenko-Karpinski, S., Smirnov, A., Wiesner, T. F., & Györke, S. (2001). Dynamic Regulation of Sarcoplasmic Reticulum Ca2+ Content and

Release by Luminal Ca2+-Sensitive Leak in Rat Ventricular Myocytes. *Biophysical Journal*, *81*(2), 785–798. doi:10.1016/S0006-3495(01)75741-4

Luo, C., & Rudy, Y. (1991). A model of the ventricular cardiac action potential. Depolarization, repolarization, and their interaction. *Circulation Research*, *68*(6), 1501 –1526. doi:10.1161/01.RES.68.6.1501

Lygren, B., Carlson, C. R., Santamaria, K., Lissandron, V., McSorley, T., Litzenberg, J., Lorenz, D., et al. (2007). AKAP complex regulates Ca2+ re-uptake into heart sarcoplasmic reticulum. *EMBO Rep*, *8*(11), 1061–1067. doi:10.1038/sj.embor.7401081

Maravall, M., Mainen, Z. F., Sabatini, B. L., & Svoboda, K. (2000). Estimating Intracellular Calcium Concentrations and Buffering without Wavelength Ratioing. *Biophysical Journal*, *78*(5), 2655–2667. doi:10.1016/S0006-3495(00)76809-3

Marks, A. R. (2001). Ryanodine Receptors/Calcium Release channels in Heart Failure and Sudden Cardiac Death. *Journal of Molecular and Cellular Cardiology*, *33*(4), 615–624. doi:10.1006/jmcc.2000.1343

Marrion, N. V., & Tavalin, S. J. (1998). Selective activation of Ca2+-activated K+ channels by co-localized Ca2+ channels in hippocampal neurons. *Nature*, *395*(6705), 900–905. doi:10.1038/27674

Martin, N., & Lilly, L. S. (2007). Chapter 2: The Cardiac Cycle: Mechanisms of Heart Sounds and Murmurs. *Pathophysiology of Heart Disease* (4th ed.). Philadelphia: Lippincott Williams & Wilkins.

Marx, S. O., Gaburjakova, J., Gaburjakova, M., Henrikson, C., Ondrias, K., & Marks, A. R. (2001). Coupled Gating Between Cardiac Calcium Release Channels (Ryanodine Receptors). *Circulation Research*, *88*(11), 1151 –1158. doi:10.1161/hh1101.091268

Marx, S. O., Kurokawa, J., Reiken, S., Motoike, H., D'Armiento, J., Marks, A. R., & Kass, R. S. (2002). Requirement of a Macromolecular Signaling Complex for β Adrenergic Receptor Modulation of the KCNQ1-KCNE1 Potassium Channel. *Science*, *295*(5554), 496 –499. doi:10.1126/science.1066843

Marx, S. O., Reiken, S., Hisamatsu, Y., Jayaraman, T., Burkhoff, D., Rosemblit, N., & Marks, A. R. (2000). PKA Phosphorylation Dissociates FKBP12.6 from the Calcium Release Channel (Ryanodine Receptor): Defective Regulation in Failing Hearts. *Cell*, *101*(4), 365–376. doi:10.1016/S0092-8674(00)80847-8

Mauban, J. R. H., O'Donnell, M., Warrier, S., Manni, S., & Bond, M. (2009). AKAP-Scaffolding Proteins and Regulation of Cardiac Physiology. *Physiology*, *24*(2), 78 –87. doi:10.1152/physiol.00041.2008

McLean, I. W., & Nakane, P. K. (1974). PERIODATE-LYSINE-PARAFORMALDEHYDE FIXATIVE A NEW FIXATIVE FOR IMMUNOELECTRON MICROSCOPY. *Journal of Histochemistry & Cytochemistry*, *22*(12), 1077 –1083. doi:10.1177/22.12.1077

Meng, X., Xiao, B., Cai, S., Huang, X., Li, F., Bolstad, J., Trujillo, R., et al. (2007). Three-Dimensional Localization of Serine 2808, a Phosphorylation Site in Cardiac Ryanodine Receptor. *Journal of Biological Chemistry*, *282*(35), 25929 –25939. doi:10.1074/jbc.M704474200

Merzlyak, E. M., Goedhart, J., Shcherbo, D., Bulina, M. E., Shcheglov, A. S., Fradkov, A. F., Gaintzeva, A., et al. (2007). Bright monomeric red fluorescent protein with an extended fluorescence lifetime. *Nat Meth*, *4*(7), 555–557. doi:10.1038/nmeth1062

Mirvis, D. M., & Goldberger, A. M. (2008). Chapter 13: Electrocardiography. *Braunwald's heart disease: a textbook of cardiovascular medicine* (8th ed.). Philadelphia: Saunders Elsevier.

Mitchell, G. F., Jeron, A., & Koren, G. (1998). Measurement of heart rate and Q-T interval in the conscious mouse. *American Journal of Physiology - Heart and Circulatory Physiology*, *274*(3), H747 –H751.

Navedo, M. F., Amberg, G. C., Nieves, M., Molkentin, J. D., & Santana, L. F. (2006). Mechanisms Underlying Heterogeneous Ca2+ Sparklet Activity in Arterial Smooth Muscle. *The Journal of General Physiology*, *127*(6), 611 –622. doi:10.1085/jgp.200609519

Navedo, M. F., Amberg, G. C., Votaw, V. S., & Santana, L. F. (2005). Constitutively active L-type Ca2+ channels. *Proceedings of the National Academy of Sciences of the United States of America*, *102*(31), 11112 –11117. doi:10.1073/pnas.0500360102

Navedo, M. F., Amberg, G. C., Westenbroek, R. E., Sinnegger-Brauns, M. J., Catterall, W. A., Striessnig, J., & Santana, L. F. (2007). Cav1.3 channels produce persistent calcium sparklets, but Cav1.2 channels are responsible for sparklets in mouse arterial smooth muscle. *American Journal of Physiology -*

Heart and Circulatory Physiology, *293*(3), H1359 –H1370. doi:10.1152/ajpheart.00450.2007

Navedo, M. F., Cheng, E. P., Yuan, C., Votaw, S., Molkentin, J. D., Scott, J. D., & Santana, L. F. (2010). Increased Coupled Gating of L-Type Ca2+ Channels During Hypertension and Timothy Syndrome. *Circulation Research*, *106*(4), 748 –756. doi:10.1161/CIRCRESAHA.109.213363

Navedo, M. F., Nieves-Cintrón, M., Amberg, G. C., Yuan, C., Votaw, V. S., Lederer, W. J., McKnight, G. S., et al. (2008). AKAP150 Is Required for Stuttering Persistent Ca2+ Sparklets and Angiotensin II–Induced Hypertension. *Circulation Research*, *102*(2), e1 –e11. doi:10.1161/CIRCRESAHA.107.167809

Nerbonne, J. M., & Kass, R. S. (2005). Molecular Physiology of Cardiac Repolarization. *Physiological Reviews*, *85*(4), 1205 –1253. doi:10.1152/physrev.00002.2005

Nichols, C. B., Rossow, C. F., Navedo, M. F., Westenbroek, R. E., Catterall, W. A., Santana, L. F., & McKnight, G. S. (2010). Sympathetic Stimulation of Adult Cardiomyocytes Requires Association of AKAP5 With a Subpopulation of L-Type Calcium Channels / Novelty and Significance. *Circulation Research*, *107*(6), 747 –756. doi:10.1161/CIRCRESAHA.109.216127

Nieves-Cintrón, M., Amberg, G. C., Navedo, M. F., Molkentin, J. D., & Santana, L. F. (2008). The control of Ca2+ influx and NFATc3 signaling in arterial smooth muscle during hypertension. *Proceedings of the National Academy of Sciences*, *105*(40), 15623 –15628. doi:10.1073/pnas.0808759105

Niggli, E., & Lederer, W. (1990). Voltage-independent calcium release in heart muscle. *Science*, *250*(4980), 565 –568. doi:10.1126/science.2173135

Nikolaev, V. O., Moshkov, A., Lyon, A. R., Miragoli, M., Novak, P., Paur, H., Lohse, M. J., et al. (2010). β2-Adrenergic Receptor Redistribution in Heart Failure Changes cAMP Compartmentation. *Science*, *327*(5973), 1653 –1657. doi:10.1126/science.1185988

Oliveria, S. F., Dell'Acqua, M. L., & Sather, W. A. (2007). AKAP79/150 Anchoring of Calcineurin Controls Neuronal L-Type Ca2+ Channel Activity and Nuclear Signaling. *Neuron*, *55*(2), 261–275. doi:10.1016/j.neuron.2007.06.032

Padala, M., Keeling, W. B., Guyton, R. A., & Thourani, V. H. (2011).*Circulation Journal*, *75*(5), 1028–1041.

Parker, I., & Wier, W. G. (1997). Variability in frequency and characteristics of Ca2+ sparks at different release sites in rat ventricular myocytes. *The Journal of Physiology*, *505*(Pt 2), 337 –344.

Pasca, S. P., Portmann, T., Voineagu, I., Yazawa, M., Shcheglovitov, A., Pasca, A. M., Cord, B., et al. (2011). Using iPSC-derived neurons to uncover cellular phenotypes associated with Timothy syndrome. *Nat Med*, *17*(12), 1657–1662. doi:10.1038/nm.2576

Patton, C., Thompson, S., & Epel, D. (2004). Some precautions in using chelators to buffer metals in biological solutions. *Cell Calcium*, *35*(5), 427–431. doi:10.1016/j.ceca.2003.10.006

Pesic, A., Madden, J. A., Pesic, M., & Rusch, N. J. (2004). High Blood Pressure Upregulates Arterial L-Type Ca2+ Channels. *Circulation Research*, *94*(10), e97 –e104. doi:10.1161/01.RES.0000131495.93500.3c

Pragnell, M., De Waard, M., Mori, Y., Tanabe, T., Snutch, T. P., & Campbell, K. P. (1994). Calcium channel beta-subunit binds to a conserved motif in the I-II cytoplasmic linker of the alpha 1-subunit. *Nature*, *368*(6466), 67–70.

Qin, J., Valle, G., Nani, A., Nori, A., Rizzi, N., Priori, S. G., Volpe, P., et al. (2008). Luminal Ca2+ Regulation of Single Cardiac Ryanodine Receptors: Insights Provided by Calsequestrin and its Mutants. *The Journal of General Physiology*, *131*(4), 325 –334. doi:10.1085/jgp.200709907

Reichenbach, H., Meister, E. M., & Theile, H. (1992). [The heart-hand syndrome. A new variant of disorders of heart conduction and syndactylia including osseous changes in hands and feet]. *Kinderarztl Prax*, *60*(2), 54–56.

Reuter, H. (1979). Properties of two inward membrane currents in the heart. *Annu Rev Physiol*, *41*, 413–424.

Richter, T., Floetenmeyer, M., Ferguson, C., Galea, J., Goh, J., Lindsay, M. R., Morgan, G. P., et al. (2008). High-Resolution 3D Quantitative Analysis of Caveolar Ultrastructure and Caveola–Cytoskeleton Interactions. *Traffic*, *9*(6), 893–909. doi:10.1111/j.1600-0854.2008.00733.x

Robert A Harrington, Mark E Silverman, & Charles F Wooley. (2011). Chapter 1. A History of the Heart, Cardiac Diseases, and the Development of Cardiovascular Medicine as a Specialty: Introduction. In V Fuster, R A Walsh, & R A Harrington (Eds.), *Hurst's The Heart* (13th ed.). McGraw-Hill. Retrieved

from http://www.accessmedicine.com.offcampus.lib.washington.edu/content.aspx?aid=7800101

Rolls, H. K., Stevenson, W. G., Strichartz, G. R., & Lilly, L. S. (2007). Chapter 11: Mechanisms of Cardiac Arrhythmias. *Pathophysiology of Heart Disease* (4th ed.). Philadelphia: Lippincott Williams & Wilkins.

Rosamond, W., Flegal, K., & Furie, K. (2008). A report from the American Heart Association Statistics Committee and Stroke Statistics Subcommittee. *Circulation*, *117*(4), e25–e146.

Rossow, C. F., Dilly, K. W., Yuan, C., Nieves-Cintrón, M., Cabarrus, J. L., & Santana, L. F. (2009). NFATc3-dependent loss of Ito gradient across the left ventricular wall during chronic β adrenergic stimulation. *Journal of Molecular and Cellular Cardiology*, *46*(2), 249–256. doi:10.1016/j.yjmcc.2008.10.016

Rossow, C. F., Minami, E., Chase, E. G., Murry, C. E., & Santana, L. F. (2004). NFATc3-Induced Reductions in Voltage-Gated K+ Currents After Myocardial Infarction. *Circulation Research*, *94*(10), 1340 –1350. doi:10.1161/01.RES.0000128406.08418.34

Rubart, M, Patlak, J. B., & Nelson, M. T. (1996). Ca2+ currents in cerebral artery smooth muscle cells of rat at physiological Ca2+ concentrations. *The Journal of General Physiology*, *107*(4), 459 –472. doi:10.1085/jgp.107.4.459

Rubart, Michael, & Zipes, D. P. (2005). Mechanisms of sudden cardiac death. *The Journal of Clinical Investigation*, *115*(9), 2305–2315.

Rubart, Michael, & Zipes, D. P. (2008). Chapter 35: Genesis of Cardiac Arrhythmias: Electrophysiologic Considerations. *Braunwald's heart disease: a textbook of cardiovascular medicine* (8th ed.). Philadelphia: Saunders Elsevier.

Sah, R., Ramirez, R. J., & Backx, P. H. (2002). Modulation of Ca2+ Release in Cardiac Myocytes by Changes in Repolarization Rate. *Circulation Research*, *90*(2), 165 –173. doi:10.1161/hh0202.103315

Saka, Y., Hagemann, A. I., Piepenburg, O., & Smith, J. C. (2007). Nuclear accumulation of Smad complexes occurs only after the midblastula transition in Xenopus. *Development*, *134*(23), 4209 –4218. doi:10.1242/dev.010645

Sanguinetti, M. C., & Tristani-Firouzi, M. (2006). hERG potassium channels and cardiac arrhythmia. *Nature*, *440*(7083), 463–469. doi:10.1038/nature04710

Santana, L F, Kranias, E. G., & Lederer, W. J. (1997). Calcium sparks and excitation-contraction coupling in phospholamban-deficient mouse ventricular myocytes. *The Journal of Physiology*, *503*(Pt 1), 21 –29.

Santana, L.F., Cheng, H., Gómez, A. M., Cannell, M. B., & Lederer, W. J. (1996). Relation Between the Sarcolemmal Ca2+ Current and Ca2+ Sparks and Local Control Theories for Cardiac Excitation-Contraction Coupling. *Circulation Research*, *78*(1), 166 –171. doi:10.1161/01.RES.78.1.166

Santana, Luis F., & Navedo, M. F. (2010). Natural inequalities: why some L-type Ca2+ channels work harder than others. *The Journal of General Physiology*, *136*(2), 143 –147. doi:10.1085/jgp.200910391

Sato, D., Xie, L.-H., Sovari, A. A., Tran, D. X., Morita, N., Xie, F., Karagueuzian, H., et al. (2009). Synchronization of chaotic early afterdepolarizations in the

genesis of cardiac arrhythmias. *Proceedings of the National Academy of Sciences*, *106*(9), 2983 –2988. doi:10.1073/pnas.0809148106

Scholz, D. G., Kitzman, D. W., Hagen, P. T., Ilstrup, D. M., & Edwards, W. D. (1988). Age-related changes in normal human hearts during the first 10 decades of life. Part I (Growth): A quantitative anatomic study of 200 specimens from subjects from birth to 19 years old. *Mayo Clin Proc*, *63*(2), 126–136.

Scott, J. D., & Santana, L. F. (2010). A-Kinase Anchoring Proteins. *Circulation*, *121*(10), 1264 –1271. doi:10.1161/CIRCULATIONAHA.109.896357

Selvin, P. R. (1995). [13] Fluorescence resonance energy transfer. *Biochemical Spectroscopy*, Methods in Enzymology (Vol. Volume 246, pp. 300–334). Academic Press. Retrieved from http://www.sciencedirect.com/science/article/pii/0076687995460152

Shah, R. V., & Fifer, M. A. (2007). Chapter 9: Heart Failure. *Pathophysiology of Heart Disease* (4th ed.). Philadelphia: Lippincott Williams & Wilkins.

Shan, J., Kushnir, A., Betzenhauser, M. J., Reiken, S., Li, J., Lehnart, S. E., Lindegger, N., et al. (2010). Phosphorylation of the ryanodine receptor mediates the cardiac fight or flight response in mice. *The Journal of Clinical Investigation*, *120*(12), 4388–4398.

Shi, C., & Soldatov, N. M. (2002). Molecular Determinants of Voltage-dependent Slow Inactivation of the Ca2+ Channel. *Journal of Biological Chemistry*, *277*(9), 6813 –6821. doi:10.1074/jbc.M110524200

Shioya, T. (2007). A simple technique for isolating healthy heart cells from mouse models. *The Journal of Physiological Sciences*, *57*(6), 327–335.

Sipido, K. R., Volders, P. G. ., Vos, M. A., & Verdonck, F. (2002). Altered Na/Ca exchange activity in cardiac hypertrophy and heart failure: a new target for therapy? *Cardiovascular Research*, *53*(4), 782 –805. doi:10.1016/S0008-6363(01)00470-9

Sobie, E. A., Dilly, K. W., dos Santos Cruz, J., Lederer, W. J., & Saleet Jafri, M. (2002). Termination of Cardiac Ca2+ Sparks: An Investigative Mathematical Model of Calcium-Induced Calcium Release. *Biophysical journal*, *83*(1), 59–78.

Soeller, C., & Cannell, M. B. (1997). Numerical simulation of local calcium movements during L-type calcium channel gating in the cardiac diad. *Biophysical Journal*, *73*(1), 97–111. doi:10.1016/S0006-3495(97)78051-2

Soldatov, N. M., Oz, M., O'Brien, K. A., Abernethy, D. R., & Morad, M. (1998). Molecular Determinants of L-type Ca2+ Channel Inactivation. *Journal of Biological Chemistry*, *273*(2), 957 –963. doi:10.1074/jbc.273.2.957

Soldatov, N. M., Zühlke, R. D., Bouron, A., & Reuter, H. (1997). Molecular Structures Involved in L-type Calcium Channel Inactivation. *Journal of Biological Chemistry*, *272*(6), 3560 –3566. doi:10.1074/jbc.272.6.3560

Splawski, I., Timothy, K. W., Decher, N., Kumar, P., Sachse, F. B., Beggs, A. H., Sanguinetti, M. C., et al. (2005). Severe arrhythmia disorder caused by cardiac L-type calcium channel mutations. *Proceedings of the National Academy of Sciences of the United States of America*, *102*(23), 8089 –8096. doi:10.1073/pnas.0502506102

Splawski, I., Timothy, K. W., Sharpe, L. M., Decher, N., Kumar, P., Bloise, R., Napolitano, C., et al. (2004). CaV1.2 Calcium Channel Dysfunction Causes a Multisystem Disorder Including Arrhythmia and Autism. *Cell*, *119*(1), 19–31. doi:10.1016/j.cell.2004.09.011

Stern, M. D. (1992). Theory of excitation-contraction coupling in cardiac muscle. *Biophysical Journal*, *63*(2), 497–517. doi:10.1016/S0006-3495(92)81615-6

Stotz, S. C., & Zamponi, G. W. (2001). Identification of Inactivation Determinants in the Domain IIS6 Region of High Voltage-activated Calcium Channels. *Journal of Biological Chemistry*, *276*(35), 33001 –33010. doi:10.1074/jbc.M104387200

Suh, B.-C., Inoue, T., Meyer, T., & Hille, B. (2006). Rapid Chemically Induced Changes of PtdIns(4,5)P2 Gate KCNQ Ion Channels. *Science*, *314*(5804), 1454 –1457. doi:10.1126/science.1131163

Sumi, M., Kiuchi, K., Ishikawa, T., Ishii, A., Hagiwara, M., Nagatsu, T., & Hidaka, H. (1991). The newly synthesized selective Ca2+calmodulin dependent protein kinase II inhibitor KN-93 reduces dopamine contents in PC12h cells. *Biochemical and Biophysical Research Communications*, *181*(3), 968–975. doi:10.1016/0006-291X(91)92031-E

Tadross, M. R., Park, S. A., Veeramani, B., & Yue, D. T. (2009). Robust approaches to quantitative ratiometric FRET imaging of CFP/YFP fluorophores under confocal microscopy. *Journal of Microscopy*, *233*(1), 192–204. doi:10.1111/j.1365-2818.2008.03109.x

Tadross, M. R., & Yue, D. T. (2010). Systematic mapping of the state dependence of voltage- and Ca2+-dependent inactivation using simple open-channel measurements. *The Journal of General Physiology*, *135*(3), 217 –227. doi:10.1085/jgp.200910309

Talan, M. I., Ahmet, I., Xiao, R.-P., & Lakatta, E. G. (2011). β2 AR Agonists in Treatment of Chronic Heart Failure: Long Path to Translation. *Journal of Molecular and Cellular Cardiology*, *51*(4), 529–533. doi:10.1016/j.yjmcc.2010.09.019

Tasken, K., & Aandahl, E. M. (2004). Localized Effects of cAMP Mediated by Distinct Routes of Protein Kinase A. *Physiological Reviews*, *84*(1), 137 –167. doi:10.1152/physrev.00021.2003

Thiel, W. H., Chen, B., Hund, T. J., Koval, O. M., Purohit, A., Song, L.-S., Mohler, P. J., et al. (2008). Proarrhythmic Defects in Timothy Syndrome Require Calmodulin Kinase II. *Circulation*, *118*(22), 2225 –2234. doi:10.1161/CIRCULATIONAHA.108.788067

Tour, O., Adams, S. R., Kerr, R. A., Meijer, R. M., Sejnowski, T. J., Tsien, R. W., & Tsien, R. Y. (2007). Calcium Green FlAsH as a genetically targeted small-molecule calcium indicator. *Nat Chem Biol*, *3*(7), 423–431. doi:10.1038/nchembio.2007.4

Tunquist, B. J., Hoshi, N., Guire, E. S., Zhang, F., Mullendorff, K., Langeberg, L. K., Raber, J., et al. (2008). Loss of AKAP150 perturbs distinct neuronal processes in mice. *Proceedings of the National Academy of Sciences*, *105*(34), 12557 –12562. doi:10.1073/pnas.0805922105

Van Haastert, P. J., Van Driel, R., Jastorff, B., Baraniak, J., Stec, W. J., & De Wit, R. J. (1984). Competitive cAMP antagonists for cAMP-receptor proteins. *Journal of Biological Chemistry*, *259*(16), 10020 –10024.

Vatta, M., Ackerman, M. J., Ye, B., Makielski, J. C., Ughanze, E. E., Taylor, E. W., Tester, D. J., et al. (2006). Mutant Caveolin-3 Induces Persistent Late Sodium Current and Is Associated With Long-QT Syndrome. *Circulation*, *114*(20), 2104 –2112. doi:10.1161/CIRCULATIONAHA.106.635268

Vijayaraghavan, S., Goueli, S. A., Davey, M. P., & Carr, D. W. (1997). Protein Kinase A-anchoring Inhibitor Peptides Arrest Mammalian Sperm Motility. *Journal of Biological Chemistry*, *272*(8), 4747 –4752. doi:10.1074/jbc.272.8.4747

Vincent, G. M., Timothy, K. W., Leppert, M., & Keating, M. (1992). The Spectrum of Symptoms and QT Intervals in Carriers of the Gene for the Long-QT Syndrome. *N Engl J Med*, *327*(12), 846–852. doi:10.1056/NEJM199209173271204

Volders, P. G. A., Vos, M. A., Szabo, B., Sipido, K. R., de Groot, S. H. M., Gorgels, A. P. M., Wellens, H. J. J., et al. (2000). Progress in the understanding of cardiac early afterdepolarizations and torsades de pointes: time to revise current concepts. *Cardiovascular Research*, *46*(3), 376 –392. doi:10.1016/S0008-6363(00)00022-5

Walsh, D. A., Perkins, J. P., & Krebs, E. G. (1968). An Adenosine 3’,5’-Monophosphate-dependant Protein Kinase from Rabbit Skeletal Muscle. *Journal of Biological Chemistry*, *243*(13), 3763 –3765.

Wang, M.-C., Collins, R. F., Ford, R. C., Berrow, N. S., Dolphin, A. C., & Kitmitto, A. (2004). The Three-dimensional Structure of the Cardiac L-type Voltage-gated Calcium Channel. *Journal of Biological Chemistry*, *279*(8), 7159 –7168. doi:10.1074/jbc.M308057200

Wang, S. Q., Stern, M. D., Ríos, E., & Cheng, H. (2004). The quantal nature of Ca2+ sparks and in situ operation of the ryanodine receptor array in cardiac cells. *Proceedings of the National Academy of Sciences of the United States of America*, *101*(11), 3979 –3984. doi:10.1073/pnas.0306157101

Wang, S.-Q., Song, L.-S., Lakatta, E. G., & Cheng, H. (2001). Ca2+ signalling between single L-type Ca2+ channels and ryanodine receptors in heart cells. *Nature*, *410*(6828), 592–596. doi:10.1038/35069083

Weiss, J. N., Nivala, M., Garfinkel, A., & Qu, Z. (2011). Alternans and Arrhythmias. *Circulation Research*, *108*(1), 98 –112. doi:10.1161/CIRCRESAHA.110.223586

Wier, W. G., Egan, T. M., López-López, J. R., & Balke, C. W. (1994). Local control of excitation-contraction coupling in rat heart cells. *The Journal of Physiology*, *474*(3), 463 –471.

Woodruff, M. L., Sampath, A. P., Matthews, H. R., Krasnoperova, N. V., Lem, J., & Fain, G. L. (2002). Measurement of cytoplasmic calcium concentration in the rods of wild-type and transducin knock-out mice. *The Journal of Physiology*, *542*(3), 843 –854. doi:10.1113/jphysiol.2001.013987

Xiang, Y. K. (2011). Compartmentalization of β-Adrenergic Signals in Cardiomyocytes. *Circulation Research*, *109*(2), 231 –244. doi:10.1161/CIRCRESAHA.110.231340

Xiang, Y., & Kobilka, B. K. (2003). Myocyte Adrenoceptor Signaling Pathways. *Science*, *300*(5625), 1530 –1532. doi:10.1126/science.1079206

Xiao, R.-P. (2001). {beta}-Adrenergic Signaling in the Heart: Dual Coupling of the {beta}2-Adrenergic Receptor to Gs and Gi Proteins. *Science Signaling*, *2001*(104), re15. doi:10.1126/stke.2001.104.re15

Xiao, R.-P., Zhu, W., Zheng, M., Cao, C., Zhang, Y., Lakatta, E. G., & Han, Q. (2006). Subtype-specific α1- and β-adrenoceptor signaling in the heart. *Trends in Pharmacological Sciences*, *27*(6), 330–337. doi:10.1016/j.tips.2006.04.009

Xiao, R.-P., Zhu, W., Zheng, M., Chakir, K., Bond, R., Lakatta, E. G., & Cheng, H. (2004). Subtype-specific β-adrenoceptor signaling pathways in the heart and their potential clinical implications. *Trends in Pharmacological Sciences*, *25*(7), 358–365. doi:10.1016/j.tips.2004.05.007

Xie, L.-H., & Weiss, J. N. (2009). Arrhythmogenic consequences of intracellular calcium waves. *American Journal of Physiology - Heart and Circulatory Physiology*, *297*(3), H997 –H1002. doi:10.1152/ajpheart.00390.2009

Yamaguchi, H., Hara, M., Strobeck, M., Fukasawa, K., Schwartz, A., & Varadi, G. (1998). Multiple Modulation Pathways of Calcium Channel Activity by a β Subunit. *Journal of Biological Chemistry*, *273*(30), 19348 –19356. doi:10.1074/jbc.273.30.19348

Yarotskyy, V, & Elmslie, K. S. (2007). Roscovitine, a cyclin-dependent kinase inhibitor, affects several gating mechanisms to inhibit cardiac L-type (Ca(V)1.2) calcium channels. *British Journal of Pharmacology*, *152*(3), 386–395. doi:10.1038/sj.bjp.0707414

Yarotskyy, Viktor, Gao, G., Peterson, B. Z., & Elmslie, K. S. (2009). The Timothy syndrome mutation of cardiac CaV1.2 (L-type) channels: multiple altered gating mechanisms and pharmacological restoration of inactivation. *The Journal of Physiology*, *587*(3), 551 –565. doi:10.1113/jphysiol.2008.161737

Yazawa, M., Hsueh, B., Jia, X., Pasca, A. M., Bernstein, J. A., Hallmayer, J., & Dolmetsch, R. E. (2011). Using induced pluripotent stem cells to investigate cardiac phenotypes in Timothy syndrome. *Nature*, *471*(7337), 230–234. doi:10.1038/nature09855

Young, J. L., & Libby, P. (2007). Chapter 5: Atherosclerosis. *Pathophysiology of Heart Disease* (4th ed.). Philadelphia: Lippincott Williams & Wilkins.

Yuan, W., & Bers, D. M. (1994). Ca-dependent facilitation of cardiac Ca current is due to Ca-calmodulin-dependent protein kinase. *American Journal of Physiology - Heart and Circulatory Physiology*, *267*(3), H982 –H993.

Zachariah, J. P., Vasan, R. S., & D'Agostino, R. B. (2011). Chapter 2. The Burden of Increasing Worldwide Cardiovascular Disease. In V. Fuster, R. A. Walsh, & R. A. Harrington (Eds.), *Hurst's The Heart* (13th ed.). McGraw-Hill. Retrieved from http://www.accessmedicine.com.offcampus.lib.washington.edu/content.aspx?aid=7800303

Zhang, D., Gaussin, V., Taffet, G. E., Belaguli, N. S., Yamada, M., Schwartz, R. J., Michael, L. H., et al. (2000). TAK1 is activated in the myocardium after pressure overload and is sufficient to provoke heart failure in transgenic mice. *Nat Med*, *6*(5), 556–563. doi:10.1038/75037

Zhang, H., Makarewich, C. A., Kubo, H., Wang, W., Duran, J. M., Li, Y., Berretta, R. M., et al. (2012). Hyperphosphorylation of the Cardiac Ryanodine Receptor at Serine 2808 Is Not Involved in Cardiac Dysfunction After Myocardial Infarction / Novelty and Significance. *Circulation Research*, *110*(6), 831 –840. doi:10.1161/CIRCRESAHA.111.255158

Zhang, J.-F., Ellinor, P. T., Aldrich, R. W., & Tsien, R. W. (1994). Molecular determinants of voltage-dependent inactivation in calcium channels. *Nature*, *372*(6501), 97–100. doi:10.1038/372097a0

Zimetbaum, P. J., & Josephson, M. E. (2008). Pathophysiology of the long QT syndrome. *UpToDate*. Waltham, MA.

Zuhlke, R. D., Pitt, G. S., Deisseroth, K., Tsien, R. W., & Reuter, H. (1999). Calmodulin supports both inactivation and facilitation of L-type calcium channels. *Nature*, *399*(6732), 159–162. doi:10.1038/20200

Zühlke, R. D., & Reuter, H. (1998). Ca2+-sensitive inactivation of L-type Ca2+ channels depends on multiple cytoplasmic amino acid sequences of the α1C subunit. *Proceedings of the National Academy of Sciences*, *95*(6), 3287 – 3294.

Appendix A: Markov model quantification of coupled gating

By using the methods of Chung and Kennedy, we modeled the channels in our current and Ca^{2+} records as *L* identical, discrete-time, binary homogeneous Markov processes (Chung & Kennedy, 1996). At any time *k*, a vector of *L* binary terms, corresponding to either the open or closed state, describes the current state of the system:

$$S_k \equiv \left(s_k^{(1)}, \ldots, s_k^{(L)}\right).$$

Each binary process has the following transition probability v_{ij}:

$$v_{ij} = P\left(s_{k+1}^{(r)} = q_j \middle| s_k^{(r)} = q_i\right), \qquad i, j \in \{1,2\}; \forall 1 \leq r \leq L.$$

For a system with only two pores that are not coupled, then the transition matrix **V** is:

$$\mathrm{V} = \begin{bmatrix} \zeta & 1-\zeta \\ 1-\rho & \rho \end{bmatrix},$$

where ζ is the probability of a closed channel to stay closed and ρ is the probability of an open channel to remain open. For *L* pores that are independent (not coupled), the transition matrix is the following $2^L \times 2^L$ Kronecker product:

$$P^{(l)} \triangleq \underbrace{V \otimes V \otimes \cdots \otimes V}_{L \text{ times}}$$

For the tightly coupled case, the transition matrix is:

$$P^{(c)} \triangleq \begin{bmatrix} \zeta & \cdots & 1-\zeta \\ \vdots & \ddots & \vdots \\ 1-\rho & \cdots & \rho \end{bmatrix}.$$

For partially coupled pores, the transition matrix is the linear combination of the independent and coupled cases via the coupling coefficient κ, which is the probability of coupled gating:

$$P \triangleq (1-\kappa)P^{(l)} + \kappa P^{(c)}.$$

And if we assume degeneracy and complete identity of channels within a cluster, then we can reduce the problem down to a (L+1) × (L+1) dimension aggregated transition matrix A:

$$\mathrm{A}=\mathrm{A}^{(I)} + \mathrm{A}^{(C)} \triangleq LPR = (1-\kappa)LP^{(l)}R + \kappa LP^{(c)}R,$$

Where L is (L+1) × 2^L where a component is zero unless if state $j \in$ aggregated state i, then it is $\binom{L}{i}^{-1}$. A component of R is 0 unless if state $j \in$ aggregated state i, then it is 1.

The model is parameterized by the set:

$$\Theta = \{\zeta, \rho, \kappa\}.$$

We use the built in HMMestimate function in Matlab to find the empirical transition matrix Â, we then estimate the parameter set Θ by:

$$\Theta = \arg\min \frac{1}{2}\left\|\mathrm{A}(\Theta)\text{-}\widehat{\mathrm{A}}\right\|$$

```
%Hidden Markov Model Analysis of Ca2+ Sparklets
%by Edward Cheng, 3/16/09
%
clear all

fname=input('Please enter file name (including extension):','s');

Data1=importdata(fname);  %open file

time=transpose(Data1(:,1));    %vector of time
ca_conc=transpose(Data1(:,2)); %vector of calcium concentration
change



global quantal;
quantal=37.9; %nM, the quantal level of Ca2+ change per single
channel opening,
%obtained from signal mass analysis from Navedo et al.
%J Gen Physiol. 2006 Jun;127(6):611-22.

states=zeros(1,length(time)); %initiate states vector
closedtime=0;opentime1=0; opentime2=0; opentime3=0;
opentime4=0; %initialize variable for open time with
%1,2,....3 channels open
opentime=0; %initialize variable for total open time
```

```
closedtime=0; %initialize variable for total closed time

ca_conc0=0; %initialize a variable to store all data associated
w/closed state to calculate std dev
ca_conc1=0; %initialize variable to store all data associated w/1
channel open
ca_conc2=0; %ditto for 2 channels
ca_conc3=0; %ditto for 3
ca_conc4=0; %ditto for 4

OC=0; %initialize variable to store open-to-closed events
CO=0; %initalize variable to store closed-to-open events

%50% threshold analysis to assign states to each timepoint.
for i=1:length(time)
    if ca_conc(i)<(quantal/2)
        states(i)=0; %state is closed (0 channel open)
        if i>1
            if states(i-1)>0
                OC=OC+(states(i-1)-states(i)); %increment OC if
previous state is at a higher conductance state
            end
        end
        closedtime=closedtime+1;  %update closedtime length
        ca_conc0(closedtime)=ca_conc(i); %store data to closed
```

```
state data vector
    elseif ca_conc(i)>=(quantal/2) && ca_conc(i)<(3*quantal/2)
        states(i)=1;
        if i>1
            if states(i-1)>1
                OC=OC+(states(i-1)-states(i)); %increment OC
            elseif states(i-1)<1
                CO=CO+1; %increment CO if prev state is closed
            end
        end
        opentime1=opentime1+1;
        opentime=opentime+1;
        ca_conc1(opentime1)=ca_conc(i);
    elseif ca_conc(i)>=(3*quantal/2) && ca_conc(i)<(5*quantal/2)
        states(i)=2;
        if i>1
            if states(i-1)>2
                OC=OC+(states(i-1)-states(i)); %increment OC
            elseif states(i-1)<2
                CO=CO+(states(i)-states(i-1)); %increment CO if
prev state is lower
            end
        end
        opentime2=opentime2+1;
        opentime=opentime+2; %2 channels are open at once
```

```
        ca_conc2(opentime2)=ca_conc(i);
    elseif ca_conc(i)>=(5*quantal/2) && ca_conc(i)<(7*quantal/2)
        states(i)=3;
        if i>1
            if states(i-1)>3
                OC=OC+(states(i-1)-states(i)); %increment OC
            elseif states(i-1)<3
                CO=CO+(states(i)-states(i-1)); %increment CO if
prev state is lower
            end
        end
        opentime3=opentime3+1;
        opentime=opentime+3; %3 channels are open at once
        ca_conc3(opentime3)=ca_conc(i);
    elseif ca_conc(i)>=(7*quantal/2) %&& ca_conc(i)<(9*quantal/2)
        states(i)=4;
        if i>1
            if states(i-1)>4
                OC=OC+(states(i-1)-states(i)); %increment OC
            elseif states(i-1)<4
                CO=CO+(states(i)-states(i-1)); %increment CO if
prev state is lower
            end
        end
        opentime4=opentime4+1;
```

```
        opentime=opentime+4; %4 channels are open at once
        ca_conc4(opentime4)=ca_conc(i);
    end
end

nPs=opentime/length(time); %calculate the multiple open probability
nPs
Ps=(opentime1+opentime2+opentime3+opentime4)/length(time); %calcula
te open probability Ps

std_dev0=std(ca_conc0); %calculate std dev of data assoc w/each
quantal level
std_dev1=std(ca_conc1);
std_dev2=std(ca_conc2);
std_dev3=std(ca_conc3);
std_dev4=std(ca_conc4);

bin_ca_conc=zeros(1,length(time)); %initialize vector to store our
binned ca_conc data

%%
%Since the Baum-Welch HMM algorithm in Matlab used to estimate the
transition matrix requires
%the "sequence" of observables to be integers, let's bin our data,
with bin size based on
```

```
%the distribution (std dev) of the raw calcium change data.  An
integer number,
%rank based on the calcium change level, is assigned to each bin,
which
%gives us the sequence of integer states needed to run the function
%hmmestimate
bin_ca_conc=bin_seq( ca_conc,states,std_dev0,std_dev1,std_dev2,std_
dev3,std_dev4 );



%%
%%Now from the nPs, we can calculate the transition matrix IF our
%channels are completely independent (as well as time invariant).
%Based on the assumption that the channels are degenerate, we'll
see if it
%is correct.  Formula for transition matrix in the case of channel
%degeneracy is from Klein et al. Biometrics. 1997 Sep;53(3):870-84.



%Initialize transition matrix for the case when all channels are
identical
%& independent
TransitionIndependent=zeros(5);
```

```
%calculate transition probabilities, see Kelin et al. for more
details
i=1; %initialize i
while i<=5
    j=1; %initialize j
    while j<=5
        k=max(i-j,0);
        l=1;
        kmax=min(5-j,i-1);
        summation=zeros(1,kmax-k+1);
        while l<=length(summation)
            summation(l)=nchoosek(i-1,k)*nchoosek(5-i,k+j-i)*(1-
poo)^k*poo^(i-k-1)*(1-pcc)^(k+j-i)*pcc^(5-j-k);
            l=l+1;
            k=k+1;
        end
        TransitionIndependent(i,j)=sum(summation);
        j=j+1;
    end
    i=i+1;
end

%Matlab considers states as a Markov chain starting with state '1',
so need
%to add 1 to make the closed state as state 1
```

```
states=states+1;
```

The following script was written to symbolically the fully stochastic gating transition matrices A_one to A_*n*

```
V=[z 1-z;1-r r];

P_I=V; %initialize P_I, transition matrix for stochastic case

for i=1:L-1
    P_I=kron(P_I,V);
end


%populate fully coupled case transition matrix
n=2^L;
for i=1:n
    for j=1:n
        if i==1
            if j==1
                P_C(i,j)=z;

            elseif j==n
                P_C(i,j)=1-z;
```

```
        else
            P_C(i,j)=0;
        end
    elseif i==2
        if j==1
            P_C(i,j)=0.5;
        elseif j==n
            P_C(i,j)=0.5;
        else
            P_C(i,j)=0;
        end
    elseif i==n-1
        if j==1
            P_C(i,j)=0.5;
        elseif j==n
            P_C(i,j)=0.5;
        else
            P_C(i,j)=0;
        end
    elseif i==n
        if j==1
            P_C(i,j)=1-r;

        elseif j==n
```

```
                P_C(i,j)=r;

            else
                P_C(i,j)=0;
            end
        else
            P_C(i,j)=0;
        end
    end
end

Openlevel=zvector(L);

%populate matrix L_mat to map onto aggregated state
for i=1:L+1
    for j=1:2^L
        if Openlevel(j)==i
            L_mat(i,j)=(nchoosek(L,i))^-1;
        else
            L_mat(i,j)=0;
        end
    end
end

%populate matrix R_mat to map onto aggregated transition matrix
```

```
for j=1:2^L
    for i=1:L+1
        if Openlevel(j)==i
            R_mat(j,i)=1;
        else
            R_mat(j,i)=0;
        end
    end
end

A=(1-k)*L_mat*P_I*R_mat+k*L_mat*P_C*R_mat;
```

Curriculum vitae

Education

2006-Present	Doctor of Medicine	Medical Scientist Training Program University of Washington, Seattle, WA
2008-2012	Doctor of Philosophy	Department of Physiology and Biophysics University of Washington, Seattle, WA
2004-2006	Bachelor of Science	Biomedical Engineering, magna cum laude Washington University in St. Louis, St. Louis, MO
2002-2004	Associates of Arts	Chemistry Pasadena City College, Pasadena, CA

Research experience

2008-2012 PI: Dr. Fernando Santana Department of Physiology and Biophysics
University of Washington, Seattle, WA

- Discovered the necessary role of AKAP150 in causing the arrhythmogenic phenotype for LQT8 in cardiac myocytes (G406R) using fluorescence calcium imaging and patch-clamp techniques.
- CO-discovered coupled gating phenomena in $Ca_v1.2$ L-type Ca^{2+} channels with colleagues.

Summer 2007 PI: Dr. Alex Clowes Department of Pathology
University of Washington, Seattle, WA

- Confirmed results from a microarray study that the prostaglandin transporter SLCO2A1 is up-regulated in vascular smooth muscle cells that were exposed to a pro-apoptotic cocktail, Fas-L and cycloheximide.

Summer 2006 PI: Dr. Daniel Chiu Department of Chemistry
University of Washington, Seattle, WA

- Fabricated a novel setup using a spiral shaped phase plate to generate higher order Lagrange-Gaussian laser beams used in optical trapping.
- Improved the method by which diffraction grating designs created by computer simulation were translated into optical masks used in micro-fabrication.

2004-2006 PI: Dr. Joshua Maurer Department of Chemistry
Washington University in St. Louis, St. Louis, MO

- Designed and performed the synthesis of oligo (ethylene glycol)-terminated alkanethiols used in the formation of self-assembled monolayers.
- Cloned extracellular domain of axonal guidance growth cues.

Summer 2005 PI: Dr. David St. Jean Small Molecules Division
Amgen Corporation, Thousand Oaks, CA

- Developed a novel tandem cyclization reaction mediated by samarium(II) iodide.

Summer 2004 PI: Dr. Nikki Zacharias Neurion Corporation, Pasadena, CA
PI: Dr. Dennis Dougherty Department of Chemistry and Chemical Engineering
California Institute of Technology, Pasadena, CA

- Synthesized protected natural and unnatural amino acids used in the study of ligand gated ion channels.
- Purified dCA dinucleotides using fast-protein liquid chromatography.

Honors

2005 Dr. Robert J. and Kathryn W. Calcaterra Scholarship
2005 Biomedical Engineering Department Junior Class Award for Academic Excellence
2004 Gustav Kurt Mesmer Scholarship
2004 Honors Extraordinary in Chemistry and Physics
2004 William C. Miller Physics Scholarship
2004 Michilinda Women's Association Scholarship
2004, 2003 Alice and Don Slater General Scholarship
2003 William C. Miller Chemistry Scholarship
2003 Freshman Chemistry Student of the Year

Publications

Dixon RE, Yuan C, Cheng EP, Navedo MF, Santana LF. Ca^{2+} amplification by oligomerization of L-type $Ca_v1.2$ channels. *Proc Natl Acad Sci U S A*. 2012 Jan 31;109(5):1749-54.

Cheng EP, Yuan C, Navedo MF, Dixon RE, Nieves-Cintrón M, Scott JD, Santana LF. Restoration of normal L-type Ca2+ channel function during Timothy syndrome by ablation of an anchoring protein. *Circulation Research*. 2011 Jul 22;109(3):255-61.

Santana LF, Cheng EP, Lederer WJ. How does the shape of the cardiac action potential control calcium signaling and contraction in the heart?. *Journal of Molecular and Cellular Cardiololgy*. 2010 Dec;49(6):901-3.

Navedo MF, Cheng EP, Yuan C, Votaw S, Molkentin JD, Scott JD, Santana LF. Increased coupled gating of L-type Ca2+ channels during hypertension and Timothy syndrome. *Circulation Research*. 2010 Mar 5;106(4):748-56.

Conference presentations

Cheng EP, Yuan C, Navedo MF, Santana LF. (2010, February 21). Coupled gating of L-type calcium channels. Presented at the 54th Biophysical Society Meeting, San Francisco, CA.

Cheng EP, Kenagy RD, Clowes, AW. (2008, February 1). Knockdown of the prostaglandin transporter in smooth muscle cells enhanced expression of inflammatory cytokines. Presented at the WSMRF Conference, Camel, CA.

Cheng EP and St Jean D. (2005, November 5). *A Novel Cyclization Mediated by SmI_2*. Presented at the Pew Midstates Undergraduate Research Symposium in the Physical Sciences and Mathematics at The University of Chicago.

Teaching experience

Spring 2010	PBIO 506 Human Physiology	Responsible for teaching a 2 hour long review session per week.
Fall 2009	PBIO 505 Human Physiology	Responsible for teaching a 2 hour long review session per week.
Fall 2008	HuBio 514 Biochemistry	Responsible for leading a 1 hour long discussion section per week.

Work experience

2002-2004	Sport Chalet, La Canada, CA	Sales associate
2001-2002	United States Army, Ft. Knox, KY	MOS 19K, M1A1 tank crewman